

Structure-activity relationships, biological evaluation and structural studies of novel pyrrolonaphthoxazepines as antitumor agents

This is the peer reviewed version of the following article:

Original:

Brindisi, M., Ulivieri, C., Alfano, G., Gemma, S., de Asís Balaguer, F., Khan, T., et al. (2019). Structure-activity relationships, biological evaluation and structural studies of novel pyrrolonaphthoxazepines as antitumor agents. EUROPEAN JOURNAL OF MEDICINAL CHEMISTRY, 162, 290-320 [10.1016/j.ejmech.2018.11.004].

Availability:

This version is available <http://hdl.handle.net/11365/1063071> since 2018-11-26T12:29:01Z

Published:

DOI: <http://doi.org/10.1016/j.ejmech.2018.11.004>

Terms of use:

Open Access

The terms and conditions for the reuse of this version of the manuscript are specified in the publishing policy. Works made available under a Creative Commons license can be used according to the terms and conditions of said license.

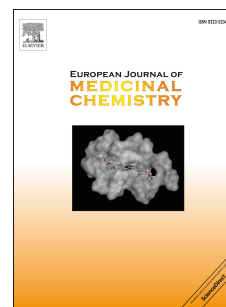
For all terms of use and more information see the publisher's website.

(Article begins on next page)

Accepted Manuscript

Structure-activity relationships, biological evaluation and structural studies of novel pyrrolonaphthoxazepines as antitumor agents

Margherita Brindisi, Cristina Ulivieri, Gloria Alfano, Sandra Gemma, Francisco de Asís Balaguer, Tuhina Khan, Alessandro Grillo, Giulia Chemi, Grégory Menchon, Andrea E. Prota, Natacha Olieric, Daniel Lucena-Agell, Isabel Barasoain, J. Fernando Diaz, Angela Nebbioso, Mariarosaria Conte, Ludovica Lopresti, Stefania Magnano, Rebecca Amet, Paula Kinsella, Daniela M. Zisterer, Ola Ibrahim, Jeff O'Sullivan, Lucia Morbidelli, Roberta Spaccapelo, Cosima Baldari, Stefania Butini, Ettore Novellino, Giuseppe Campiani, Lucia Altucci, Michel O. Steinmetz, Simone Brogi



PII: S0223-5234(18)30952-8

DOI: <https://doi.org/10.1016/j.ejmech.2018.11.004>

Reference: EJMECH 10861

To appear in: *European Journal of Medicinal Chemistry*

Received Date: 16 July 2018

Revised Date: 11 October 2018

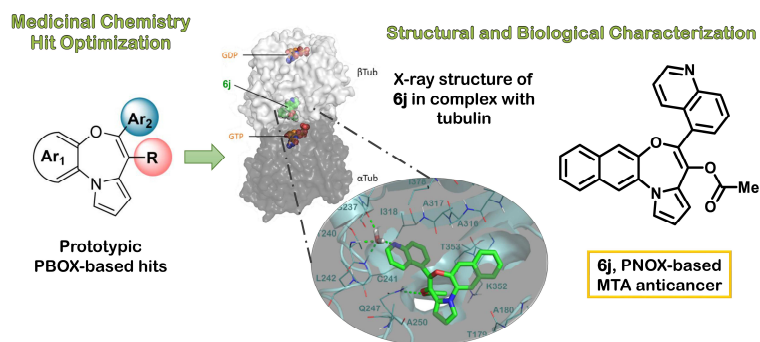
Accepted Date: 2 November 2018

Please cite this article as: M. Brindisi, C. Ulivieri, G. Alfano, S. Gemma, F. de Asís Balaguer, T. Khan, A. Grillo, G. Chemi, Gré. Menchon, A.E. Prota, N. Olieric, D. Lucena-Agell, I. Barasoain, J.F. Diaz, A. Nebbioso, M. Conte, L. Lopresti, S. Magnano, R. Amet, P. Kinsella, D.M. Zisterer, O. Ibrahim, J. O'Sullivan, L. Morbidelli, R. Spaccapelo, C. Baldari, S. Butini, E. Novellino, G. Campiani, L. Altucci, M.O. Steinmetz, S. Brogi, Structure-activity relationships, biological evaluation and structural studies of novel pyrrolonaphthoxazepines as antitumor agents, *European Journal of Medicinal Chemistry* (2018), doi: <https://doi.org/10.1016/j.ejmech.2018.11.004>.

This is a PDF file of an unedited manuscript that has been accepted for publication. As a service to our customers we are providing this early version of the manuscript. The manuscript will undergo copyediting, typesetting, and review of the resulting proof before it is published in its final form. Please note that during the production process errors may be discovered which could affect the content, and all legal disclaimers that apply to the journal pertain.

Graphical Abstract

POTENT PRO-APOPTOTIC TUBULIN BINDING AGENTS



Structure-Activity Relationships, Biological Evaluation and Structural Studies of Novel Pyrrolonaphthoxazepines as Antitumor Agents

Margherita Brindisi,^{a,b} Cristina Ulivieri,^{b,c} Gloria Alfano,^{a,b} Sandra Gemma,^{a,b} Francisco de Asís Balaguer,^d Tuhina Khan,^a Alessandro Grillo,^{a,b} Giulia Chemi,^{a,b} Grégory Menchon,^{e,f} Andrea E. Prota,^{e,f} Natacha Olieric,^{e,f} Daniel Lucena-Agell,^d Isabel Barasoain,^d J. Fernando Diaz,^d Angela Nebbioso,^g Mariarosaria Conte,^h Ludovica Lopresti,^{b,c} Stefania Magnano,ⁱ Rebecca Amet,ⁱ Paula Kinsella,ⁱ Daniela M. Zisterer,ⁱ Ola Ibrahim,^j Jeff O'Sullivan,^j Lucia Morbidelli,^{b,c} Roberta Spaccapelo,^k Cosima Baldari,^{b,c} Stefania Butini,^{a,b,*} Ettore Novellino,^l Giuseppe Campiani,^{a,b,*} Lucia Altucci,^g Michel O. Steinmetz,^{e,f} Simone Brogi^{a,b}

^aEuropean Research Centre for Drug Discovery and Development (NatSynDrugs), University of Siena, Department of Biotechnology, Chemistry and Pharmacy, DoE Department of Excellence 2018-2022, via Aldo Moro 2, I-53100 Siena, Italy

^bIstituto Toscano Tumori, University of Siena, via Aldo Moro 2, I-53100 Siena, Italy

^cDepartment of Life Sciences, via Aldo Moro 2, I-53100 Siena, Italy

^dDepartment of Physical and Chemical Biology, Centro de Investigaciones Biológicas, Consejo Superior de Investigaciones Científicas, Ramiro de Maeztu 9, 28040 Madrid, Spain

^eLaboratory of Biomolecular Research, Division of Biology and Chemistry, Paul Scherrer Institut, 5232 Villigen, Switzerland

^fUniversity of Basel, Biozentrum, 4056 Basel, Switzerland

^gDepartment of Precision Medicine, University of Campania Luigi Vanvitelli, Vico L. de Crecchio 7, 80138 Naples, Italy

^hIRCCS, SDN, Via E. Gianturco 113, 80143, Naples, Italy

ⁱSchool of Biochemistry and Immunology, Trinity Biomedical Sciences Institute, Trinity College Dublin, 152-160 Pearse Street, Dublin 2, Ireland

^jSchool of Dental Science, Trinity College Dublin, Lincoln Place, Dublin 2, Ireland

^kDepartment of Experimental Medicine, University of Perugia, P.le Gambuli, I-06132 Perugia, Italy

^lDepartment of Pharmacy, University of Napoli Federico II, DoE Department of Excellence 2018-2022, Via D. Montesano 49, 80131 Napoli, Italy

KEYWORDS. Apoptosis, antitumor agents, microtubule-targeting agent, tubulin, X-ray crystallography, molecular modeling.

Corresponding Authors:

*Stefania Butini, Tel. +390577234161, email: butini3@unisi.it

**Giuseppe Campiani, Tel. +390577234172, email: campiani@unisi.it

Abstract

Microtubule-targeting agents (MTAs) are a class of clinically successful anti-cancer drugs. The emergence of multidrug resistance to MTAs imposes the need for developing new MTAs endowed with diverse mechanistic properties. Benzoxazepines were recently identified as a novel class of MTAs. These anticancer agents were thoroughly characterized for their antitumor activity, although, their exact mechanism of action remained elusive. Combining chemical, biochemical, cellular, bioinformatics and structural efforts we developed improved pyrrolonaphthoxazepines antitumor agents and their mode of action at the molecular level was elucidated. Compound **6j**, one of the most potent analogues, was confirmed by X-ray as a colchicine-site MTA. A comprehensive structural investigation was performed for a complete elucidation of the structure-activity relationships. Selected pyrrolonaphthoxazepines were evaluated for their effects on cell cycle, apoptosis and differentiation in a variety of cancer cells, including multidrug resistant cell lines. Our results define compound **6j** as a potentially useful optimized hit for the development of effective compounds for treating drug-resistant tumors.

1. Introduction

Microtubules (MTs) are the principal component of the cell cytoskeleton involved in a variety of crucial cell processes in eukaryotes such as growth, proliferation, trafficking, motility and autophagy [1-3]. In particular, MTs are found in mammalian cells and are involved in two different mitosis phases: interphase and division [1]. MTs consist of $\alpha\beta$ -tubulin heterodimers that polymerize in a polarized way by a nucleation-elongation mechanism adding non-covalently dimers at the ends of MTs and forming hollow tubes. The terminal parts of the MT (denoted the plus- and minus-end) are continuously alternating between elongation and shortening periods - a property denoted dynamic instability [4] and which is highly regulated by accessory proteins in cells. It is well-known that cancer cells display an altered mitosis rate. Therefore, interfering with MT dynamics by microtubule-targeting agents (MTAs), represents one of the most important targets in cancer therapy [5]. MTAs can display different interaction sites on both α - and β -tubulin [6, 7]. The most well-characterized sites include: i) the well-known taxane site, targeted by compounds such as taxol (**1**), located on β -tubulin in a profound hydrophobic cleft; ii) the site targeted by laulimalide (**2**) that binds to β -tubulin in a different pocket from the taxane site; iii) the vinca site located at the plus-end edge near the GTP binding site of β -tubulin, targeted by compounds such as vinblastine (**3**); and iv) the colchicine site situated at the tubulin intradimer interface between the α - and β -tubulin subunit and targeted by MTAs such as colchicine (**4**) and nocodazole (Figure 1) [8]. Additional very well characterized sites are the maytansine site [9] and the pironetin site [10]. The colchicine site is one of the most important binding pockets for MTAs and compounds acting on this site (nocodazole, **5**) are well-known microtubule-destabilizing agents (MDAs).

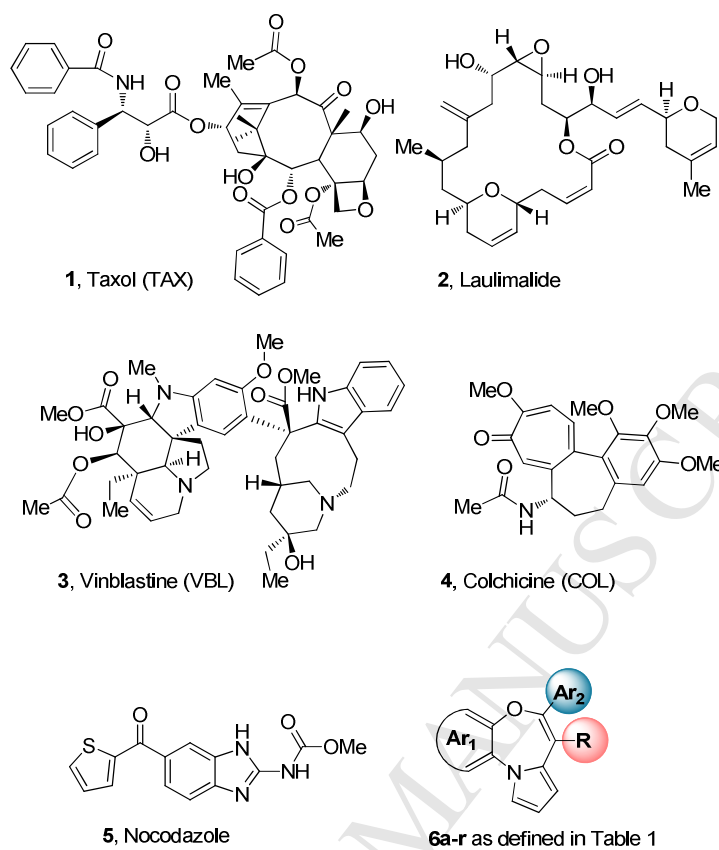


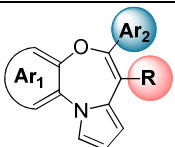
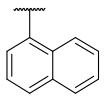
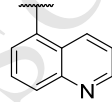
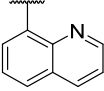
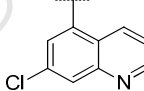
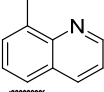
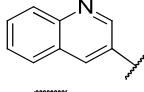
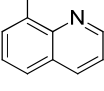
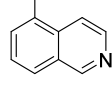
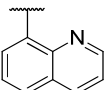
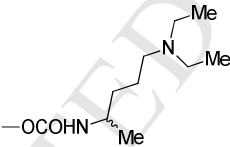
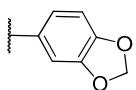
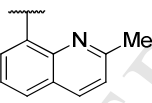
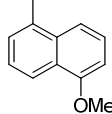
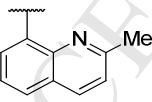
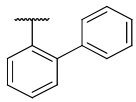
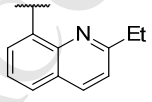
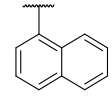
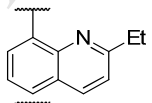
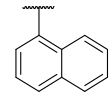
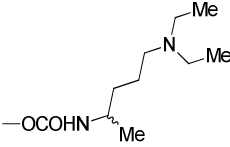
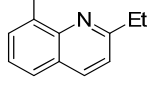
Figure 1. Representative MTAs (**1-5**) and general structure of title compounds **6a-r**.

Alteration of MT dynamics can lead to cell cycle arrest and consequently to cell death by apoptosis in dividing cells. Additionally, the capability of MTAs to interact with the autophagy process, could suggest an additional therapeutic benefit by blocking or stimulating the process. Part of the cytotoxic effect of compound **1**, indeed, comprises the capability of blocking autophagosome maturation [11], while the other MTAs such as **3** and **4** are able to stimulate autophagy. This latter mechanism could contribute to their anticancer activity [12-15]. Following our interest in the field [16-18], in this scenario, pyrrolo-1,5-benzoxazepines, typified by the 4-acetoxy-5-(1-naphthyl) naphtho[2,3-*b*]pyrrolo[2,1-*d*][1,4]oxazepine (**PNOX**, Table 1) and analogues were developed as MDAs and were thoroughly characterized assessing their antitumor

activity. In particular, compound **PNOX** and related analogues were shown to inhibit the growth of a number of cancer cell lines such as ovarian carcinoma cell lines, oral squamous carcinoma cells, acute lymphoblastic leukemia cells, neuroblastoma cells, human colon cancer cells, malignant hematopoietic cells, breast tumor cells, prostate cancer cells, embryo cell lines and other myeloma and leukemia cells [17, 19-26]. With the aim of further improving the class of benzoxazepine anticancers (antitumor potency and drug-like properties) and to fully elucidate their mechanism of action, we extended our studies by further decorating and/or modifying the original scaffold at different levels [27]. In particular, taking into account the high lipophilicity of the early developed analogues, typified by **PNOX** (cocrystallization/soaking of **PNOX** and related molecules with tubulin was unsuccessful), we attempted to attenuate lipophilicity by introducing specific structural modifications such as polar groups and/or heteroatoms. We herein present a multidisciplinary approach to the discovery of novel naphthoxazepine analogues with improved physicochemical properties, and a crystallographic study to unveil the binding site and mode of action on tubulin and microtubules of the novel analogues is discussed. A set of pyrrolonaphth(benz)oxazepine (**PNOX**) was synthesized (**6a-r**, Table 1) and appropriate biochemical studies were undertaken for establishing the affinity of selected analogues on isolated tubulin. The effects of the novel compounds were also evaluated against a relevant panel of different types of cancer cells including MDR cell lines. Finally, we carried out studies to assess the influence of the newly developed derivatives on the cell cycle, apoptosis and differentiation and to establish their effect on the autophagy process. These studies provided essential insight into the mechanism of action of the new benzoxazepines and useful hints for the future design of improved analogues. A SAR study is discussed. This work identified compound

6j as the most promising anticancer agent of the whole series, potentially useful as a novel interesting hit for the development of effective compounds for treating drug-resistant tumors.

Table 1. Novel **PNOX** derivatives **6a-r**.

							
Cpd	Ar ₁	Ar ₂	R	Cpd	Ar ₁	Ar ₂	R
PNOX	naphtho[2,3]		OCOMe	6j	naphtho[2,3]		OCOMe
6a	naphtho[2,3]		OCOMe	6k	naphtho[2,3]		OCOMe
6b	naphtho[2,3]		OCONMe ₂	6l	naphtho[2,3]		OCOMe
6c	naphtho[2,3]		OCONEt ₂	6m	naphtho[2,3]		OCOMe
6d	naphtho[2,3]			6n	naphtho[2,3]		OCOMe
6e	naphtho[2,3]		OCOMe	6o	naphtho[2,3]		OCOMe
6f	naphtho[2,3]		OCONEt ₂	6p	benzo		OCOMe
6g	naphtho[2,3]		OCOMe	6q	naphtho[2,3]		NHCOMe
6h	naphtho[2,3]		OCONMe ₂	6r	naphtho[2,3]		
6i	naphtho[2,3]		OCONEt ₂				

2. Results and Discussion

2.1 Chemistry

The general retrosynthetic scheme for the synthesis of novel compounds **6a-r** is described in Figure 2. As represented, the synthesis of the key pyrrolobenzoxazepinone template could derive from an alkylation reaction between pyrrolylphenol derivatives (**8**) and the suitable α -bromo esters (**9a-e**) providing the arylalkyl ether skeleton to undergo intramolecular cyclization generating key ketones **7**.

Due to the lengthy and often problematic synthesis of α -bromobenzyl derivatives and in order to identify a more general and expedite chemical route to target compounds, we subsequently envisioned a novel straightforward Mitsunobu-based route for the construction of the key arylalkyl ether template. Accordingly, a glyoxylate intermediate could represent a convenient access to the required α -hydroxyester derivatives (**10a-g**) to undergo Mitsunobu reaction with the pyrrolylphenol derivatives (**8**). This revised path also provided a 3-step shorter route to the desired pyrrolobenzoxazepinone template **7**. In Figure 2 we also reported the fragments engaged for the construction of the key cyclic ketone **7** sub-grouped according to the employed route.

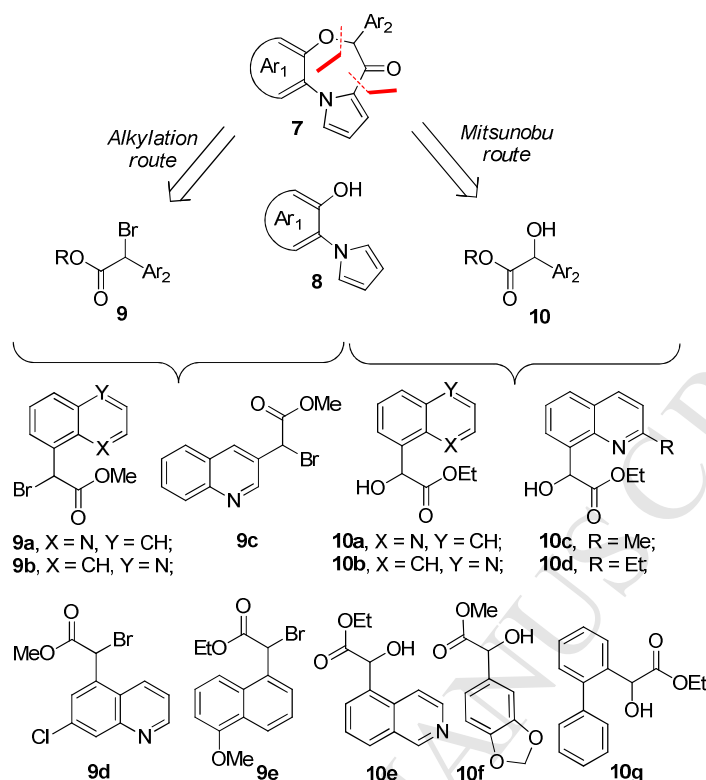
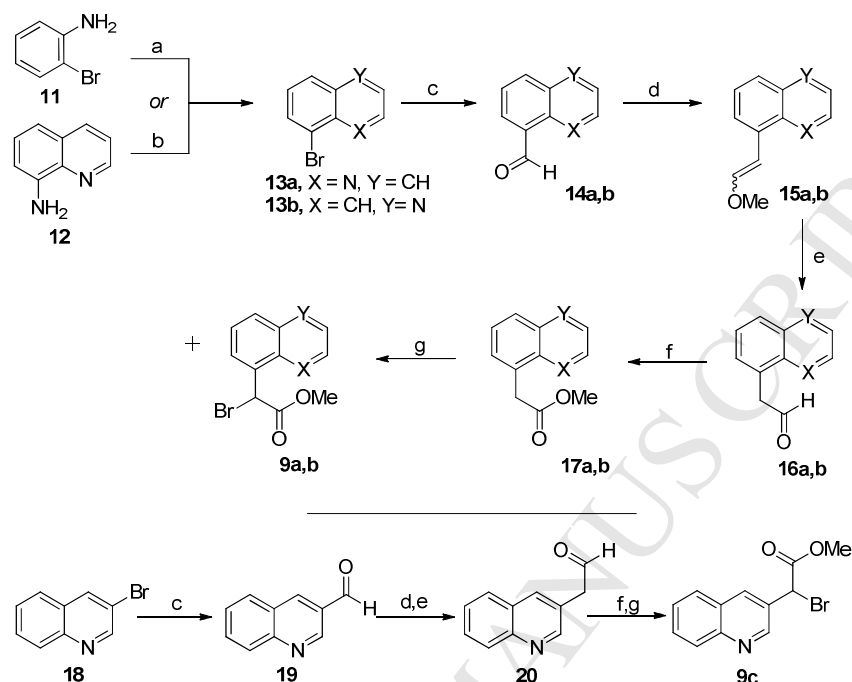


Figure 2. Retrosynthetic pathways for the construction of the pyrrolobenzoxazepinone core **7** and representation of α -bromoester derivatives **9a-e** and α -hydroxyesters **10a-g**.

In Scheme 1 is reported the synthetic route for the construction of the quinoline-based α -bromoderivatives **9a-c** bearing an 8-, 5- and 3-quinolyl aromatic portion, respectively. In a first instance, 8-bromoquinoline **13a** was obtained by Skraup reaction on 2-bromoaniline **11** in the presence of glycerol, nitrobenzene and Fe(II) sulfate under strongly acidic conditions. Due to the poor yields provided by this method, a second route was envisaged, employing 8-aminoquinoline **12**, Cu(II) bromide and *tert*-butyl nitrite [28]. 8-Bromoquinoline **13a** and the commercially available 5-bromoquinoline **13b** were reacted with *N,N*-dimethylformamide (DMF) in the presence of *n*-butyllithium at $-78\text{ }^{\circ}\text{C}$ providing the corresponding formyl derivatives **14a,b**. Subsequently, aldehyde homologation was performed by reacting intermediates **14a,b** with (methoxymethyl)triphenylphosphonium chloride in the presence of sodium

bis(trimethylsilyl)amide as the base. The resulting enol ethers **15a,b** were effectively cleaved in acidic medium providing the homologated aldehydes **16a,b** [29]. Oxidation with *N*-iodosuccinimide (NIS), in the presence of potassium carbonate and methanol [30], led to the corresponding methyl esters **17a,b**, which underwent radicalic bromination in the presence of *N*-bromosuccinimide (NBS), thus providing the desired bromo-derivatives **9a,b**.

The chemical route employed for the synthesis of compound **9c** entirely traced that adopted for the synthesis of compounds **9a,b**. Accordingly, formylation of the bromoderivative **18** followed by homologation of the resulting aldehyde **19** provided the corresponding enol ether finally hydrolyzed to the corresponding homologated aldehyde **20**. The oxidation of this latter to methyl ester, followed by radicalic bromination, led to intermediate compound **9c**.

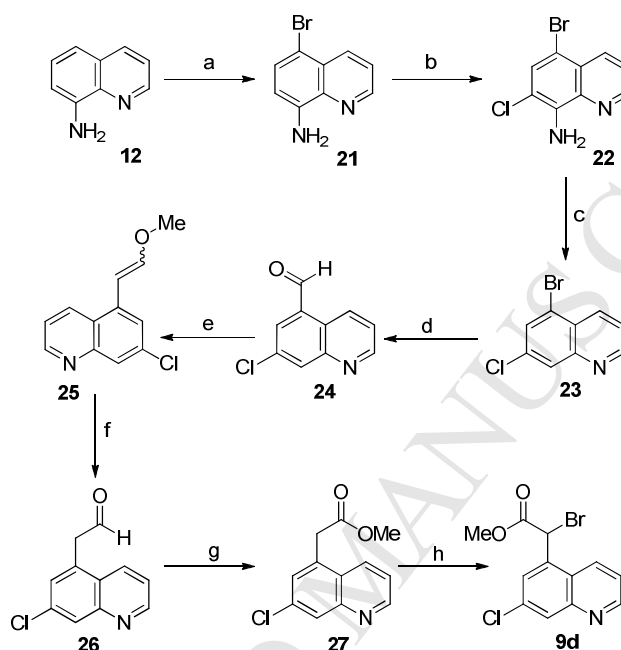
Scheme 1. Synthesis of α -bromoester derivatives **9a-c**.^a

^aReagents and conditions: (a) Glycerol, PhNO₂, FeSO₄·7H₂O, conc. H₂SO₄, 150 °C, 7 h; (b) CuBr₂, *t*BuONO, dry MeCN, 75 °C, 12 h; (c) *n*BuLi (2.5 M solution in *n*-hexane), DMF, dry THF, -78 °C, 10 min; (d) (methoxymethyl)triphenylphosphonium chloride, NaN(TMS)₂, dry THF, 0 °C, 2 h; (e) 6 N HCl, acetone, 50 °C, 3 h; (f) NIS, K₂CO₃, MeOH, rt, 3 h; (g) NBS, AIBN, CCl₄, 85 °C, 12 h.

The synthesis of compound **9d** is reported in Scheme 2. 8-Aminoquinoline **12** was brominated at 5-position with NBS in acetonitrile providing intermediate **21**. This latter was reacted with *N*-chlorosuccinimide (NCS) to afford 5-bromo-7-chloro-8-aminoquinoline derivative **22**. Reductive deamination in the presence of sodium nitrite and hypophosphorous acid provided 5-bromo-7-chloroquinoline **23** [31]. Conversion of **23** into the corresponding aldehyde derivative **24** was achieved by treatment with DMF in the presence of *n*-buthyllithium. The following steps for the synthesis of compound **9d** entirely traced those reported in Scheme 1 for the synthesis of compounds **9a-c**. Accordingly, formation of enol ether **25** was followed by hydrolysis to the

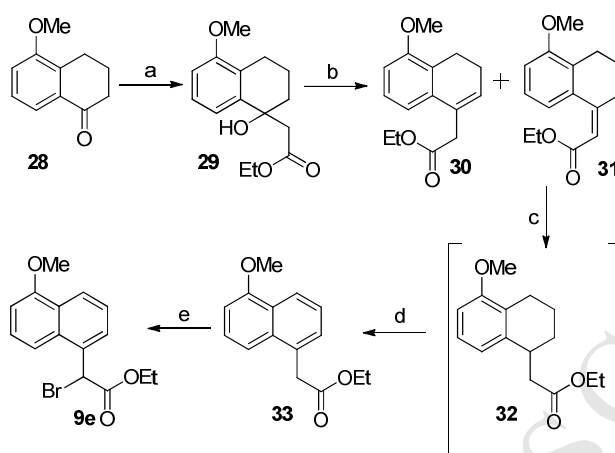
corresponding homologated aldehyde **26**. Oxidation of this latter to methyl ester **27** followed by radicalic bromination led to bromo-derivative **9d**.

Scheme 2. Synthesis of α -bromoester derivative **9d**.^a



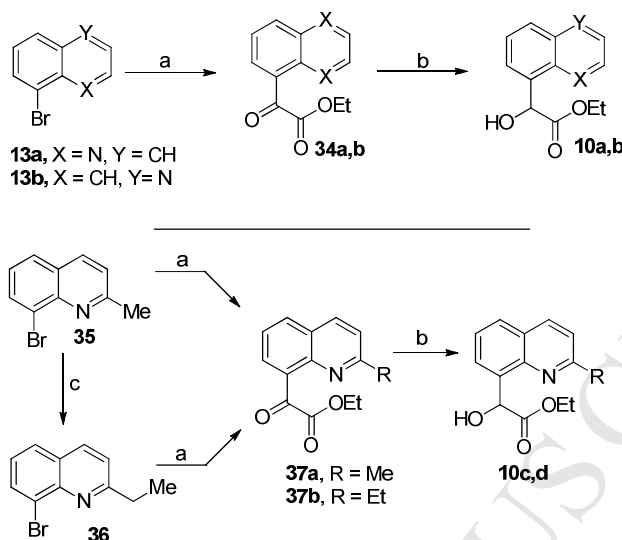
^aReagents and conditions: (a) NBS, MeCN, 25 °C, 1 h; (b) NCS, MeCN, 75 °C, 12 h; (c) H₃PO₂, NaNO₂, conc.H₂SO₄, water, from 25 °C to 60 °C, 3 h; (d) *n*-BuLi (2.5 M solution in *n*-hexane), dry DMF, dry THF, -78 °C, 15 min; (e) (methoxymethyl)triphenylphosphonium chloride, NaN(TMS)₂, dry THF, 0 °C, 3 h; (f) 6 N HCl, acetone, 25 °C, 4 h; (g) NIS, K₂CO₃, MeOH, 25 °C, 3 h; (h) NBS, AIBN, CCl₄, 85 °C, 8 h.

Compound **9e** was synthesized as reported in Scheme 3. 5-Methoxytetralone **28** was treated with dry ethyl acetate in the presence of lithium *bis*(trimethylsilyl)amide. The resulting β -hydroxyester **29** was dehydrated in the presence of trifluoroacetic acid providing a mixture of regioisomers **30** and **31**, both submitted to catalytic hydrogenation, employing cyclohexene as hydrogen source to afford intermediate **32**, immediately submitted to oxidation with DDQ in order to provide the corresponding aromatic derivative **33** [32]. Radicalic bromination with NBS led to bromo-derivative **9e**.

Scheme 3. Synthesis of α -bromoester derivative **9e**.^a

^aReagents and conditions: (a) $\text{LiN}(\text{TMS})_2$, dry EtOAc, dry THF, from -78°C to -70°C , 1 h; (b) toluene, TFA, 110°C , 3 h; (c) cyclohexene, 1,4-dioxane, 10% Pd/C, 101°C , 12 h; (d) toluene, DDQ, 110°C , 3 h; (e) NBS, AIBN, CCl_4 , 80°C , 12 h.

The synthesis of α -hydroxyesters **10a-d** is reported in Scheme 4. Bromoquinolines **13a,b** were converted into their corresponding ethyl glyoxylates derivatives **34a,b** by treatment with diethyl oxalate in the presence of *n*-butyllithium [33]. Selective reduction of the ketone functionality was achieved by reaction with sodium borohydride in dry THF, providing α -hydroxyester derivatives **10a,b**. The synthesis of compounds **10c,d** bearing 2-alkyl substituted quinoline rings started from 8-bromo-2-methylquinoline **35** prepared from 2-bromoaniline and crotonaldehyde as previously reported [34]. 8-Bromo-2-ethylquinoline **36** was derived from **35** by treatment with methyl iodide after deprotonation with lithium diisopropylamide (LDA). Both bromoquinoline derivatives **35** and **36** were reacted with diethyl oxalate in the presence of *n*-butyllithium providing glyoxalyl derivatives **37a,b**. Reduction of the ketone functionality in the presence of sodium borohydride led to the corresponding alcohols **10c,d**.

Scheme 4. Synthesis of α -hydroxyesters **10a-d**.^a

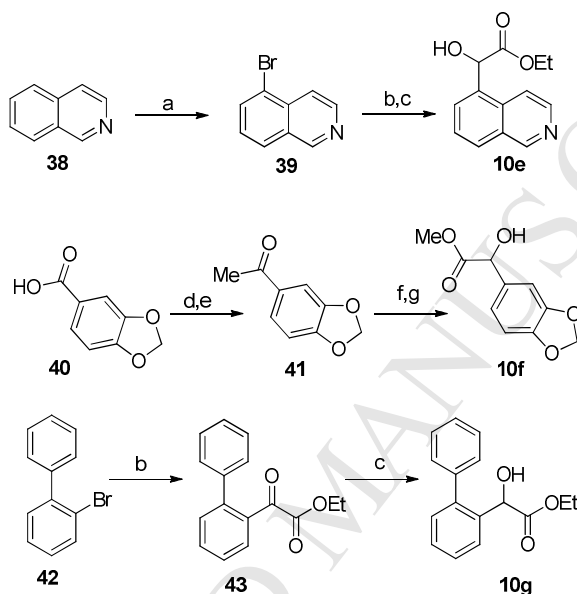
^aReagents and conditions: a) *n*BuLi, (2.5 M solution in *n*-hexane), diethyl oxalate, dry THF, -78 °C, 10 min; b) NaBH₄, dry THF, 25 °C, 30 min; (c) LDA, MeI, dry THF, from -78 °C to 0 °C, 5 h.

The synthesis of compounds **10e-g** is described in Scheme 5. Isoquinoline **38** was brominated at C-5 by treatment with NBS in the presence of sulfuric acid providing bromoderivative **39** [35]. Reaction with diethyl oxalate in the presence of *n*-butyllithium followed by reduction in the presence of sodium borohydride led to alcohol **10e**.

The synthesis of compound **10f** started from piperonylic acid **40** which was converted into the corresponding Weinreb amide that was reacted with methylmagnesium bromide in dry tetrahydrofuran readily providing the desired methyl ketone **41**. This latter compound was then submitted to intramolecular Cannizzaro reaction performed with selenium dioxide in the presence of Amberlyst A-26 in a dioxane/water mixture providing the α -hydroxyacid derivative [36], immediately converted to the corresponding methyl ester **10f** with methyl iodide in the presence of potassium carbonate.

The biphenyl derivative **10g** was prepared starting from bromoderivative **42**. This latter compound was converted into its glyoxylate derivative **43** and to alcohol **10g** as previously described.

Scheme 5. Synthesis of α -hydroxyesters **10e-g**.^a

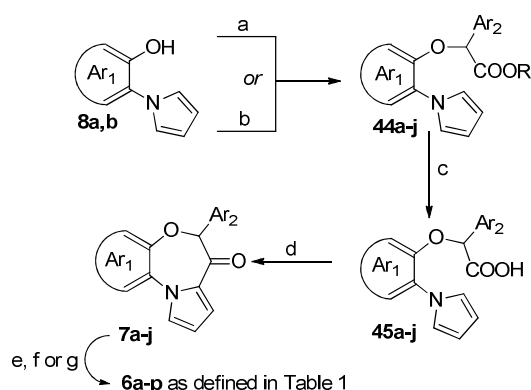


^aReagents and conditions: (a) NBS, H₂SO₄, from -25 °C to 25 °C, 24 h (b) *n*-BuLi (2.5 M in *n*-hexane), diethyl oxalate, dry THF, -78 °C, 10 min; (c) NaBH₄, dry THF, 25 °C, 4 h; (d) *N,O*-dimethylhydroxylamine hydrochloride, EDCI, HOBT, DIPEA, dry dichloromethane (DCM), 0 °C, 12 h; (e) MeMgBr (3 M solution in THF), dry THF, 1 h, 0 °C; (f) SeO₂, Amberlyst A-26, dioxane, water, 24 h, 90 °C; (g) MeI, K₂CO₃, dry DMF, 25 °C, 3 h.

The synthesis of final compounds **6a-p** is reported in Scheme 6. Arylpyrroles **8a,b** were submitted to alkylation or Mitsunobu reaction according to the availability of α -bromo- or α -hydroxyester derivatives providing aryl-alkyl ethers **44a-j**. Key compounds **6a** and **6j** were synthesized employing both the original alkylation route and then the shorter Mitsunobu route, in order to scale up molecules for further biological assays. Subsequently, alkaline hydrolysis with aqueous sodium hydroxide afforded carboxylic acid derivatives **45a-j**. These latter intermediates were submitted to intramolecular Friedel-Crafts reaction in the presence of phosphorous

pentachloride providing key cyclic ketones **7a,j**. Final compound **6a** was obtained by adding acetyl chloride to the potassium enolate deriving by treatment of the cyclic ketone **7a** with potassium *tert*-butoxide. Carbamate-containing compounds **6b** and **6c** were obtained by treatment of the same potassium enolate with dimethylcarbamoyl chloride and diethylcarbamoyl chloride, respectively. Compound **6d** was obtained by reacting the potassium enolate of ketone **7a** with *N*¹,*N*¹-diethylpentane-1,4-diamine and triphosgene in the presence of *N,N*-DIPEA. Compounds **6e-i** were also obtained by enolization of suitable ketones **7f,g** employing potassium *tert*-butoxide and following reactions with acetyl chloride, dimethyl- or diethylcarbamoyl chloride.

In the case of the cyclic ketone **7b**, bearing the 5-substituted quinolyl moiety, the enolization in the presence of potassium *tert*-butoxide led to complete decomposition of the ketone. Therefore, after a series of attempts, the use of sodium *bis*(trimethylsilyl)amide at -78 °C was identified as the best condition to efficiently form the enolate, subsequently reacted with acetyl chloride providing final compound **6j**. The same enolization protocol was also successfully applied to final compounds **6k-p**.

Scheme 6. Synthesis of final compounds **6a-p**.^a

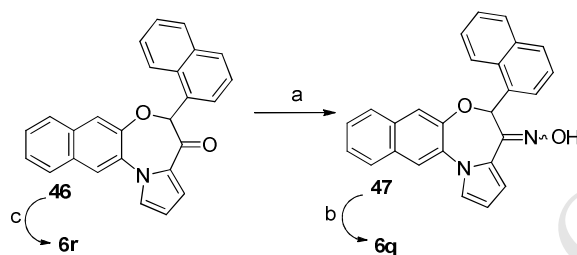
Cpd	Ar ₁	Ar ₂	R	Cpd	Ar ₁	Ar ₂	R
44a	naphtho[2,3]		Me	44f	naphtho[2,3]		Et
44b	naphtho[2,3]		Me	44g	naphtho[2,3]		Et
44c	naphtho[2,3]		Me	44h	naphtho[2,3]		Et
44d	naphtho[2,3]		Me	44i	naphtho[2,3]		Me
44e	naphtho[2,3]		Et	44j	benzo		Et

^aReagents and conditions: (a) K₂CO₃, 18-crown-6, dry DMF, 90 °C, 12 h for **44a-e**; (b) PPh₃, DIAD, dry DCM, from 0 °C to 25 °C, 24 h for **44a,b** and **44f-j**; (c) 5% NaOH_{aq}, THF, MeOH, rt, 2 h for **45 a-c, e-h,j**, 0.25 N LiOH, MeCN, 25 °C for **45d,i**; (d) PCl₅, dry DCM, 40 °C, 12 h; (e) KO^tBu, acetyl chloride, dry THF, rt, 8 h for **6a,e,g** or NaN(TMS)₂, acetyl chloride, dry THF, -78 °C, 4 h for **6j-p**; (f) KO^tBu, dimethylcarbamoyl chloride, dry THF, rt, 8 h, for **6b,h** or KO^tBu, diethylcarbamoyl chloride, dry THF, rt, 8 h, for **6c,f,i**; (g) KO^tBu, triphosgene, N¹,N¹-diethylpentane-1,4-diamine, N,N-DIPEA, 25 °C, 14 h, for **6d**.

The preparation of compounds **6q,r** is reported in Scheme 7. Ketone **46** [37] was converted into the corresponding oxime **47** by treatment with hydroxylamine hydrochloride in the presence of pyridine. Conversion to the corresponding enamide-containing compound **6q** was performed with acetic anhydride in the presence of sodium bisulfite [38]. Ketone **46** was also treated with

potassium hydride, and the corresponding potassium enolate was reacted with triphosgene and *N,N*-diethylbutan-1,3-diamine, finally providing final compound **6r**.

Scheme 7. Synthesis of compounds **6q,r**.^a



^aReagents and conditions: (a) $\text{NH}_2\text{OH}\cdot\text{HCl}$, piridine, dry MeOH, 120 °C, 12 h; (b) Ac_2O , NaHSO_3 , CuI, 1,2-DCE, 120 °C, 12 h; (c) KH (30% suspension in mineral oil), triphosgene, *N,N'*-diethylpentane-1,4-diamine, *N,N*-DIPEA, dry THF, 25 °C, 12 h.

Solubility for **6j** and **PNOX** was experimentally measured. *In silico* we determined the solubility values of a series of MTAs. Calculations performed by QikProp (QikProp, version 4.3, Schrödinger, LLC, New York, NY, 2015) highlighted the improved solubility of **6j** (-6.272 mol/dm^3) over **PNOX** (-6.814 mol/dm^3) and other well-known drugs such as tivantinib (-6.277 mol/dm^3), DJ-101 (-6.685 mol/dm^3) and lexibulin (-6.499 mol/dm^3). On the other hand, experimental data from literature and calculated solubility of **6j** proved to be lower than combretastatin (calculated -4.517 mol/dm^3) and colchicine (**4**) (calculated -4.961 mol/dm^3 , experimental 7 mg/mL).

The water solubility of **6j** and **PNOX** were experimentally determined also by HPLC analysis [39]. HPLC experiments demonstrated that the introduction of a specific structural modification has improved water solubility of **6j** over PNOX (solubility at pH = 7.4 was 26.04 μM for **PNOX**, and 458.26 μM for **6j** (0.2 mg/mL), see Table S1), being similar to those reported for nocodazole ($< 1 \text{ mg/mL}$) and tivantinib ($< 1 \text{ mg/mL}$).

2.2 Biological investigation.

2.2.1 Cell based assays in HL-60 and GIST-T1 cells

As a preliminary approach to determine the potential of the newly synthesized derivatives we performed a screening on the HL-60 cell line to determine the cell viability following treatment (Table 2). This preliminary investigation was performed on a small set of quinolyl-derivatives (**6a-c,j,l**) and also ketone intermediates **7a,b** were included. Cell viability was assessed using an AlamarBlue cell viability assay (cells were seeded at 4000/well in a 96-well plate and cell viability measured after 72 h of drug treatment). This test highlighted an exceptional potency for some of the tested compounds which exhibited very promising IC_{50} values in the high nanomolar range (**6a**, IC_{50} = 262.7 nM; **6b**, IC_{50} = 299.5 nM; **6j**, IC_{50} = 294.5 nM).

Table 2. Viability tests as IC_{50} (μ M) values for a panel of compounds tested in HL-60 cells.

Cmpd	HL-60
	IC_{50} (μ M)
6a	0.2627
6b	0.2995
6c	4.582
6j	0.2945
6l	6.462
7a	1.075
7b	2.767

HL-60 cells (300,000 cells/ml) were seeded into 96-well plates and were treated in triplicate with vehicle (0.1% (v/v) DMSO) or the indicated compounds for 72 h. The cells were then incubated in 10% (v/v) AlamarBlue™ and its reduction to a fluorescent state measured at excitation 544 nm and emission 590 nm using a multi-well fluorimeter. IC_{50} values are the mean of at least three separate determinations. Standard errors were all within 10% of the mean.

Based on these data we sought to explore the efficacy of the best performing analogues in inhibiting the survival of the gastrointestinal stromal tumor cell line GIST-T1. The results indicated that the compounds were active in inhibiting cell viability even at 1 μ M. Viability was further inhibited by applying a concentration of an order of magnitude higher (Figure 3).

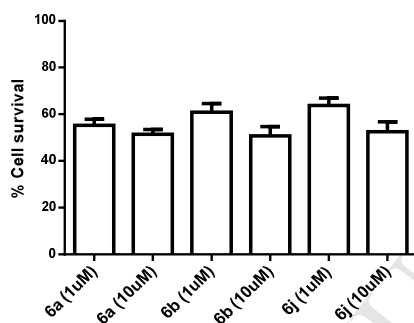


Figure 3. Percentage of cell viability in a gastrointestinal stromal tumor cell line (GIST-T1) treated with **6a**, **6b** and **6j** each tested at both 1 μ M and 10 μ M. Viability was assessed using an AlamarBlue cell viability assay cells were seeded at 4000/well in a 96-well plate and cell viability was measured after 48 h of drug treatment. Data represents mean \pm the S.E.M of three biological replicates.

This preliminary investigation prompted us to expand the structure-activity relationships at both the C4 and C5 of the pyrrolonaphthoxazepine nucleus, to systematically interrogate the ability of our compounds to interfere with cell cycle progression and to evaluate the potential pro-apoptotic effect in HL-60 cells. Thus, intranucleosomal DNA fragmentation was determined by flow cytometry [40] on HL-60 cells treated with a 10 μ M concentration of the new derivatives in comparison with **PNOX** (Figure 4A). The results show that most compounds induced a significant enhancement in the percentage of apoptotic cells (with hypodiploid or “sub- G_0/G_1 ” DNA content) compared to vehicle. Flow cytometric analysis of cell cycle progression also determined that the pro-apoptotic effects of the new compounds correlate with

the blockage of the cell cycle in the G2M phase (Figure 4B), further suggesting that compounds-induced apoptosis is secondary to cell cycle arrest.

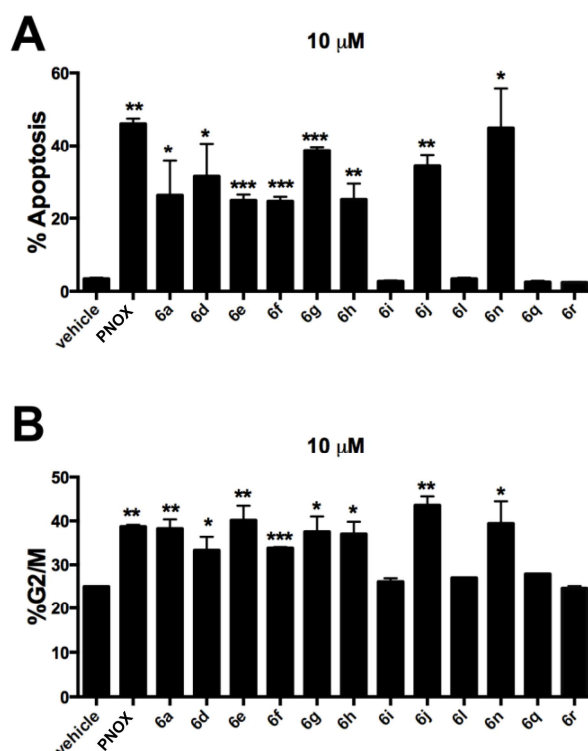


Figure 4. Effect of compounds **PNOX**, **6a**, **6d-j**, **6l,n,q,r** on apoptosis in HL-60 cells. Cells were treated with 10 μ M of title compounds for 24 h and DNA content was measured by flow cytometry. Control samples were treated with vehicle (0.1% DMSO). The bar graphs show the percentage of cells in the sub-G₀/G₁ peak (% apoptosis) (A) and the percentage of cells in the G2M phase (B). Data are mean \pm SD (n > 3), *p < 0.05, **p < 0.01, ***p < 0.001 vs vehicle.

From these preliminary tests we found that the improvement of the water solubility was achieved while leaving unaltered or even improving the pro-apoptotic potential of the new analogues.

2.2.2 Effect of selected compounds on tubulin polymerization.

The effect of the selected compounds (**PNOX** and **6a,d,f,g,h,j,m,n**) on tubulin polymerization was monitored by performing turbidity time course experiments to monitor absorbance at 350 nm (Figures 5-7 and Table 3). Since microtubules are large structures, their formation is reflected in turbidity of the solution, allowing to follow the assembly reaction [41].

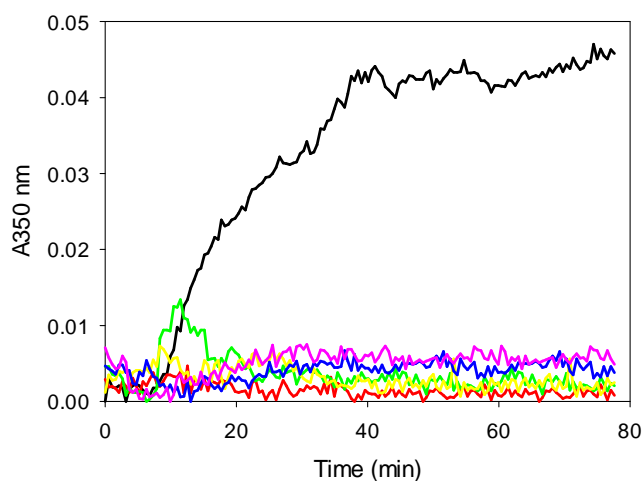


Figure 5. Turbidity time course for the assembly of 25 μM tubulin at 37 $^{\circ}\text{C}$ in the presence of 27.5 μM of the compounds followed at 350 nm. Black line (DMSO, vehicle), red line (**PNOX**), blue line (**6a**), green line (**6e**), pink line (**6g**), yellow line (**6j**).

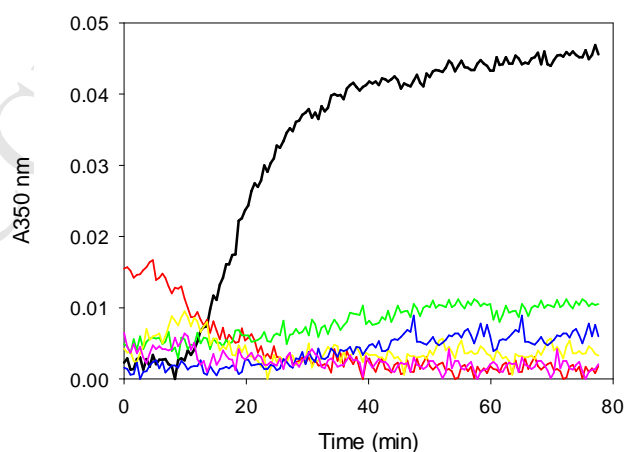


Figure 6. Turbidity time course for the assembly of 25 μM tubulin at 37 $^{\circ}\text{C}$ in the presence of 27.5 μM of the compounds followed at 350 nm. Black line (DMSO, vehicle), green line (**6d**), yellow line (**6f**), pink line (**6h**), red line (**6m**), blue line (**6n**).

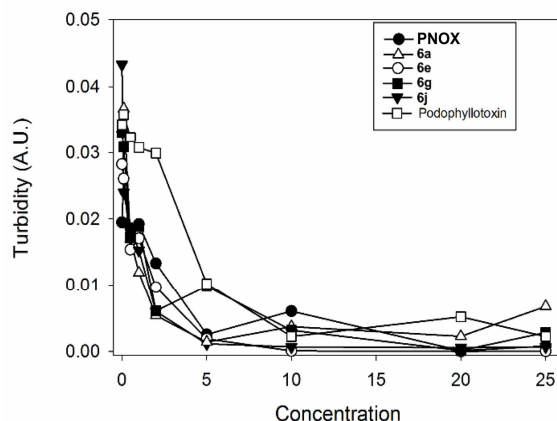


Figure 7. Stoichiometry of the tubulin depolymerization in the presence of compounds: **PNOX**, **6a**, **6e**, **6g**, **6j** and the reference compound podophyllotoxin.

As it can be seen (Figures 5 and 6), when added stoichiometrically all the compounds tested were able to inhibit the polymerization of pure tubulin in conditions in which the protein is able to assembly into microtubules (black lines) indicating that they directly interact with tubulin and that the interaction results in the inhibition of the polymerization capacity of the protein.

Following on, we wanted to estimate the stoichiometry needed to inhibit the assembly reaction. As shown in Figure 7, all the compounds are able to inhibit the assembly of tubulin at sub-stoichiometric ratios with tubulin in a colchicine-like manner, suggesting that they may inhibit the tubulin association by binding to the colchicine site. To support this hypothesis, we planned to determine the binding constant by competition experiments. In view of the chemical structure of the compounds it was possible to hypothesize that they would exhibit fluorescent behavior in the near UV. Accordingly, it was found that the compounds were fluorescent at 450 nm upon

excitation at 320 nm. Upon addition of an excess of tubulin, the fluorescence of the compounds increased. We then tried to use this property to determine the binding constant by a competition assay with the colchicine site MDA podophyllotoxin [42]. However, it was found that upon podophyllotoxin addition the samples became turbid. We attributed this behavior to the low solubility of the compounds in the medium, which we found to be lower than 5 μM in our test conditions. To overcome the problem, we designed a method based on analytical ultracentrifugation in which the compounds dissociated by competition with podophyllotoxin were sedimented and we could measure the amount of compound bound in the presence of podophyllotoxin at the solubility limits of the compound, which are of the order of sub- μM (see Experimental Section). From these measurements, the binding constants of the compounds could be determined (Table 3) and the binding site was confirmed to be the one of **4**, because of the competition with podophyllotoxin (Figure S1).

Table 3. Binding constants (K_b) of the compounds to dimeric tubulin calculated by AUC at 25 °C (10^7 M^{-1}).

Cpd	PNOX	6a	6d	6e	6f	6g	6h	6j	6m	6n
K_b	4.4 ± 1.5	115 ± 37	114 ± 48	4.4 ± 1.1	9 ± 5	0.3 ± 0.1	5 ± 1	7 ± 3	16 ± 4	2 ± 1

2.2.3 Structural insight into the 6j-tubulin complex

We sought to solve the **6j**-tubulin complex structure by X-ray crystallography (Figure 8A) in order to define the mode of interaction of the novel analogues at the molecular level. To this end, we soaked **6j** into a crystal formed by a protein complex composed of two $\alpha\beta$ -tubulin heterodimers (T_2), the stathmin-like protein RB3 (R) and tubulin tyrosine ligase (TTL); the complex is denoted $T_2\text{R-TTL}$ [43, 44]. Using this approach, the **6j**-tubulin structure was

determined to 2.4 Å resolution (Figures 8B and 9A; Table S2). Any attempt using **PNOX** was unsuccessful mainly due to its poor solubility.

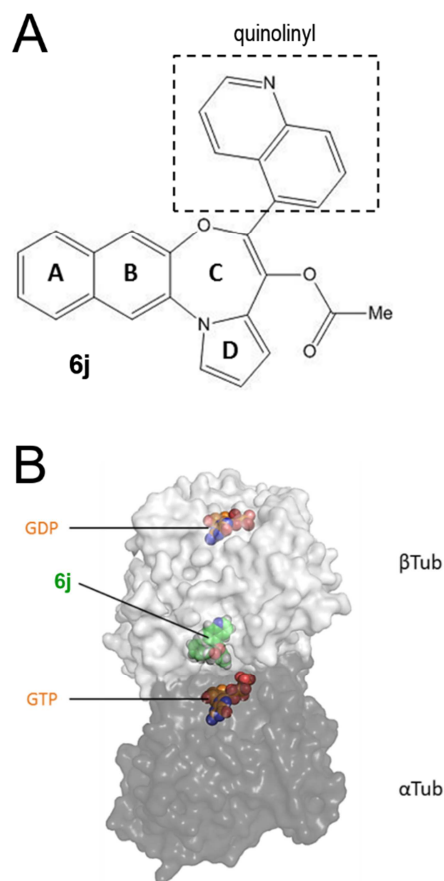


Figure 8. X-ray crystallographic studies on **6j**. (A) Chemical structure of **6j**. The A, B, C and D cycles are part of the naphtho-pyrrolo-benzoxazepine moiety. The quinolinyl moiety is highlighted by a dashed box. (B) Overall view of the X-ray crystal structure of the **6j**-tubulin complex. The α - and β -tubulin subunits are represented in dark and light gray surface representation, respectively. **6j** and the guanosine nucleotide molecules are shown in green and orange spheres representation, respectively.

6j binds to the colchicine site of tubulin, which is formed by residues of helices H7 and H8, strands S8 and S9 and loop T7 of β -tubulin and of loop T5 of α -tubulin (Figure 9A). The

superimposition of the β -tubulin chains of the free (PDB ID 4I55 [43]) and **6j**-bound tubulin structures revealed a flip of the T7 loop of β -tubulin as well as a change in the conformation of the T5 loop of α -tubulin upon ligand binding (Figure S2). These structural adaptations are necessary to accommodate the ligand in its binding site and have already been observed for other colchicine-site ligands [45, 46].

We then investigated the detailed **6j**-tubulin binding mode. The fused system, acetoxyl and quinolyl moieties of **6j** are buried into the colchicine site, making most of the hydrophobic interactions with the β -tubulin part of the dimer (Figures 8A,B). The interaction is further stabilized by a hydrogen-bond formed between the carbonyl of the acetoxyl group of **6j** and β Q247 of the T7 loop of β -tubulin, as well as a water-mediated contact between the nitrogen of the quinolyl moiety of **6j** and the main chain carbonyl of β G237 and amine groups of β T240 and β C241 from the H7 helix of β -tubulin. Moreover, the pyrrolonaphthoxazepine moiety is stacked between the sidechains of both K254 and K352 residues of β -tubulin. The NZ nitrogen of K352 is 5.7 Å distant from the center of the pyrrole ring of **6j**, suggesting that a cation- π stacking interaction can be established (Figure 9).

To compare the tubulin-binding mode of **6j** with that of **4**, we superimposed the β -tubulin chains from the **4**-tubulin (PDB ID 4O2B [45]) and **6j**-tubulin structures (RMSD chain D of **4** onto chain D of **6j** 0.29 Å over 2732 atoms; Figure 9B). We observed no functional common groups between **4** and **6j** molecules that occupy the same position in their respective binding pockets. The major differences are observed for the conformations of both the α T5 and β T7 loops. Compared to **4**, the bulky pyrrolonaphthoxazepine moiety of **6j** induces a flip of α T179 by establishing more hydrophobic contacts to the α T5-loop (Figure 9B). The conformational flip of the β T7 loop is induced by the acetoxyl moiety of **6j** by displacing the side chain of L248.

Together with L255 this residue is involved in the stabilization of the trimethoxy-substituted A ring of **4**. The hepta-membered C ring moiety of **4** superimposes with the naphthyl group of the naphthoxazepine moiety of **6j**, thereby establishing comparable hydrophobic contacts to tubulin. One common feature is a water-mediated contact between the 2-methoxy group of **4** and the main chain carbonyl group of β V238 and the main chain amine group of β C241 of β -tubulin; in the vicinity, a water-mediated contact is also formed with the nitrogen of the quinolyl moiety of **6j** (see above and Figure 9A). β A250 appears to be largely involved in hydrophobic contacts with both compounds (with pyrrole moiety of **6j** and with the hepta-membered ring and the trimethoxyphenyl moiety of **4**) (for an overall view of superposition between compounds **4** and **6j** see Figure S3).

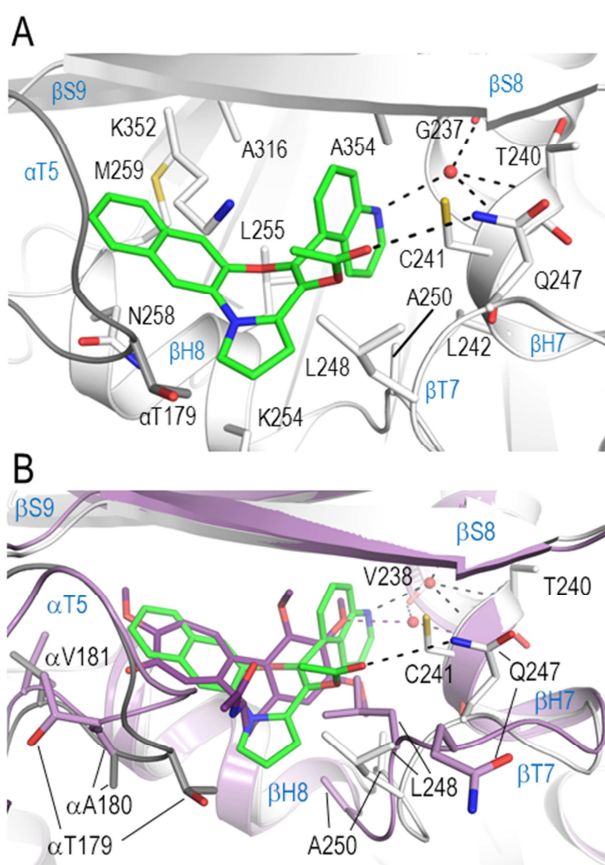


Figure 9. Detailed interactions between tubulin and **6j**. (A) Close-up view of the interaction mode between **6j** and tubulin. **6j** and interacting tubulin residues are shown in green and grey sticks representation, respectively. Tubulin secondary structural elements are labeled with blue letters. (B) Superimposition of the **6j**-tubulin (**6j** in green sticks) and **4**-tubulin (PDB ID 4O2B; **4** in violet sticks) complex structures. In both figures, oxygen, nitrogen and sulfur atoms are colored in red, blue and yellow, respectively. Hydrogen bonds are represented by black dotted lines, and the water molecules are displayed as a red sphere. Tubulin secondary structural elements are labeled with blue letters.

Together, these results define **6j** as a new tubulin colchicine binder. It is well established that colchicine-site ligands inhibit microtubule polymerization by preventing the “curved-to-straight” conformational switch accompanying tubulin assembly into microtubules [45, 46]. Inspection of the **6j** binding mode in the “curved” (T₂R-TTL) and “straight” (PDB ID 1JFF) tubulin states revealed that the ligand destabilizes microtubules by a similar mechanism (not shown).

Moreover, for providing a comprehensive analysis about the binding mode of the new compound **6j** into the colchicine binding site, in addition to the above performed analysis with the colchicine (PDB ID 4O2B), we further analyzed 40 tubulin-ligand complexes in which the ligands targeted the colchicine binding site (PDB IDs: 3DU7, 3HKC, 3HKD, 3N2G, 3N2K, 4O2A, 4YJ2, 4YJ3, 5CA0, 5CA1, 5CB4, 5C8Y, 5GON, 5H7O, 5JCB, 5JVD, 5LYJ, 5NG1, 5M7E, 5M7G, 5M8G, 5OSK, 5O7A, 5XAF, 5XAG, 5XLZ, 5XKF, 5XKG, 5XKH, 5XLT, 5YLJ, 5YLS, 5YL2, 5Z4U, 6BRF, 6BR1, 6BRY, 6BS2, 6FKL, 6FKJ). The analysis highlighted the crucial role of the hydrophobic contacts for interacting with the colchicine binding site. Accordingly, the quinoline moiety and the tricyclic portion of **6j** were overlapped by the hydrophobic portions of the examined ligands to strongly interact with the binding site. Notably,

with respect to the selected ligands, **6j** is the only compound able to target the residue β Q247 by a H-bond with its acetoxyl group. In fact, none of the other examined ligands is able to form the mentioned contact. This further investigation pointed out the novel pattern of interaction that could be useful for the rational design of ligands able to maximize the contacts into the colchicine binding site on tubulin.

2.2.4 Molecular Dynamics (MD) simulation on the **6j**-tubulin complex.

In order to assess the contribution of structural moieties to the affinity of **6j** for tubulin in the colchicine site, as well as to evaluate the stability of the binding mode found by crystallographic studies, we performed a Molecular Dynamics (MD) simulation employing Desmond software on the **6j**-tubulin complex (Figure 10). The MD study could also be able to establish the role of the water molecule in the binding mode of **6j**. For the calculation we used chains C and D from the crystal structure after appropriate preparation (see the Experimental Section for further details). During the MD simulation, after about 20 ns, the complex showed an overall stability with low Root Mean Square Deviation (RMSD) of the protein and the ligand (Figure 10A). Regarding the pattern of interaction of **6j** with tubulin, we noted that the main contacts were maintained as underlined by the dynamic analysis of the simulation interaction diagram (Figure 10B). In particular, the pyrrolobenzoxazepine moiety is involved in i) strong contacts with the α -tubulin V181 with additional hydrophobic contacts with M259, A316, and I318 of β -tubulin and ii) a strong cation- π stacking with K352 of β -tubulin. The quinoline nucleus interacts by several hydrophobic contacts with C241, L242, L248, A250, L255, A354 and I378 of β -tubulin. Hydrophobic interactions are the main contacts that govern the affinity of **6j** for the colchicine site. In fact, as reported in Figures 10C,D we noted a limited number of polar contacts, mainly water mediated, as confirmed by the crystal structure. The nitrogen of quinoline nucleus is able

to maintain the water mediated H-bonds with G237, C241 and T240 and in addition can form a water mediated H-bond with the backbone of V238. The acetyl function lacks a direct H-bonding with Q247 that becomes sporadically water mediated.

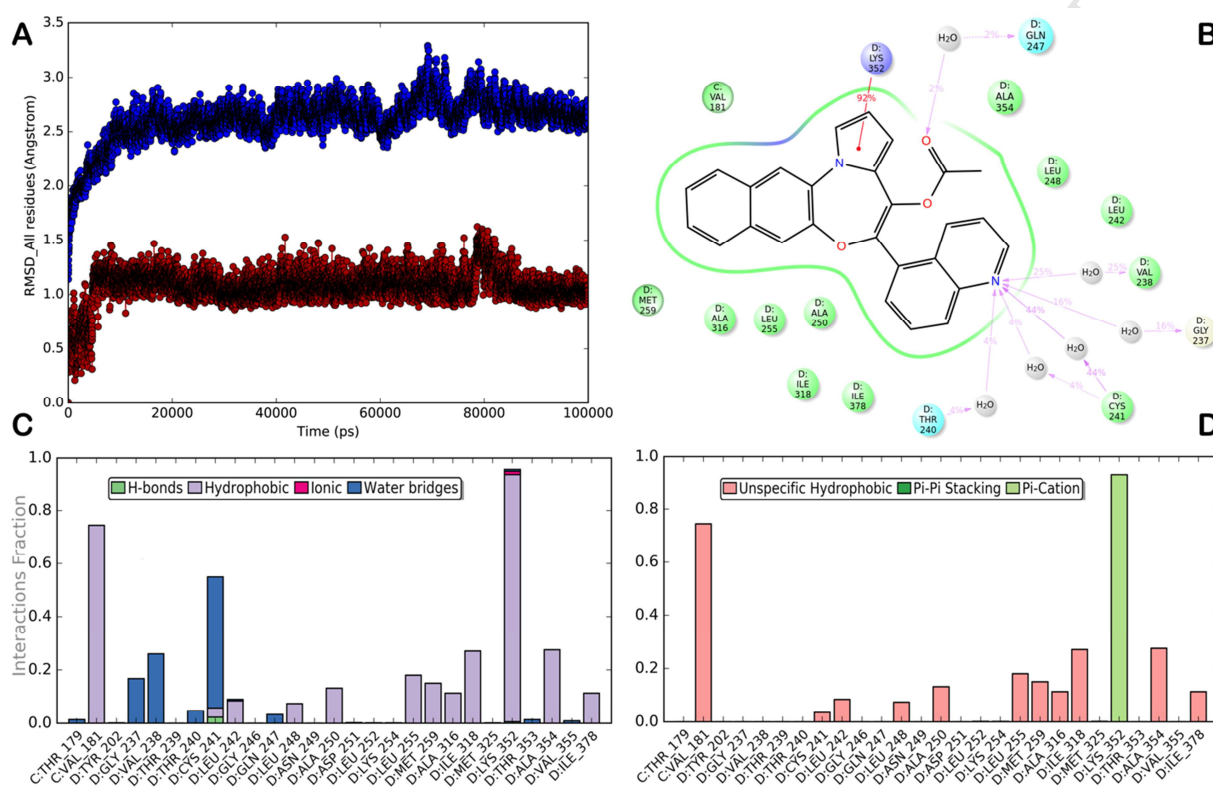


Figure 10. Molecular dynamics of **6j**-tubulin complex outputs. (A) RMSD (Root Mean Square Deviation) of the complex **6j**-tubulin (RMSD of the protein in a line formed by blue circles; RMSD of the ligand in a line formed by red circles). RMSD were calculated between the final conformation and the starting conformation through the 100 ns of the MD simulation. (B) **6j**-tubulin interactions monitored throughout the simulation. The represented water molecule interacting with G237, V238, T240 and C241 is the same, different to the water molecule interacting with Q247. (C) Protein-ligand interactions are categorized into four types: H-bonds, hydrophobic, ionic and water bridges. (D) Hydrophobic contacts of the ligand into the colchicine binding site over the course of the trajectory.

2.2.5 Structure-activity Relationship studies.

Combining the experimental data (K_b and ΔG_{bind} ; in the following discussion ΔG_{bind} values are referred to $\Delta G_{\text{bind}25^\circ\text{C}}$) and molecular docking studies, a systematic and inclusive SAR study of the synthesized compounds (**6a-r**) was performed for investigating the behavior of the developed compounds within the colchicine binding site of the β -tubulin and to explain their activity and potency. Regarding **6j**, we found that the adopted molecular docking protocol (scoring function GoldScore implemented in GOLD software) was able to correctly accommodate the ligand into the active site with low RMSD (0.45) with respect to the crystal structure (Figure S4). For **6j**, the ΔG_{bind} value confirms its strong binding to the colchicine binding site of β -tubulin ($K_b = 7 \pm 3 \times 10^7 \text{ M}^{-1}$; $\Delta G_{\text{bind}} = -10.7 \text{ kcal/mol}$). The effect of different positioning of the heterocyclic nitrogen atom was explored and, in general, with respect to the original members, an increase of binding affinity was found, although to different extents. In fact, compounds **6a** and **6m** (8-substituted quinoline and 5-substituted isoquinoline, respectively) act as low and high nanomolar tubulin binders, respectively ($K_b \text{ 6a} = 115 \pm 37 \times 10^7 \text{ M}^{-1}$; $K_b \text{ 6m} = 16 \pm 4 \times 10^7 \text{ M}^{-1}$). Notably, compound **6a** was found to be one of the most potent tubulin-binders of the series. Even though compounds **6a** and **6m** are accommodated in a similar fashion as found for **6j** (Figure 11 and Figure S5 respectively), the different position of the nitrogen atom on quinoline nucleus clearly influences their binding mode. Although **6a,m** cannot form the water mediated contacts shown by **6j**, they display a higher hydrophobic contribution which is responsible for the increased tubulin affinity especially in the case of **6a**. In fact, compound **6a** is able to maximize the hydrophobic contacts with the residues V238, L242, I318 and I378. The reported data highlights the strong binding behavior with a reduction of ΔG_{bind} ($\Delta G_{\text{bind}} \text{ 6a} = -12.4 \text{ kcal/mol}$ and $\Delta G_{\text{bind}} \text{ 6m} = -11.2 \text{ kcal/mol}$ (Table 3).

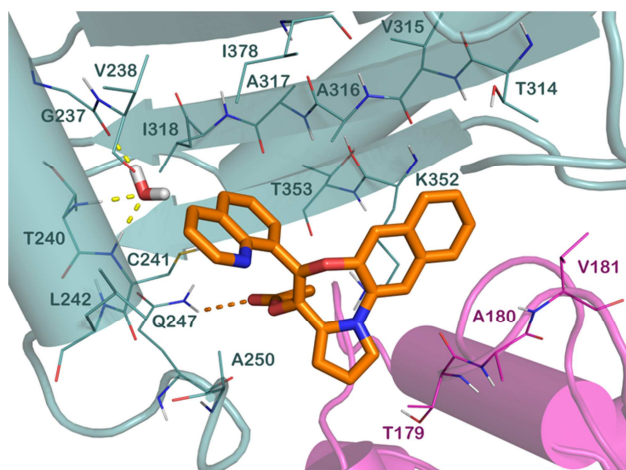


Figure 11. Complex of **6a**-tubulin (orange sticks, α -tubulin in magenta cartoon and β -tubulin in dark green cartoon) as found by means of molecular docking calculation.

In contrast, the introduction of an ethyl group on the quinoline ring of **6a** at 2-position (compound **6g** in Figure S6) significantly decreased potency against tubulin (**6g**, $K_b = 0.3 \pm 0.1 \times 10^7 \text{ M}^{-1}$; $\Delta G_{\text{bind}} = -8.8 \text{ kcal/mol}$). This could most likely be ascribed to the increment of the steric hindrance on the quinoline substituent. For this reason, the docking study on the mentioned compounds highlighted a slightly different orientation of the core of the molecules with reduced interaction with K352. This binding mode brings the oxygen atom of the carbonyl group at 3.5 \AA from the sidechain of Q247 precluding the specific polar contacts. The introduction of a Me group on the quinoline ring of **6a** at C-2 led to a compound, **6e**, with a significant binding affinity against tubulin ($K_b = 4.4 \pm 1.1 \times 10^7 \text{ M}^{-1}$). This confirms the relevant role of the hydrophobic patch at the colchicine binding site targeted by the quinoline substituted ring (Figure S7), maintaining interaction with Q247. The ΔG_{bind} of -10.4 kcal/mol also supports its high affinity for the colchicine binding site.

The introduction of more hydrophobic nuclei as in compounds **PNOX** and **6e** seems to be well tolerated, although with a slight decrease of binding affinity. This observation supports the easier

displacement of the water molecule when more hydrophobic nuclei were introduced (**PNOX** and **6e**), without a significant decrease of affinity, indicating that the water molecules should not be fundamental for the activity of the ligands based on the scaffold herein described. In fact, these compounds present comparable binding affinities to tubulin, although slightly lower, to that found for **6j**. Remarkably, the introduction of a nitrogen atom at C-5 as in **6j** led to a more soluble compound with respect to **PNOX** (hydrophobic analogue) while maintaining tubulin affinity (Figure S8 and Table 3; ΔG_{bind} **PNOX** = -10.4 kcal/mol). The introduction of a different fused ring such as benzodioxole at a different position as in **6n** (Figure S9) seems to be well tolerated, with a slight decrease of binding affinity (**6n**, $K_b = 2 \pm 1 \times 10^7 \text{ M}^{-1}$; $\Delta G_{\text{bind}} = -10.0$ kcal/mol) with respect to **6j**, while the 3-quinoline moiety of **6l** is not tolerated as confirmed by the docking calculation (Figure S10). This is due to the different interactions showed for the two compounds (**6l** and **6n**). In particular, **6n** forms water mediated H-bond as found for **6j** but the different orientation of the R_1 substituent did not allow the compound to reach an optimal accommodation to establish polar contacts with Q247, due to the fact that the oxygen from the carbonyl group was found at 3.6 Å from the Q247 side chain (Figure S9). On the contrary, **6l** with a quinolin-3-yl substituent differently oriented with respect to that of **6j**, showed a limited potency mainly due to the steric hindrance and the absence of the water mediated interactions. In particular, the different orientation of the quinoline moiety did not allow compound **6l** to establish efficient hydrophobic interactions with V238, L242, I318 and I378, the stacking with K352 and H-bonding with the Q247 side chain (carbonyl group at 3.9 Å) (Figure S10). Modification of the R_2 site (carbamates) led to a sub-series of analogues with different affinity against tubulin. The introduction of the dimethylamino group (**6h**) gave a potency similar to **PNOX** (**6h**, $K_b = 5 \pm 1 \times 10^7 \text{ M}^{-1}$; $\Delta G_{\text{bind}} = -10.5$ kcal/mol). Compound **6h** is accommodated into

the colchicine binding site in a similar fashion found for **6j** (Figure S11). The diethylamino derivative **6f** showed a potency similar to **6j** (Figure S12) (**6f**, $K_b = 9 \pm 5 \times 10^7 \text{ M}^{-1}$; $\Delta G_{\text{bind}} = -10.9 \text{ kcal/mol}$). Further, the elongation of the chain at R_2 position as in compound **6d**, bearing a urethane functionality containing a flexible lateral chain with extra protonatable nitrogen, led to one of the best compounds in term of binding affinity towards tubulin. Additionally, both enantiomers of **6d** showed a similar accommodation into the colchicine binding site, indicating the lack of a stereoselective interaction. As depicted in Figure S13, despite the flexible chain, **6d** showed a relevant number of docked solutions of both the *R*- (82%) and *S*-enantiomer (74%), with a further polar contact established between the protonated nitrogen of the flexible lateral chain and the backbone of T353 by both enantiomers. Accordingly, compound **6d** showed a $K_b = 114 \pm 48 \times 10^7 \text{ M}^{-1}$ and a ΔG_{bind} of -12.3 kcal/mol .

2.2.6 Effect of selected compounds on tumor cell lines.

A subset of the most promising analogues was characterized for their potential anticancer properties in different tumor cell lines, including both sensitive and multidrug resistant cells.

2.2.6.1 Effect on A2780 and A2780AD human ovarian carcinoma cells, NIH3T3 and P-gp overexpressing NIH-MDR-G185 cells

The effects of compounds **PNOX**, **6a**, **6d-h**, **6j**, **6l-n** on A2780 and A2780AD human ovarian carcinoma cells, mouse embryo NIH 3T3 and P-gp overexpressing NIH-MDR-G185 (3T3Col) cells was investigated. A2780 and 3T3 cells are sensitive to chemotherapy, whereas A2780AD and 3T3Col cells have acquired resistance by means of P-glycoprotein overexpression. We determined the IC_{50} values of the aforementioned compounds and compared them with those measured for **1**, **3** and **4** (Table 4).

As it can be seen all the compounds are effective in killing cancer cells in the low micro/high nanomolar ranges, which is in agreement with the binding affinities in the high nanomolar range. It should be noticed that the IC₅₀ values determined are within the solubility range of the drugs (except for **6g**, whose IC₅₀ 1 μ M is far over the determined solubility 0.064 μ M) thus the values obtained should be considered with this limitation and are probably overestimated being the actual values lower than those resulting from the assay. Interestingly all the compounds are extremely effective in the resistant cell lines, indicating that either they are poor substrates for P-glycoprotein (one of the main reasons for antitumoral drug resistance) [47] or that their affinity for tubulin is stronger than for P-glycoprotein [48].

Table 4. Cytotoxicity assessment of different compounds on the growth of two human ovarian carcinoma cell lines (A2780 and A2780AD) and two embryo cell lines (NIH 3T3 and NIH-MDR-G185).^a

Cpd	A2780 ^b	A2780AD	R/S ^c	3T3	3T3col	R/S
PNOX	249 \pm 17	240 \pm 33	0.96	126 \pm 4	306 \pm 24	2.42
6a	76 \pm 13	79 \pm 15	1.03	34 \pm 4	68 \pm 13	2
6d	1900 \pm 200	1350 \pm 50	0.71	2300 \pm 300	2500 \pm 600	1.08
6e	285 \pm 26	310 \pm 24	1.08	126 \pm 10	278 \pm 19	2.20
6f	3050 \pm 250	2250 \pm 50	0.73	4950 \pm 750	9000 \pm 100	1.81
6g	1000 \pm 0.03	950 \pm 5	0.95	540 \pm 79	790 \pm 100	1.46
6h	900 \pm 100	826.5 \pm 17	0.91	408.5 \pm 7	1051.5 \pm 148	2.57
6j	80 \pm 12	92 \pm 16	1.15	42 \pm 9	84 \pm 16	2
6m	300.75 \pm 122	810 \pm 48	2.69	375.3 \pm 1	876 \pm 144	2.33
6n	2050 \pm 50	7100 \pm 2600	3.46	2775 \pm 375	2040 \pm 520	0.73
1	3.3 \pm 0.5	700 \pm 79	212.12	25 \pm 3	4875 \pm 1000	195
3	0.5 \pm 0.01	44 \pm 3	88	1 \pm 0.02	70.4 \pm 7	70.4

4	13.1 ± 4	500 ± 20	38.2	25 ± 4	1117 ± 117	44.7
----------	----------	----------	------	--------	------------	------

^aIC₅₀ values of the ligands determined in ovarian carcinoma cells A2780, P-gp overexpressing A2780AD cells, mouse embryo NIH 3T3 and P-gp overexpressing NIH-MDR-G185. IC₅₀ value is the concentration that gives 50% inhibition of cell growth; ^bIC₅₀ values (nM) are the mean ± SE of three independent assays; ^cThe relative resistance of the resistant cell lines obtained by dividing the IC₅₀ of the resistant cell line by that of the parental cell line.

2.2.6.2 Effect on A549, B16F10, B16F1, PC9 and HCC827 cells

We further characterized **PNOX** in primary human melanocytes (HEMA), human primary melanoma cell line A375 and metastatic melanoma 501MEL cell lines on their cell cycle profile (Figures S14-S16), and we engaged further cell-based assays for a sub-series of new compounds with different binding affinity against tubulin. In particular, we assessed efficacy for **PNOX**, **6a**, **6j** and **6l** against the following tumor cell lines: A549, lung adenocarcinoma; B16F10, mouse melanoma (metastatic); B16F1, mouse melanoma; PC9, lung adenocarcinoma; HCC827, lung adenocarcinoma with EGFR mutation (Figure 12).

The efficacy of **6a**, **6j** and **6l** on cell survival was investigated on different tumor cell lines both of mouse and human origin, representative of melanoma and lung tumors. Cells were exposed to increasing concentrations (0.1, 1 and 10 μM) in medium containing 5% serum. Cell viability was evaluated by the MTT assay after 18 h of incubation. **PNOX** was kept as reference compound. Data demonstrates that **6a** and **6j** showed an inhibitory effect overlapping the one elicited by **PNOX**, while **6l** was devoid of any activity. The inhibitory effect was marked in all tumor cell lines except HCC827, characterized by a doubling time of ca. 50-60 h (Figure 12).

Based on the computational and experimental data, we observed that the tubulin affinity correlates with growth inhibition of tumor cell lines. In fact, we noted that **6a**, possessing a strong affinity against tubulin, is able to behave as tumor cell growth inhibitor at higher concentration with respect to compounds **PNOX** and **6j**. Compound **6l**, containing the 3-substituted quinoline is almost inactive against all the selected tumor cell lines. This is fully

consistent with the predicted lack of affinity towards tubulin of **6l** that is not able to correctly accommodate the quinoline nucleus into the colchicine binding site.

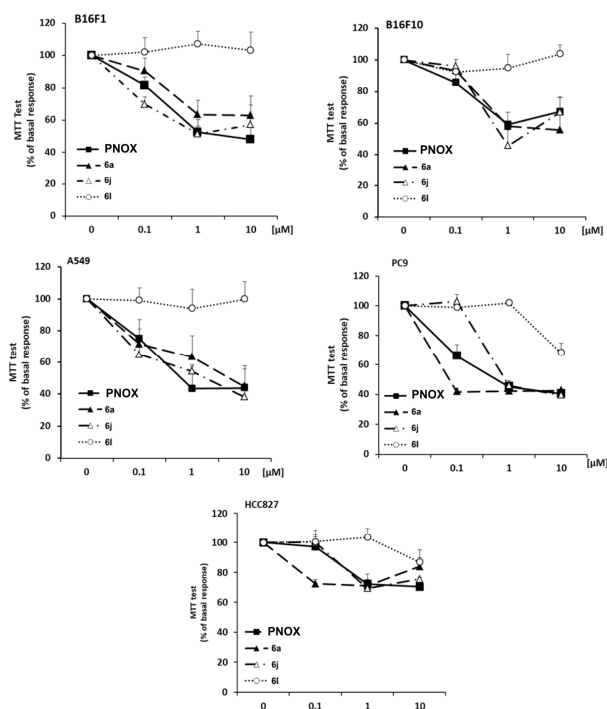


Figure 12. Effect of compounds **PNOX**, **6a**, **6j** and **6l** against the following cell lines: A549, lung adenocarcinoma; B16F10, mouse melanoma (metastatic); B16F1, mouse melanoma; PC9, lung adenocarcinoma; HCC827, lung adenocarcinoma with EGFR mutation. Cells were exposed to the test substances for 18 h in presence of 5% serum.

For PC9 and HCC827 cell lines we also performed a western blot analysis in order to gain additional information regarding their possible mechanism of action as pro-apoptotic agents. As shown in Figure 13A, compounds **PNOX** and **6j** were able to promote caspase 3-mediated apoptosis in the tested cell lines. Moreover, the western blot reported in Figure 13B documented an increase of the inhibitory protein of cell cycle p21 and reduction of cyclin D1. Based on these results we can conclude that our developed compounds are able to block tumor cell cycle

(increasing p21 and reducing cyclin D1 expression) and induce apoptosis, being as effective as **PNOX**.

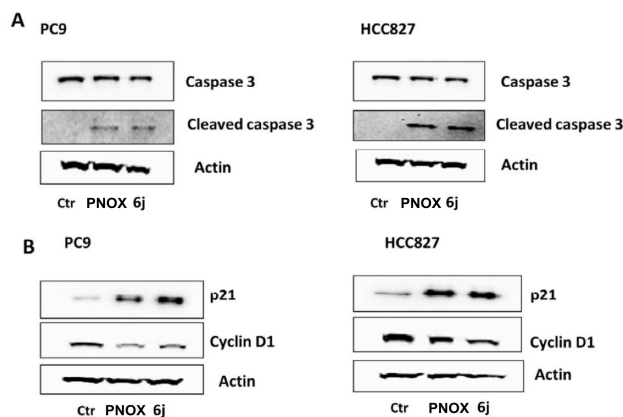


Figure 13. Western blot analysis. (A) caspase 3 activation; (B) cell cycle proteins. Cells were exposed to **PNOX** and **6j** (10 μM) for 18 h in presence of 5% serum.

2.2.6.3 Effects on cell cycle and differentiation in NB4 cell line

To extend the investigation of their biological effects, compounds **6a**, **6e**, **6j**, and **6n** were also evaluated in the promyelocytic leukemia (APL) NB4 cell line in terms of cell cycle progression, cell death and cell differentiation. NB4 cells were treated with four different concentrations (50 and 100 nM, 1 and 10 μM) for 24 h, in comparison with **PNOX**.

The compounds were able to induce a dose-dependent block in G1 phase, compared to the control (Figure S17A) indicating that compounds are able to affect cell cycle progression. Interestingly, in the APL context the cell cycle block is mainly in G1 phase (**PNOX**, **6a**, **6e**, **6j**), suggesting a context-dependent effect on the type of cell cycle block. Furthermore, compound **6n**, which in this context is less potent in cell death induction, induces a G2/M block, indicating a possible link with cell death and cell cycle blocks. In addition, treatment for 24 h induced cell death, revealed by the percentage of cells in pre-G1 phase (Figure S17B). Flow cytometric analysis of propidium iodide stained cells showed the capability of the compounds to induce

dose-dependent cell death (Figure 14A). Compound **6n** was not able to affect cell-cycle progression as well as cell death (Figures 14A and S17A,B). Moreover, effects on granulocytic differentiation, revealed by CD11c staining, were also tested in a dose dependent manner. The differentiation induction reached a maximum value at 1 μ M concentration and, then, decreased likely due to the occurrence of cell death (Figure 14B). To better understand the role of these compounds on cell differentiation, NB4 cells were treated with these drugs at a concentration of 500 nM and in co-treatment with ATRA (All Trans Retinoic Acid), a renowned differentiation modulator. While as expected in these timeframes, cell cycle progression and cell death were less affected by ATRA co-treatment (Figures 15A and S18A,B), NB4 differentiation was strongly regulated by ATRA, and high values were reached in combination, particularly for **6j**. A strong differentiating effect was obtained after combination with **6j** (Figure 15B). This biological effect indicates potential therapeutic applications in differentiation therapy.

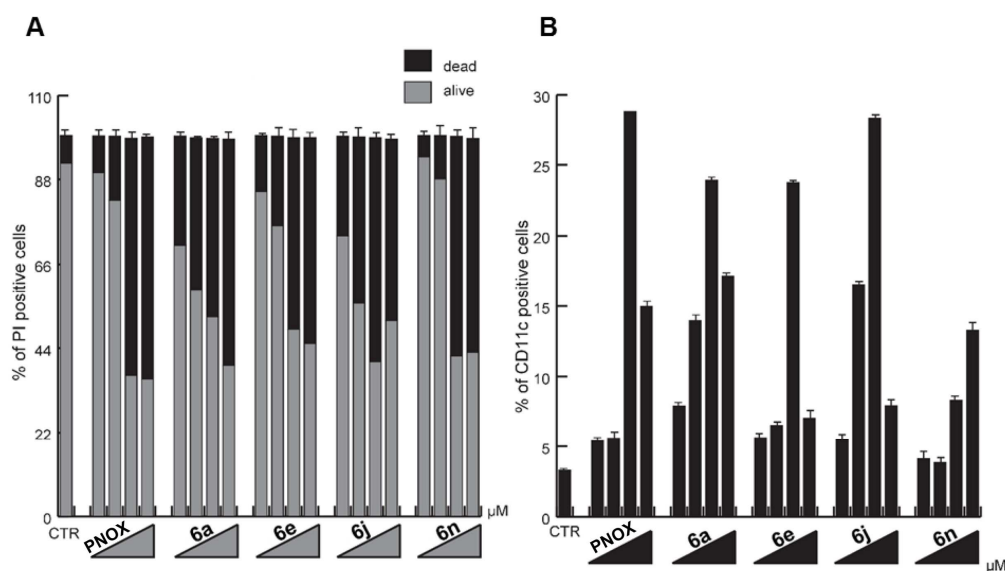


Figure 14. Biological assays on NB4 cells. (A) propidium iodide assay (B) CD11c expression levels at 24 h after treatment with compounds **PNOX**, **6a**, **6e**, **6j** and **6n** used at 50 and 100 nM, 1 and 10 μ M. Data are represented as mean \pm S.E.M of biological triplicates.

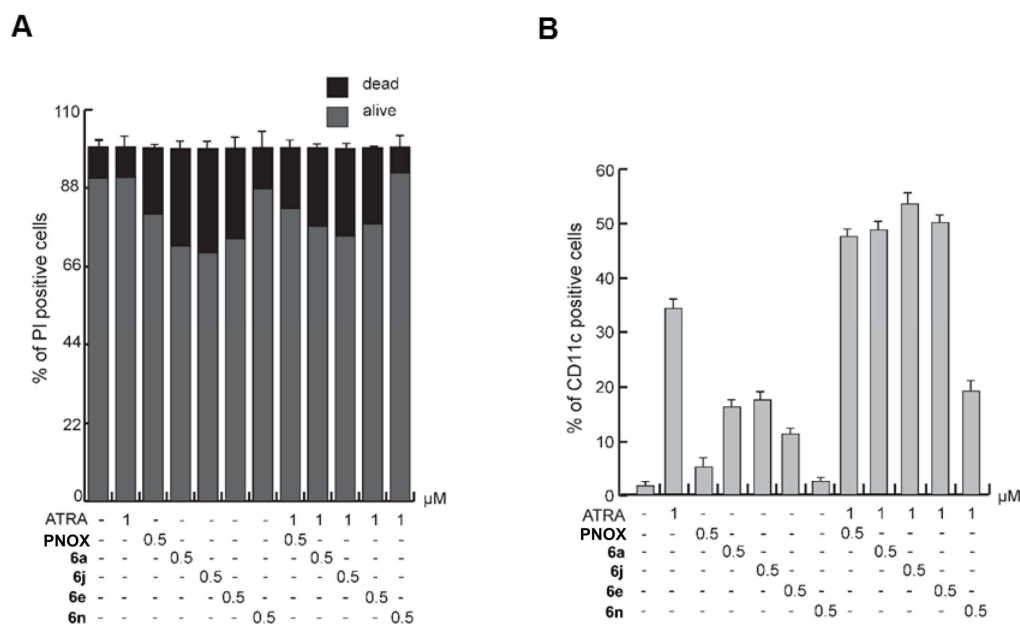


Figure 15. Biological assays on the promyelocytic leukemia NB4 with and without ATRA treatment. (A) Propidium iodide assay and (B) CD11c expression levels at 24 h after treatment with compounds **PNOX**, **6a**, **6e**, **6j** and **6n** used at the concentration of 0.5 μ M with and without ATRA used at the concentration of 1 μ M. Data are represented as mean \pm S.E.M. of biological triplicates.

2.2.6.4 Effect on tongue carcinoma (SCC4), multiple myeloma (NCI-H929), and Ca9.22 gingival squamous carcinoma (p53 mutated) cell lines

Compounds **PNOX**, **6j** and **6p** were also evaluated in for their effect on viability on tongue carcinoma (SCC4) and multiple myeloma (NCI-H929), and Ca9.22 gingival squamous carcinoma (p53 mutated) cell lines (Table 5). As shown, compounds **PNOX** and **6j** demonstrated comparable efficacy in SCC4 and NCI-H929 cells, while, compound **6p** demonstrated negligible efficacy in both cell lines.

Table 5. Cytotoxicity assessment of compounds **PNOX** and **6j** and **6p** on the growth on tongue carcinoma (SCC4) and multiple myeloma (NCI-H929), and Ca9.22 gingival squamous carcinoma (p53 mutated) cell lines.

Cpd	h	IC ₅₀ (μM)		
		SCC4 ^a	NCI-H929 ^b	Ca9.22 ^c
PNOX	24	nt	nt	0.210
	48	0.160	0.376	0.170
	72	nt	nt	0.083
6j	24	nt	nt	31.6
	48	0.222	0.363	13.4
	72	nt	nt	4.5
6p	24	nt	nt	8.0
	48	9.37	>50	6.3
	72	nt	nt	4.5

^aIC₅₀ values determined in tongue carcinoma (SCC4) cells; cells were treated with increasing concentrations of each compound for 48 h. Data represent the mean of three independent experiments. ^bIC₅₀ values determined in multiple myeloma (NCI-H929) cells; cells were treated with increasing concentrations of each compound for 48 h. Data represent the mean of three independent experiments. ^cIC₅₀ values determined in Ca9.22 gingival squamous carcinoma (p53 mutated) cells; cells were treated with increasing concentrations of each compound for 24 h, 48 h and 72 h. Data represent the mean of three independent experiments. We have previously reported the IC₅₀ values for **PNOX** in Ca9.22 cells [21] and they are shown here again for comparison purposes.

As **PNOX** and **6j** were giving promising IC₅₀ values these compounds were further tested for their pro-apoptotic ability through flow cytometric analysis of Annexin V/Propidium iodide stained cells. This dual staining method can distinguish between early apoptosis and late apoptosis. As can be seen from Figure 16 (panels A and B), both compounds induced substantial apoptosis (over 40%) following a 48 h treatment in SCC4 and NCI-H929 cells. Regarding

Ca9.22 cells (Figure 16, panel C), **6j** does not seem to be effective at 500 nM when compared to the other cell lines, while **6p** displays only modest efficacy.

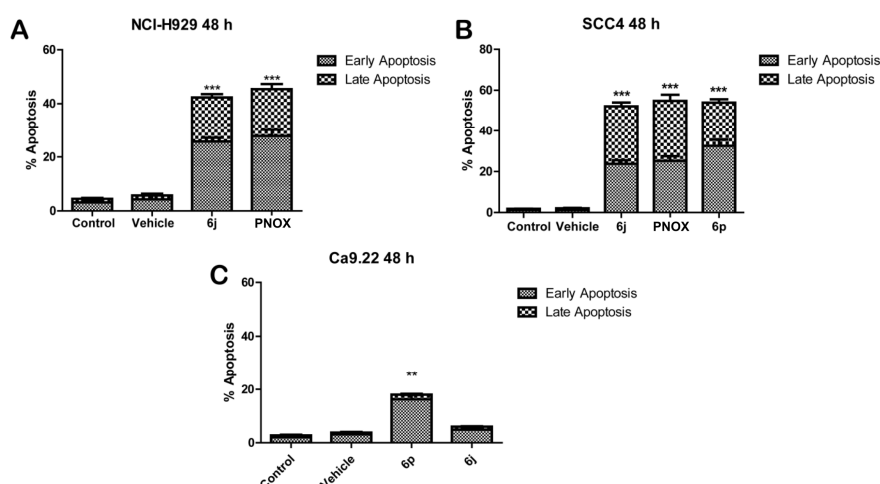


Figure 16. (A) NCI-H929 cells were seeded at a density of 30×10^4 cells/mL and were left untreated (control) or treated with either vehicle (1% EtOH (v/v)) or 500 nM of **PNOX** and **6j** for 48 h. (B) SCC4 cells were seeded at a density of 15×10^4 cells/mL and were treated with either vehicle control (1% EtOH (v/v)) or 500 nM of **6j** or **PNOX** or 50 μ M **6p** for 48 h. (C) Ca9.22 cells were seeded at a density of 30×10^4 cells/mL and were treated with either vehicle control (1% EtOH (v/v)) or 500 nM **6p**, or 500 nM of **6j** for 48 h.

After incubation cells were harvested and stained with Annexin V/Propidium Iodide (PI) and were analyzed by flow cytometry using BD FACs Accuri software. 10,000 cells were gated on vehicle treated cells. Values represent the mean \pm S.E.M of three independent experiments (n=3). Statistical analysis was performed using a T-test. **p = 0.001”.

2.2.7 Autophagy studies

Dysfunction of autophagy is implied in several diseases including cancer where it may either inhibit or promote cancer cell proliferation depending on the tumor setting [49]. To address the impact of compounds on both basal and induced autophagy we measured the accumulation of the

LC3B-II protein by immunoblot. LC3B-II is indeed exclusively located on autophagic vesicles and it is one of the most widely used markers to monitor autophagy since LC3B-II levels are considered directly correlated to the abundance of autophagosomes in the cells. However, since autophagy is a dynamic process, accumulation of LC3B-II within the cells does not necessarily correspond to an increase of autophagy but could reflect a reduction in autophagosome turnover. We therefore compared the amount of LC3B-II in compound-treated samples both in presence or absence of chloroquine (CQ), a well-known inhibitor of lysosomal activity and autophagy (Figure 17).

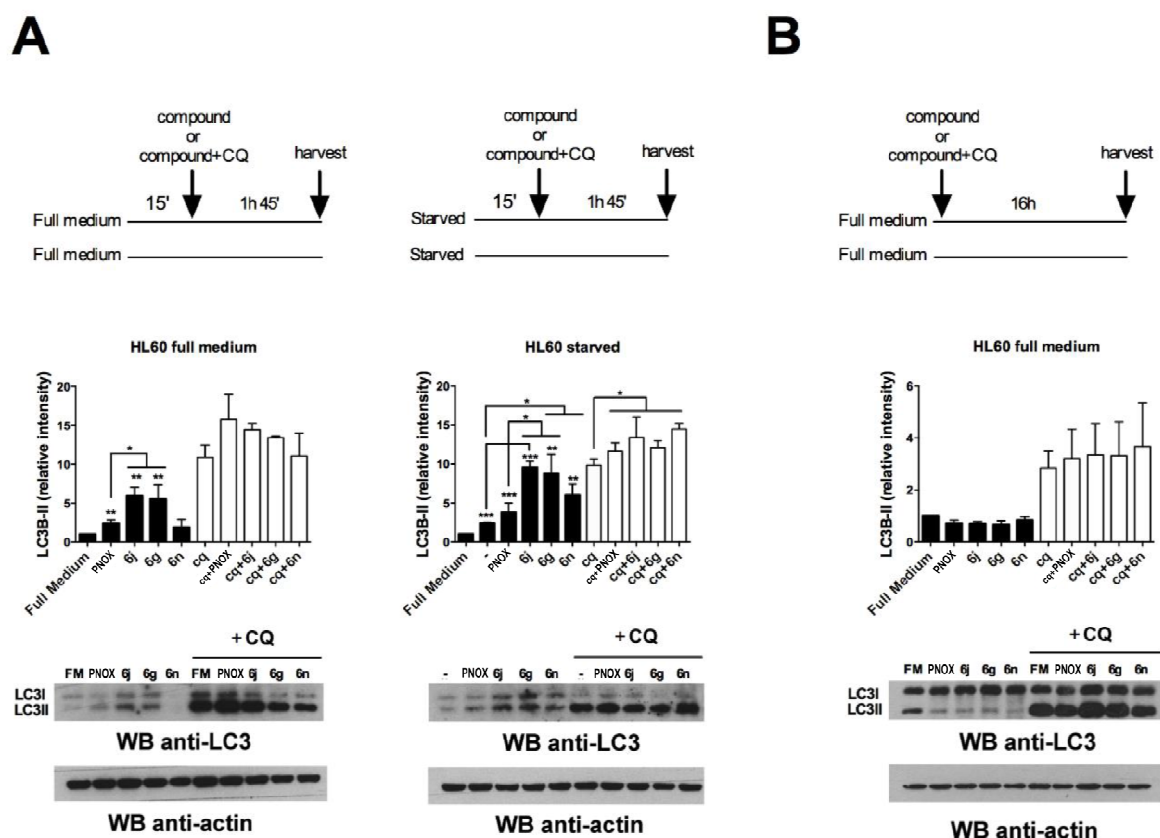


Figure 17. Immunoblot analysis of LC3B-II levels in HL-60 cells cultured in serum supplemented RPMI 1640 (full medium) or in Earle's Balanced Salts (EBS) medium (starved) and treated with 10 μ M of compounds **PNOX**, **6g**, **6j** or **6n** in presence or absence of 40 μ M

chloroquine (CQ) for 1 h 45 min (A) or 16 h (B). Control immunoblot with anti-actin antibodies of the same filters are shown. Densitometric analysis of LC3B-II amount from three independent experiments was performed and normalized with actin level. Bar graphs show the relative intensity of LC3B-II. *, $p < 0.05$ **, $p < 0.01$ versus full medium as calculated by Student's T-test.

HL-60 cells were treated with compounds for 1 h 45 min and accumulation of LC3B-II was measured by immunoblot (Figure 17A). Significant higher levels of LC3B-II, which were further increased in presence of the lysosomal inhibitor CQ, were found in samples treated with **PNOX**, **6g** and **6j** compared with cells maintained in full medium indicating that these compounds are able to induce accumulation of autophagosomes in HL-60 cells in basal condition (Figure 17A). Moreover, **6g** and **6j** appeared to be more effective when compared with **PNOX** (Figure 17A). To investigate the effect of these compounds on autophagy induced by serum deprivation, cells were starved for 15 min before the addition of the compounds and the levels of LC3B-II measured in presence or absence of CQ after 1 h 45 min of treatment. Accumulation of LC3B-II was significantly higher in serum starved samples co-treated with **6g**, **6j** and **6n** compared with untreated and **PNOX**-treated samples indicating that **6g** and **6j** are the most effective derivatives on the autophagic process in both basal and serum starved conditions. Moreover, a reduction of the LC3B-II protein was found in treated samples, but not in the same samples co-treated with CQ, following longer treatment (16 h) in serum supplemented medium compared with untreated cells. The enhancement of LC3B-II accumulation in samples treated with CQ, a lysosomal inhibitor, compared with CQ-untreated samples may be indicative of a pro-autophagic effect of compounds rather than of an inhibitory effect on the autophagic process. In support of a pro-autophagic effect of the novel analogues in HL-60 cells, short treatment (1 h 45 min) with

compounds in serum supplemented samples resulted in the increase of LC3II-B levels which is further enhanced in samples co-treated with CQ (Figure 17A). Despite this analysis of the autophagic flux (difference in the levels of LC3II-B in presence or absence of lysosomal inhibitors) which reflects the net amount of LC3II-B delivered to lysosomes, suggests a pro-autophagic effect, additional assays are required to better characterize the pro-autophagic effect of novel compounds. Our preliminary data demonstrated that our novel analogues are able to target the autophagic process and that **6g** and **6j** are the best performing analogues so far identified when tested at 10 μ M.

3. Conclusion

In summary, we explored the structure-activity relationships of a pyrrolonaphthoxazepine class of anticancer agents, and described the development of a series of potent pro-apoptotic MDAs with nanomolar affinity. Compounds were characterized by crystallographic, biological, bioinformatics and medicinal chemistry studies. In particular, we have assessed the binding affinity to tubulin for selected compounds and we have solved the X-ray structure of one of the most promising compounds in complex with tubulin. This allowed us to unveil the binding site on tubulin for this class of MDAs, thus gaining insights into their binding mode and mechanism of action. We assessed their ability to inhibit the growth of a large group of tumor cells, including multidrug-resistant cell lines and we investigated the mechanism of action of a sub-series of compounds on cell cycle in different cell lines, unveiling for some of them the activation of caspase 3-mediated apoptosis. Finally, the role of selected compounds on the autophagic process was investigated by the quantification of LC3B-II protein. The obtained data suggested a relevant therapeutic potential for the newly developed compound **6j** and some of its analogues as effective anticancer agents displaying efficacy on multiple cancer cell lines.

Additionally, the molecular insight derived from analysis of the X-ray structure of **6j** in complex with tubulin will pave the way to the discovery of novel optimized compounds as potential antitumor agents.

4. Experimental Section

4.1. Chemistry

4.1.1. General Remarks. Unless otherwise specified, materials were purchased from commercial suppliers and used without further purification. Reaction progress was monitored by TLC using silica gel 60 F254 (0.040-0.063 μm) with detection by UV. Silica gel 60 (0.040-0.063 μm) was used for column chromatography. ^1H NMR and ^{13}C NMR spectra were recorded on a Varian 300 MHz spectrometer or a Bruker 400 MHz spectrometer by using the residual signal of the deuterated solvent as internal standard. Splitting patterns are described as singlet (s), doublet (d), triplet (t), quartet (q), and broad (br); the value of chemical shifts (δ) are given in ppm and coupling constants (J) in Hertz (Hz). ESI-MS spectra were performed by an Agilent 1100 Series LC/MSD spectrometer. IR spectra were recorded on a Agilent Cary 630 FTIR spectrophotometer and are reported as cm^{-1} . Melting points were determined in Pyrex capillary tubes using an Electrothermal 8103 apparatus and are uncorrected. Yields refer to purified products and are not optimized. All moisture-sensitive reactions were performed under argon atmosphere using oven-dried glassware and anhydrous solvents. Final compounds were analyzed by combustion analysis (CHN) to confirm purity > 95% (Table S3).

4.1.2 8-Bromoquinoline (13a). Method 1. $\text{FeSO}_4 \cdot 7\text{H}_2\text{O}$ (121 mg, 0.44 mmol) and PhNO_2 (1.78 g, 14.53 mmol) were heated at 110 $^\circ\text{C}$. In a separate flask 2-bromoaniline **11** (2.50 g, 14.53 mmol) and glycerol were sequentially added to conc. H_2SO_4 and the resulting mixture heated at 70 $^\circ\text{C}$. This solution was then added to the PhNO_2 $\text{FeSO}_4 \cdot 7\text{H}_2\text{O}$ at 110 $^\circ\text{C}$ and the mixture was

heated at 150 °C for 7 h. After cooling to room temperature, the mixture was poured into ice and neutralized to pH = 8 with 4 N NaOH. The aqueous phase was extracted 10 times with EtOAc. The combined organic layers were dried over anhydrous sodium sulfate, filtered and concentrated. The residue was purified by flash chromatography on silica gel (50% petroleum ether in DCM) to afford the title compound as a brown oil (60% yield).

Method 2. To a solution of copper (II) bromide (7.00 g, 31.36 mmol) and *tert*-butyl nitrite (5.40 g, 52.28 mmol) in dry acetonitrile (90 mL) was added 8-aminoquinoline **12** (3.77 mg, 26.14 mmol) at room temperature and the mixture was stirred at 65 °C for 12 h. Acetonitrile was evaporated, then Et₂O and water were added and the precipitate filtered. The aqueous phase was extracted 3 times with Et₂O. The combined organic layers were dried over anhydrous sodium sulfate, filtered and concentrated. The residue was purified by flash chromatography on silica gel (30% EtOAc in petroleum ether) to afford the title compound as a brown oil (76% yield). ¹H NMR (CDCl₃, 300 MHz) δ 9.05 (dd, 1H, *J*₁ = 1.5 Hz, *J*₂ = 4.2 Hz), 8.18 (dd, 1H, *J*₁ = 1.5 Hz, *J*₂ = 8.4 Hz), 8.05 (dd, 1H, *J*₁ = 1.2 Hz, *J*₂ = 7.2 Hz), 7.78 (d, 1H, *J* = 7.8 Hz), 7.50-7.38 (m, 2H); ESI-MS *m/z* 209.9 [M+H]⁺, 231.9 [M+Na]⁺.

4.1.3 Quinoline-8-carbaldehyde (14a). To a solution of **13a** (100 mg, 0.48 mmol) in dry THF (1.5 mL) at -78 °C *n*BuLi (2.5 M in *n*-hexane, 300 μL, 0.72 mmol) was added dropwise. The resulting solution turned to red and DMF (192 μL, 2.49 mmol) was added. After 10 min at -78 °C the mixture was quenched with water. The reaction was poured into a saturated aqueous solution of NaHCO₃ (10 mL) and extracted with EtOAc (3 x 10 mL). The combined organic layers were dried over anhydrous sodium sulfate, filtered and concentrated. The residue was purified by flash chromatography on silica gel (10% EtOAc in *n*-hexane) to afford the title compound as a yellow solid (53% yield). ¹H NMR (CDCl₃, 300 MHz) δ 11.44 (s, 1H), 9.03 (dd,

$J_1 = 1.8$ Hz, $J_2 = 4.2$ Hz, 1H), 8.31 (dd, $J_1 = 1.2$ Hz, $J_2 = 7.2$ Hz, 1H), 8.23 (dd, $J_1 = 1.8$ Hz, $J_2 = 8.1$ Hz, 1H), 8.08 (dd, $J_1 = 1.5$ Hz, $J_2 = 8.4$ Hz, 1H), 7.66 (t, $J = 7.8$ Hz, 1H), 7.50 (dd, $J_1 = 4.5$ Hz, $J_2 = 8.4$ Hz, 1H); ESI-MS m/z 158 $[M+H]^+$; 180 $[M+Na]^+$.

4.1.4 Quinoline-5-carbaldehyde (14b). Compound **14b** was obtained from **13b** (500 mg, 2.4 mmol) following the procedure described for the preparation of **14a**. The residue was purified by flash chromatography on silica gel (16% EtOAc in *n*-hexane) to afford the title compound as a yellow solid (66% yield). ^1H NMR (CDCl_3 , 300 MHz) δ 10.37 (s, 1H), 9.62 (d, 1H, $J = 8.7$ Hz), 9.02 (t, 1H, $J = 2.1$ Hz), 8.38 (d, 1H, $J = 8.7$ Hz), 8.07 (dd, 1H, $J_1 = 5.4$ Hz, $J_2 = 7.2$ Hz), 7.92-7.88 (m, 1H), 7.58 (dd, 1H, $J_1 = 4.5$ Hz, $J_2 = 8.7$ Hz); ESI-MS m/z 158 $[M+H]^+$.

4.1.5 8-(2-Methoxyvinyl)quinoline (15a). (Methoxymethyl)-triphenylphosphonium chloride (76 mg, 0.223 mmol) was suspended in dry THF (1.0 mL) and then sodium *bis*(trimethylsilyl)amide (1 M solution in THF, 300 μL , 0.3 mmol) was added at 0 °C. The solution immediately became dark red colored. After 30 minutes at 0 °C, aldehyde **14a** (40 mg, 0.255 mmol) dissolved in dry THF (1.0 mL) was added and the resulting mixture was stirred at 0 °C for 30 min. The reaction was monitored by TLC. After 1 h stirring at room temperature, H_2O was added and the aqueous layer was extracted twice with ethyl acetate. The combined organic layers were dried over anhydrous sodium sulfate, filtered and concentrated. The residue was purified by flash chromatography on silica gel (10% EtOAc in *n*-hexane) to afford the title compound as a yellow oil (63% yield). ^1H NMR (CDCl_3 , 300 MHz) (mixture of *cis* and *trans* isomers) δ 8.91 (td, 1H $J_1 = 1.8$ Hz, $J_2 = 3.9$ Hz), 8.43 (dd, 1H, $J_1 = 1.5$ Hz, $J_2 = 7.5$ Hz), 8.12 (dt, 1H, $J_1 = 2.1$ Hz, $J_2 = 8.1$ Hz), 7.69 (dd, 1H, $J_1 = 1.2$ Hz, $J_2 = 7.5$ Hz), 7.62 (dd, 1H, $J_1 = 1.2$ Hz, $J_2 = 8.1$ Hz), 7.54-7.36 (m, 3H), 6.96 (d, 1H, $J = 13.2$ Hz), 6.71 (d, $J = 7.2$ Hz), 6.45 (d, 1H, $J = 7.2$ Hz, 1H), 3.85 (s, 3H), 3.84 (s, 3H); ESI-MS m/z 186 $[M+H]^+$.

4.1.6 5-(2-Methoxyvinyl)quinoline (15b). Compound **15b** was obtained from **14b** (400 mg, 2.55 mmol) following the procedure described for the preparation of **15a**. The residue was purified by flash chromatography on silica gel (30% EtOAc in *n*-hexane) to afford the title compound as a yellow oil (84% yield). ¹H NMR (CDCl₃, 300 MHz) (mixture of *cis* and *trans* isomers) δ 8.91-8.87 (m, 1H), 8.41 (d, 1H, *J* = 8.4 Hz), 8.05 (d, 1H, *J* = 7.2 Hz), 7.95 (dd, 1H, *J*₁ = 5.4 Hz, *J*₂ = 8.1 Hz), 7.70-7.60 (m, 1H), 7.48-7.36 (m, 2H), 7.00 (dd, 1H, *J*₁ = 1.2 Hz, *J*₂ = 12.6 Hz), 6.42-6.36 (m, 1H), 5.81 (d, 1H, *J* = 6.9 Hz), 3.81-3.79 (m, 3H); ESI-MS *m/z* 186 [M+H]⁺.

4.1.7 2-(Quinolin-8-yl)acetaldehyde (16a). Compound **15a** (30 mg, 0.162 mmol) was dissolved in acetone (1.0 mL) and then 6 N HCl (405 μL) was added dropwise. The mixture was refluxed for 3 h. The solvent was evaporated and the resulting aqueous mixture was taken to pH = 8 with saturated aqueous NaHCO₃. The aqueous layer was extracted with EtOAc (3 x 20 mL). The combined organic layers were dried over anhydrous sodium sulfate, filtered and concentrated. The residue was purified by flash chromatography on silica gel (30% EtOAc in *n*-hexane) to afford the title compound as a red oil (54% yield). ¹H NMR (CDCl₃, 300 MHz) δ 9.93 (s, 1H), 8.91 (dd, 1H, *J*₁ = 1.8 Hz, *J*₂ = 4.2 Hz), 8.18 (dd, 1H, *J*₁ = 1.2 Hz, *J*₂ = 8.1 Hz), 7.80 (d, 1H, *J* = 8.1 Hz), 7.61-7.41 (m, 3H), 4.28 (s, 2H); ESI-MS *m/z* 180 [M+Na]⁺.

4.1.8 2-(Quinolin-5-yl)acetaldehyde (16b). Compound **16b** was obtained starting from **15b** (500 mg, 2.68 mmol) following the procedure described for the preparation of **16a**. The title compound was obtained as a dark yellow oil (94% yield). ¹H NMR (CDCl₃, 300 MHz) δ 9.80-9.78 (m, 1H), 8.95 (d, 1H, *J* = 3.6 Hz), 8.22 (d, 1H, *J* = 8.7 Hz), 8.10 (d, 1H, *J* = 8.4 Hz), 7.71 (t, 1H, *J* = 7.8 Hz), 7.49-7.44 (m, 2H), 4.14 (s, 2H); ESI-MS *m/z* 180 [M+Na]⁺.

4.1.9 Methyl 2-(quinolin-8-yl)acetate (17a). To a solution of compound **16a** (300 mg, 1.75 mmol) in MeOH (2.0 mL) *N*-iodosuccinimide (987 mg, 4.38 mmol) and potassium carbonate

(605 mg, 4.38 mmol) were sequentially added. The reaction was performed in a dark room. The resultant dark brown mixture was stirred for 3 h at 25 °C. Subsequently, water (1.0 mL) and $\text{Na}_2\text{S}_2\text{O}_3 \cdot 5\text{H}_2\text{O}$ (900 mg) were added. The aqueous phase was extracted with EtOAc (3 x 50 mL). The combined organic layers were dried over anhydrous sodium sulfate, filtered and concentrated. The residue was purified by flash chromatography on silica gel (30% EtOAc in *n*-hexane) to afford the title compound as a pale yellow oil (57% yield). ^1H NMR (CDCl_3 , 300 MHz) δ 8.92 (dd, $J_1 = 1.8$ Hz, $J_2 = 4.2$ Hz, 1H), 8.14 (d, 1 H, $J = 8.1$ Hz), 7.76 (d, 1 H, $J = 8.1$ Hz), 7.64 (d, 1 H, $J = 6.9$ Hz), 7.52-7.38 (m, 2H), 4.30 (s, 3H), 3.70 (s, 2H); ESI-MS m/z 202 $[\text{M}+\text{H}]^+$, 224 $[\text{M}+\text{Na}]^+$.

4.1.10 Methyl 2-(quinolin-5-yl)acetate (17b). Compound **17b** was obtained from **16b** (450 mg, 2.63 mmol) following the procedure described for the preparation of **17a**. The residue was purified by flash chromatography on silica gel (33% EtOAc in *n*-hexane) to afford the title compound as a pale yellow amorphous solid (70% yield). ^1H NMR (CDCl_3 , 300 MHz) δ 8.94 (t, 1H, $J = 2.4$ Hz), 8.38 (d, 1H, $J = 8.7$ Hz), 8.08 (d, 1H, $J = 8.7$ Hz), 7.68 (t, 1H, $J = 7.5$ Hz), 7.50-7.44 (m, 2H), 4.08 (s, 2H), 3.69 (s, 3H); ESI-MS m/z 202 $[\text{M}+\text{H}]^+$, 224 $[\text{M}+\text{Na}]^+$.

4.1.11 Methyl 2-bromo-2-(quinolin-8-yl)acetate (9a). To a solution of compound **17a** (130 mg, 0.64 mmol) in CCl_4 (10 mL) *N*-bromosuccinimide (126 mg, 0.71 mmol) and a catalytic amount of AIBN were added in sequence. The mixture was refluxed for 24 h in the presence of a lamp (radical reaction). Subsequently the solvent was evaporated and DCM was added. The organic layer was washed twice with water (10 mL) and then dried over anhydrous sodium sulfate, filtered and concentrated. The residue was purified by flash chromatography on silica gel (30% EtOAc in petroleum ether) to afford the title compound as a colorless oil (60% yield). ^1H NMR (CDCl_3 , 300 MHz) δ 8.96 (dd, 1H, $J_1 = 2.4$ Hz, $J_2 = 4.2$ Hz), 8.20-8.12 (m, 2H), 7.84 (dd,

1H, $J_1 = 1.5$ Hz, $J_2 = 8.1$ Hz), 7.58 (t, $J = 8.1$ Hz, 1 H), 7.45 (dd, 1H, $J_1 = 3.9$ Hz, $J_2 = 8.1$ Hz), 6.95 (s, 1H), 3.79 (s, 3H); ESI-MS m/z 281 $[M+H]^+$.

4.1.12 Methyl 2-bromo-2-(quinolin-5-yl)acetate (9b). Compound **9b** was obtained from **17b** (350 mg, 1.74 mmol) following the procedure described for the preparation of **9a**. The mixture was refluxed for 2 h. The residue was purified by flash chromatography on silica gel (33% EtOAc in *n*-hexane) to afford the title compound as a colorless oil (51% yield). ^1H NMR (CDCl_3 , 300 MHz) δ 8.95 (d, 1H, $J = 3.6$ Hz), 8.50 (d, 1H, $J = 8.4$ Hz), 8.12 (d, 1H, $J = 8.4$ Hz), 7.80-7.78 (m, 1H), 7.69-7.66 (m, 1H), 7.49-7.46 (m, 1H), 6.05 (s, 1H), 3.77 (s, 3H); ESI-MS m/z 280 $[M+H]^+$.

4.1.13 Quinoline-3-carbaldehyde (19). Compound **19** was obtained starting from **18** (500 mg, 2.40 mmol) following the procedure described for the preparation of **14a**. The residue was purified by flash chromatography on silica gel (16% EtOAc in *n*-hexane) to afford the title compound as a yellow solid (45% yield). ^1H NMR (CDCl_3 , 300 MHz) δ 10.23 (s, 1H), 9.34 (s, 1H), 8.61 (s, 1H), 8.17 (d, 1H, $J = 8.7$ Hz), 7.97 (d, 1H, $J = 7.8$ Hz), 7.86 (t, 1H, $J = 7.2$ Hz), 7.64 (t, 1H, $J = 7.8$ Hz); ESI-MS m/z 158 $[M+H]^+$.

4.1.14 2-(Quinolin-3-yl)acetaldehyde (20). Starting from **19** (600 mg, 3.82 mmol) 3-(2-methoxyvinyl)quinoline was obtained following the procedure described for the preparation of **15a**. The residue was purified by flash chromatography on silica gel (20% EtOAc in *n*-hexane) to afford 3-(2-methoxyvinyl)quinoline as a yellow oil (500 mg, 70% yield). ^1H NMR (CDCl_3 , 300 MHz) (mixture of *cis* and *trans* isomers) δ 8.97 (s, 1H), 8.85 (s, 1H), 8.42 (s, 1H), 8.03 (d, 2H, $J = 8.7$ Hz), 7.88 (s, 1H), 7.78-7.43 (m, 15H), 7.21 (d, 1H, $J = 1.5$ Hz), 6.35 (dd, 1H, $J_1 = 1.8$ Hz, $J_2 = 7.2$ Hz), 5.92 (d, 2H, $J = 12.9$ Hz), 5.37 (d, 1H, $J = 6.0$ Hz), 3.88 (d, 3H, $J = 1.8$ Hz), 3.76 (d, 3H, $J = 1.5$ Hz); ESI-MS m/z 186 $[M+H]^+$. Compound **20** was obtained starting from 3-(2-

methoxyvinyl)quinoline (1.0 g, 5.41 mmol) following the procedure described for the preparation of **16a**. The title compound was obtained as a yellow oil (97% yield). ^1H NMR (CDCl_3 , 300 MHz) δ 9.88 (s, 1H), 8.74 (d, 1H, $J = 2.1$ Hz), 8.10 (d, 1H, $J = 8.1$ Hz), 8.01 (s, 1H), 7.80 (d, 1H, $J = 8.1$ Hz), 7.71 (t, 1H, $J = 1.2$ Hz), 7.58 (t, 1H, $J = 1.2$ Hz), 3.92 (s, 2H); ESI-MS m/z 180 $[\text{M}+\text{Na}]^+$.

4.1.15 Methyl 2-bromo-2-(quinolin-3-yl)acetate (9c). Starting from **20** (1.0 g, 5.85 mmol) compound *methyl 2-(quinolin-3-yl)acetate* was obtained following the procedure described for the preparation of **17a**. The residue was purified by flash chromatography on silica gel (33% EtOAc in *n*-hexane) to afford the title compound as a pale yellow oil (29% yield). ^1H NMR (CDCl_3 , 300 MHz) δ 8.84 (d, 1H, $J = 1.8$ Hz), 8.11-8.07 (m, 2H), 7.79 (d, 1H, $J = 7.8$ Hz), 7.69 (dt, 1H, $J_1 = 1.8$ Hz, $J_2 = 8.7$ Hz), 7.54 (dt, 1H, $J_1 = 1.2$ Hz, $J_2 = 7.2$ Hz), 3.82 (s, 2H), 3.72 (s, 3H); ESI-MS m/z 202 $[\text{M}+\text{H}]^+$, 224 $[\text{M}+\text{Na}]^+$. Starting from *methyl 2-(quinolin-3-yl)acetate* (350 mg, 1.74 mmol) compound **9c** was obtained following the procedure described for the preparation of **9a**. The mixture was refluxed for 2 h. The residue was purified by flash chromatography on silica gel (25% EtOAc in *n*-hexane) to afford the title compound as a brown oil (71% yield). ^1H NMR (CDCl_3 , 300 MHz) δ 9.03 (d, 1H, $J = 1.8$ Hz), 8.35 (s, 1H), 8.11 (d, 1H, $J = 8.4$ Hz), 7.83 (d, 1H, $J = 7.8$ Hz), 7.75 (dt, 1H, $J_1 = 0.6$ Hz, $J_2 = 6.9$ Hz), 7.57 (dt, 1H, $J_1 = 0.9$ Hz, $J_2 = 6.9$ Hz), 5.54 (d, 1H, $J = 1.5$ Hz), 3.82 (d, 3H, $J = 2.4$ Hz); ESI-MS m/z 280.9 $[\text{M}+\text{H}]^+$.

4.1.16 5-Bromo-8-aminoquinoline (21). To solution of compound **12** (1.0 g, 6.94 mmol) in 46.0 mL of acetonitrile, a portion of NBS (605 mg, 3.40 mmol) was added. The reaction mixture was stirred at 25 °C for 15 min, then a second portion of NBS (667 mg, 3.75 mmol) was added. The reaction was stirred for 1 h at 25 °C. The solvent was evaporated under reduced pressure and

the residue taken up with EtOAc and washed with water (3 x 50 mL). The organic layer was dried over anhydrous sodium sulfate, filtered and concentrated. The residue was purified by flash chromatography on silica gel (10% EtOAc in petroleum ether) to afford the title compound as an amorphous yellow solid (51% yield). ^1H NMR (300 MHz, CDCl_3) δ 8.76 (d, 1H, $J = 6.0$ Hz), 8.43 (d, 1H, $J = 9.0$ Hz), 7.56 (d, 1H, $J = 12.0$), 7.48 (q, 1H, $J = 3.0$ Hz), 6.80 (d, 1H, $J = 6.0$ Hz); ESI-MS m/z 222.9 $[\text{M}+\text{H}]^+$.

4.1.17 5-Bromo-7-chloro-8-aminoquinoline (22). To a solution of compound **21** (800 mg, 3.61 mmol) in 77.0 mL of acetonitrile, *N*-chlorosuccinimide (458 mg, 3.43 mmol) was added at 25 °C. The reaction mixture was then stirred at 75 °C for 12 h. After cooling to room temperature, acetonitrile was removed under reduced pressure. The residue was taken up with EtOAc, and washed with water (3 x 70 mL). The organic layer was dried over anhydrous sodium sulfate, filtered and concentrated. The residue was purified by flash chromatography on silica gel (7% EtOAc in petroleum ether) to afford the title compound as an amorphous orange solid (70% yield). ^1H NMR (300 MHz, CDCl_3) δ 8.78 (d, 1H, $J = 4.2$ Hz), 7.69 (s, 1H), 8.43 (d, 1H, $J = 8.7$ Hz), 7.50 (q, 1H, $J = 4.2$), 5.46 (br, 2H); ^{13}C NMR (75 MHz, CDCl_3) δ 148.5, 148.4, 135.5, 133.0, 130.7, 127.4, 126.3, 122.3, 121.9. ESI-MS m/z 258.0 $[\text{M}+\text{H}]^+$.

4.1.18 5-Bromo-7-chloroquinoline (23). To a suspension of compound **22** (650 mg, 2.52 mmol) in 25 mL of water, concentrated H_2SO_4 was added dropwise at 0 °C until complete dissolution of the starting material was achieved. A solution of NaNO_2 (348 mg, 5.05 mmol) in 6.5 mL of water at 0 °C was added to the resulting bright yellow solution. The mixture was stirred for 15 min and subsequently it was added via cannula to a 50% aqueous solution of H_3PO_2 (6.0 mL) at 65 °C. The resulting mixture was stirred at 60 °C for 3 h. After cooling to room temperature, H_2SO_4 was neutralized through addition of 5 mL of a 4 N NaOH solution.

The aqueous layer was extracted with EtOAc (3 x 30 mL) and the organic layers dried over anhydrous sodium sulfate, filtered and concentrated. The residue was purified by flash chromatography on silica gel (7% EtOAc in petroleum ether) to afford the title compound as a yellow amorphous solid (12% yield). ^1H NMR (400 MHz, CDCl_3) δ 8.84 (d, 1H, $J = 3.2$ Hz), 8.40 (d, 1H, $J = 8.4$ Hz), 8.00 (s, 1H), 7.73 (s, 1H), 7.41 (q, 1H, $J = 4.4$ Hz); ESI-MS m/z 243.9 $[\text{M}+\text{H}]^+$.

4.1.19 7-Chloroquinoline-5-carbaldehyde (24). Compound **24** was obtained from **23** following the procedure described for the preparation of **14a**. The residue was purified by flash chromatography on silica gel (11% EtOAc in petroleum ether) to afford the title compound as a yellow amorphous solid (48% yield). ^1H NMR (400 MHz, CDCl_3) δ 10.22 (s, 1H), 9.46 (d, 1H, $J = 8.8$ Hz), 8.94 (dd, 1H, $J_1 = 1.2$ Hz, $J_2 = 4.0$ Hz), 8.30 (d, 1H, $J = 1.6$ Hz), 7.94 (d, 1H, $J = 2.0$ Hz), 7.52 (q, 1H, $J = 4.4$ Hz); ESI-MS m/z 192.0 $[\text{M}+\text{H}]^+$.

4.1.20 7-Chloro-5-(2-methoxyvinyl)quinoline (25). Compound **25** was obtained from **24** following the procedure described for the preparation of **15a**. The residue was purified by flash chromatography on silica gel (25% EtOAc in petroleum ether) to afford the title compound as a yellow amorphous solid (62% yield). ^1H NMR (300 MHz, CDCl_3), mixture of *cis* - *trans* isomers, δ 8.91-8.87 (m, 2H), 8.39 (t, 3H, $J = 6.9$ Hz), 8.09 (d, 1H, $J = 2.1$ Hz), 7.97 (s, 1H), 7.45-7.38 (m, 3H), 7.02 (d, 1H, $J = 12.6$ Hz), 6.46 (d, 1H, $J = 6.9$ Hz), 6.31 (d, 1H, $J = 6.3$ Hz), 5.77 (d, 1H, $J = 6.9$ Hz), 3.86 (s, 3H), 3.81 (s, 3H); ESI-MS m/z 220.0 $[\text{M}+\text{H}]^+$.

4.1.21 2-(7-Chloroquinolin-5-yl)acetaldehyde (26). Compound **26** was obtained from **25** following the procedure described for the preparation of **16a**. The product was isolated as a brown oil and submitted to the next step without further purification (73% yield). ^1H NMR (300

MHz, CDCl₃), δ 9.83 (s, 1H), 8.97 (d, 1H, J = 6.0 Hz), 8.28-8.25 (m, 2H), 7.55-7.51 (m, 2H), 4.15 (s, 2H); ESI-MS m/z 206.0 [M+H]⁺.

4.1.22 Methyl 2-(7-chloroquinolin-5-yl)acetate (27). Compound **27** was obtained from **26** following the procedure described for the preparation of **17a**. The residue was purified by flash chromatography on silica gel (20% EtOAc in petroleum ether) to afford the title compound as a white amorphous solid (59% yield). ¹H NMR (300 MHz, CDCl₃), δ 8.93 (dd, 1H, J_1 = 1.5 Hz, J_2 = 4.2 Hz), 8.32 (d, 1H, J = 7.8 Hz), 8.07 (d, 1H, J = 1.5 Hz), 7.47-7.43 (m, 2H), 4.04 (s, 2H), 3.70 (s, 3H); ESI-MS m/z 236.0 [M+H]⁺.

4.1.23 Metil 2-bromo-2-(7-chloroquinolin-5-yl)acetate (9d). Compound **9d** was obtained starting from **27** following the procedure described for the preparation of **9a**. The residue was purified by flash chromatography on silica gel (20% EtOAc in petroleum ether) to afford the title compound as a colorless oil (65% yield). ¹H NMR (300 MHz, CDCl₃), δ 8.97 (dd, 1H, J_1 = 1.5 Hz, J_2 = 4.5 Hz), 8.52 (d, 1H, J = 1.5 Hz), 8.21 (d, 1H, J = 1.5 Hz), 7.83 (d, 1H, J = 2.1 Hz), 7.54 (q, 1H, J_1 = 4.5 Hz, J_2 = 8.7 Hz), 5.98 (s, 1H), 3.70 (s, 3H); ESI-MS m/z 315.9 [M+H]⁺.

4.1.24 Ethyl 2-(1-hydroxy-5-methoxy-1,2,3,4-tetrahydronaphthalen-1-yl)acetate (29). To a solution of LHMDs (1M in THF, 14.74 mL, 14.74 mmol) in dry THF (15.8 mL) cooled to -78 °C, a solution of dry EtOAc (1.34 mL, 13.64 mmol) in dry THF (1.36 mL) was added dropwise. A solution of tetralone **28** (2.0 g, 11.34 mmol) in dry THF (2.6 mL) was added while maintaining an internal temperature below -70 °C. The resulting mixture was stirred at -70 °C for 1 h, quenched with 2 N HCl (10 mL), and allowed to warm up to 25 °C. The mixture was extracted with EtOAc (2 x 10 mL) and the combined organic layers were washed with brine, dried over anhydrous sodium sulfate, filtered and concentrated. The residue was purified by flash chromatography on silica gel (10% EtOAc in *n*-hexane) to afford the title compound as a yellow

oil (76% yield). ^1H NMR (400 MHz, CDCl_3) δ 7.20 (m, 2H), 6.75 (m, 1H), 4.2 (q, J = 6.4 Hz, 2H), 3.80 (s, 3H), 2.70 (m, 4H), 2.10 (m, 1H), 1.85 (m, 1H), 1.25 (t, J = 7.2 Hz, 3H); ESI-MS m/z 287.0 $[\text{M}+\text{H}]^+$.

4.1.25 Ethyl 2-(5-methoxy-3,4-dihydronaphthalen-1-yl)acetate (30) and ethyl 2-(5-methoxy-3,4-dihydronaphthalen-1(2H)-ylidene)acetate (31). Hydroxyester **29** (2,270 mg, 8.6 mmol) was dissolved in toluene/TFA (17 mL/0.4 mL) and the mixture was stirred at 110 °C for 3 h. The mixture was then cooled to 25 °C, diluted with EtOAc and washed with a 1 N NaOH solution (5 mL) and water (5 mL). The organic layer was washed with brine, dried over anhydrous sodium sulfate, filtered and concentrated. The resulting dark yellow residue containing a 1:2 mixture of olefins **30** and **31** was directly used in the next step (quantitative yield). ^1H NMR (300 MHz, CDCl_3) δ 7.25 (m, 0.5H), 7.15 (m, 1H), 6.80 (m, 1.5H), 6.35 (s, 0.3H), 6.00 (t, 0.7H), 4.20 (m, 2H), 3.80 (s, 3H), 3.40 (s, 1.5H), 3.20 (m, 0.5H), 2.80 (m, 2H), 2.30 (m, 1.5H), 1.85 (m, 0.5H), 1.25 (t, 1H), 1.20 (t, 2H).

4.1.26 Ethyl 2-(5-methoxynaphthalen-1-yl)acetate (33). A mixture of olefins **31** and **32** (1866 mg, 7.58 mmol) was dissolved in cyclohexene/dioxane (7.7 mL/2.6 mL). A catalytic amount of 10% Pd-C was then added and the mixture heated to reflux for 12 h. The mixture was cooled to 25 °C, filtered through a pad of celite and, after carefully washing the pad with EtOAc, concentrated under reduced pressure. The above residue containing intermediate **32** was dissolved in toluene (16.4 mL). To this was added DDQ (3,614 mg, 7.96 mmol), and the mixture heated at reflux for 3 h. The mixture was then cooled to 25 °C, and the resulting solids were removed by filtration using EtOAc as the solvent. The filtrate was concentrated to dryness and the product was purified by flash chromatography on silica gel (4% EtOAc in petroleum ether) to afford the title compound as a yellow oil (30% yield). ^1H NMR (400 MHz, CDCl_3) δ 8.27 (t, J =

5.2 Hz, 1H), 7.55 (d, $J = 8.6$ Hz, 1H), 7.48-7.41 (m, 3H), 6.85 (d, $J = 7.6$ Hz, 1H), 4.15 (q, $J = 7.2$ Hz, 2H), 4.09 (s, 2H), 4.00 (s, 3H), 1.20 (t, $J = 7.2$ Hz, 3H); ^{13}C NMR (75 MHz, CDCl_3) δ 171.6, 155.8, 133.1, 130.3, 128.5, 126.3, 125.9, 124.7, 121.8, 116.0, 103.8, 60.9, 55.5, 39.6, 14.1. ESI-MS m/z 245.2 $[\text{M}+\text{H}]^+$, 267.3 $[\text{M}+\text{Na}]^+$.

4.1.27 Ethyl 2-bromo-2-(5-methoxynaphthalen-1-yl)acetate (9e). Compound **9e** was obtained starting from **33** following the procedure described for the preparation of **9a**. The residue was purified by flash chromatography on silica gel (5% Et_2O in petroleum ether) to afford title compound as a yellow oil (30% yield). ^1H NMR (400 MHz, CDCl_3) δ 8.32 (d, $J = 8.4$ Hz, 1H), 7.79 (d, $J = 7.2$ Hz, 1H), 7.64 (d, $J = 8.4$ Hz, 1H), 7.50 (t, $J = 8.0$ Hz, 1H), 7.42 (t, $J = 8.0$ Hz, 1H), 6.85 (d, $J = 7.6$ Hz, 1H), 6.11 (s, 1H), 4.25 (q, $J = 7.6$ Hz, 2H), 3.99 (s, 3H), 1.22 (t, $J = 7.2$ Hz, 3H); ESI-MS m/z 325.0 $[\text{M}+\text{H}]^+$.

4.1.28 Ethyl 2-oxo-2-(quinolin-8-yl)acetate (34a). To a solution of compound **13a** (250 mg, 1.22 mmol) in dry THF (2.5 mL), $n\text{-BuLi}$ (2.5 M solution in $n\text{-hexane}$, 1.50 mmol) was added dropwise at -78°C . After 10 min diethyl oxalate (165 μL , 1.22 mmol) was added at -78°C . The reaction mixture was stirred at -78°C for 10 min (TLC monitoring) and then quenched with 3 mL of a saturated solution of NaHCO_3 . The aqueous layer was extracted with EtOAc (3 x 5 mL). The combined organic layers were dried over anhydrous sodium sulfate, filtered and concentrated. The residue was purified by flash chromatography on silica gel (7% EtOAc in petroleum ether) to afford the title compound as a yellow amorphous solid (20% yield). ^1H NMR (CDCl_3 , 300 MHz) δ 8.89 (dd, 1H, $J_1 = 1.5$ Hz, $J_2 = 3.9$ Hz), 8.34 (dd, 1H, $J_1 = 1.5$ Hz, $J_2 = 7.2$ Hz), 8.23 (dd, 1H, $J_1 = 1.5$ Hz, $J_2 = 8.4$ Hz), 8.10 (dd, 1H, $J_1 = 1.2$ Hz, $J_2 = 8.1$ Hz), 7.69 (t, 1H, $J = 7.8$ Hz), 7.50-7.46 (m, 1H), 4.44 (m, 2H), 1.42 (t, 3H, $J = 6.9$ Hz); ESI-MS m/z 230.0 $[\text{M}+\text{H}]^+$, 252.0 $[\text{M}+\text{Na}]^+$, 481.0 $[2\text{M}+\text{Na}]^+$.

4.1.29 Ethyl 2-oxo-2-(quinolin-5-yl)acetate (34b). Compound **34b** was prepared starting from **13b** following the procedure described for the preparation of **34a**. The residue was purified by flash chromatography on silica gel (20% to 50% EtOAc in *n*-hexane) to afford the title compound as a yellow amorphous solid (22% yield). ¹H NMR (300 MHz, CDCl₃) δ 9.39 (d, *J* = 8.7 Hz, 1H), 9.01 (d, *J* = 4.1 Hz, 1H), 8.40 (d, *J* = 8.4 Hz, 1H), 8.08 (d, *J* = 7.2 Hz, 1H), 7.81 (t, *J* = 7.9 Hz, 1H), 7.60 (dd, *J*₁ = 8.7, *J*₂ = 4.1 Hz, 1H), 4.50 (q, *J* = 7.1 Hz, 2H), 1.46 (t, *J* = 8 Hz, 3H); ESI-MS *m/z* 230.1 [M+H]⁺.

4.1.30 Ethyl 2-hydroxy-2-(quinolin-8-yl)acetate (10a). To a solution of compound **34a** (130 mg, 0.57 mmol) in dry THF (5 mL), NaBH₄ (13 mg, 0.34 mmol) was added at 25 °C. The reaction mixture was stirred at 25 °C for 30 min (TLC monitoring), and then quenched with saturated aqueous NH₄Cl (1 mL). THF was evaporated under reduced pressure and the aqueous residue extracted with EtOAc (3 x 10 mL). The combined organic layers were dried over anhydrous sodium sulfate, filtered and concentrated. The residue was purified by flash chromatography on silica gel (10% to 20% EtOAc in *n*-hexane) to afford the title compound as a pale yellow amorphous solid (26% yield). ¹H NMR (CDCl₃, 300 MHz) δ 8.87 (dd, 1H, *J*₁ = 1.8 Hz, *J*₂ = 4.5 Hz), 8.20 (dd, 1H, *J*₁ = 1.8 Hz, *J*₂ = 8.4 Hz), 7.80 (dd, 1H, *J*₁ = 1.5 Hz, *J*₂ = 8.1 Hz), 7.71 (d, 1H, *J* = 6.9 Hz), 7.57-7.52 (m, 1H), 7.44 (q, 1H, *J* = 3.9 Hz), 5.66 (s, 1H), 4.26-4.05 (m, 2H), 1.12 (t, 3H, *J* = 4.2 Hz); ESI-MS *m/z* 232.0 [M+H]⁺, 254.0 [M+Na]⁺, 485.0 [2M+Na]⁺.

4.1.31 Ethyl 2-hydroxy-2-(quinolin-5-yl)acetate (10b). Compound **10b** was prepared starting from **34b** following the procedure described for the preparation of **10a**. The residue was purified by flash chromatography on silica gel (50% DCM in acetone) to afford the title compound as a yellow amorphous solid (21% yield). ¹H NMR (300 MHz, CDCl₃) δ 8.83 (d, *J* = 4.2 Hz, 1H),

8.56 (d, $J = 8.7$ Hz, 1H), 8.05 (d, $J = 8.4$ Hz, 1H), 7.67-7.52 (m, 2H), 7.39 (dd, $J = 8.6, 4.2$ Hz, 1H), 5.76 (s, 1H), 4.27-4.03 (m, 2H), 1.10 (t, $J = 7.2$ Hz, 3H); ESI-MS m/z 231.9 $[M+H]^+$.

4.1.32 8-Bromo-2-ethylquinoline (36). To a solution of freshly distilled diisopropylamine (428 μ L, 3.06 mmol) in dry THF (10 mL), *n*-BuLi (1.6 M solution in *n*-hexane, 2.90 mmol) was added dropwise at 0 °C. The solution was stirred for 30 min and then cooled to -78 °C. The cold solution was added dropwise to a solution of compound **35** (500 mg, 2.25 mmol) in dry THF (1 mL). The reaction mixture immediately turned dark red and it was kept stirring at -78 °C for 1 h. Methyl iodide (270 μ L, 4.34 mmol) was then added and the mixture was stirred while slowly reaching 0 °C, and then poured into crushed ice and neutralized with saturated aqueous NH_4Cl . The aqueous layer was extracted with EtOAc (3 x 10 mL). The combined organic layers were dried over anhydrous sodium sulfate, filtered and concentrated. The residue was purified by flash chromatography on silica gel (10% EtOAc in petroleum ether) to afford the title compound as a yellow oil (48% yield). 1H NMR (300 MHz, $CDCl_3$) δ 8.03 (d, 1H, $J = 8.6$ Hz), 8.01 (dd, 1H, $J_1 = 7.8$ Hz, $J_2 = 1.6$ Hz), 7.73 (dd, 1H, $J_1 = 8.2$ Hz, $J_2 = 1.2$ Hz), 7.34 (d, 1H, $J = 8.2$ Hz), 7.30 (t, 1H, $J = 7.8$ Hz), 3.12-3.05 (m, 2H), 1.43 (t, 3H, $J = 7.4$ Hz); ESI-MS m/z 237.0 $[M+H]^+$.

4.1.33 Ethyl 2-(2-methylquinolin-8-yl)-2-oxoacetate (37a). Compound **37a** was prepared starting from **35** following the procedure described for the preparation of **34a**. The residue was purified by flash chromatography on silica gel (7% EtOAc in petroleum ether) to afford the title compound as a yellow amorphous solid (18% yield). 1H NMR (300 MHz, $CDCl_3$) δ 8.29 (d, $J = 7.2$ Hz, 1H), 8.12-7.96 (m, 2H), 7.65-7.54 (m, 1H), 7.38-7.21 (m, 1H), 4.47 (q, $J = 7.1$ Hz, 2H), 2.68 (s, 3H), 1.41 (t, $J = 7.2$ Hz, 3H); ESI-MS m/z 244.0 $[M+H]^+$.

4.1.34 Ethyl 2-(2-ethylquinolin-8-yl)-2-oxoacetate (37b). Compound **37b** was prepared starting from **36** following the procedure described for the preparation of **34a**. The residue was

purified by flash chromatography on silica gel (10% EtOAc in petroleum ether) to afford the title compound as a yellow amorphous solid (38% yield). ^1H NMR (300 MHz, CDCl_3) δ 8.23 (d, J = 7.3 Hz, 1H), 8.05 (d, J = 8.5 Hz, 1H), 7.98 (d, J = 8.1 Hz, 1H), 7.54 (t, J = 7.7 Hz, 1H), 7.30 (d, J = 8.5 Hz, 1H), 4.43 (q, J = 7.5 Hz, 2H), 2.92 (q, J = 7.6 Hz, 2H), 1.42-1.29 (m, 6H).

4.1.35 Ethyl 2-hydroxy-2-(2-methylquinolin-8-yl)acetate (10c). Compound **10c** was prepared starting from **37a** following the procedure described for the preparation of **10a**. The residue was purified by flash chromatography on silica gel (10% EtOAc in *n*-hexane) to afford the title compound as a yellow amorphous solid (50% yield). ESI-MS m/z 246.0 $[\text{M}+\text{H}]^+$, 268.0 $[\text{M}+\text{Na}]^+$.

4.1.36 Ethyl 2-(2-ethylquinolin-8-yl)-2-hydroxyacetate (10d). Compound **10d** was prepared starting from **37b** following the procedure described for the preparation of **10a**. The residue was pure enough to be directly employed for the subsequent step (97% yield). ^1H NMR (300 MHz, CDCl_3) δ 8.07 (d, J = 8.5 Hz, 1H), 7.74 (d, J = 8.2 Hz, 1H), 7.65 (d, J = 7.1 Hz, 1H), 7.45 (t, J = 7.6 Hz, 1H), 7.33-7.23 (m, 1H), 6.80 (br s, 1H), 5.53 (s, 1H), 4.26-4.02 (m, 2H), 3.00 (q, J = 7.6 Hz, 2H), 1.41 (t, J = 7.5 Hz, 3H), 1.15 (t, J = 7.1 Hz, 3H); ESI-MS m/z 260.0 $[\text{M}+\text{H}]^+$, 281.9 $[\text{M}+\text{Na}]^+$.

4.1.37 5-Bromoisoquinoline (39). Isoquinoline **38** (1,156 mg, 8.95 mmol) was suspended in conc. H_2SO_4 (9.7 mL) at 0 °C. After cooling to -25 °C, NBS (1,912 mg, 10.74 mmol) was added. The reaction mixture was stirred at -25 °C for 2 h and then at 25 °C for additional 24 h. Subsequently, ice was added and the mixture was treated with conc. NH_4OH (10 mL) to pH = 8-10. The resulting solution was extracted with EtOAc (3 x 10 mL). The combined organic layers were dried over anhydrous sodium sulfate, filtered and concentrated. The residue was purified by flash chromatography on silica gel (20% EtOAc in petroleum ether) to afford the title compound

as a pale pink solid (71% yield). ^1H NMR (300 MHz, CDCl_3) δ 9.24 (s, 1H), 8.65 (d, J = 5.9 Hz, 1H), 8.00-7.95 (m, 3H), 7.48 (t, J = 7.8 Hz, 1H); ESI-MS m/z 209.1 $[\text{M}+\text{H}]^+$.

4.1.38 Ethyl 2-hydroxy-2-(isoquinolin-5-yl)acetate (10e). *Ethyl 2-(isoquinolin-5-yl)-2-oxoacetate* was prepared starting from **39** following the procedure described for the preparation of **34a**. The residue was purified by flash chromatography on silica gel (25% EtOAc in petroleum ether) to afford the title compound as a pale orange amorphous solid (40% yield). ^1H NMR (400 MHz, CDCl_3) δ 9.32 (s, 1H), 8.79 (d, J = 6.0 Hz, 1H), 8.70 (d, J = 6.1 Hz, 1H), 8.27-8.17 (m, 2H), 7.69 (t, J = 7.6 Hz, 1H), 4.47 (q, J = 7.2 Hz, 2H), 1.43 (t, J = 6.8 Hz, 3H); ESI-MS m/z 230.1 $[\text{M}+\text{H}]^+$. Compound **10e** was obtained starting from *ethyl 2-(isoquinolin-5-yl)-2-oxoacetate* following the procedure described for **10a**. The residue was purified by flash chromatography on silica gel (50% EtOAc in petroleum ether) to afford title compound as a pale yellow amorphous solid (53% yield). ^1H NMR (400 MHz, CDCl_3) δ 9.24 (s, 1H), 8.54 (d, J = 6.0 Hz, 1H), 7.95-7.91 (m, 2H), 7.75 (d, J = 7.2 Hz, 1H), 7.58 (t, J = 7.6 Hz, 1H), 5.73 (s, 1H), 4.31-4.06 (m, 2H), 3.76 (s, 1H), 1.11 (t, J = 7.2 Hz, 3H); ESI-MS m/z 232.1 $[\text{M}+\text{H}]^+$.

4.1.39 1-(Benzo[d][1,3]dioxol-5-yl)ethanone (41). *N-methoxy-N-methylbenzo[d][1,3]dioxole-5-carboxamide*. To a solution of acid **40** (1.0 g, 6.01 mmol) in dry DCM (20 mL), EDCI (1,382 mg, 7.21 mmol), HOBt (974 mg, 7.21 mmol) and *N,N*-DIPEA (2 mL, 12.01 mmol) were added at 0 °C. The reaction mixture was stirred at 0 °C for 30 min, then *N,O*-dimethylhydroxylamine hydrochloride (703 mg, 7.21 mmol) and *N,N*-DIPEA (1.00 mL, 6.01 mmol) were added. The reaction mixture was stirred at 25 °C for 12 h, then quenched with saturated aqueous NaHCO_3 . The reaction was extracted with DCM (3 x 20 mL) and the combined organic layers were washed with saturated aqueous NaHCO_3 , dried over anhydrous sodium sulfate, filtered and concentrated. The residue was purified by flash chromatography on silica gel (100% chloroform)

to afford the title compound as a colorless oil (73% yield). ^1H NMR (300 MHz, CDCl_3), δ 7.30 (dd, 1H, $J_1 = 0.9$ Hz, $J_2 = 0.9$ Hz), 7.22 (s, 1H), 6.81 (d, 1H, $J = 8.7$ Hz), 6.00 (s, 2H), 3.55 (s, 3H), 3.34 (s, 3H); ESI-MS m/z 210.0 $[\text{M}+\text{H}]^+$, 231.9 $[\text{M}+\text{Na}]^+$, 425.0 $[\text{2M}+\text{H}]^+$, 440.9 $[\text{2M}+\text{Na}]^+$. To a solution of *N*-methoxy-*N*-methylbenzo[*d*][1,3]dioxole-5-carboxamide (920 mg, 4.40 mmol) in dry THF (20 mL) MeMgBr (3 M solution in Et_2O , 2.2 mL, 6.60 mmol) was added at 0 °C. The reaction mixture was stirred at 0 °C for 1 h, and then quenched with saturated aqueous NH_4Cl . THF was evaporated under reduced pressure and the residue was partitioned between DCM and water. The aqueous layer was extracted with DCM (3 x 30 mL). The combined organic layers were dried over anhydrous sodium sulfate, filtered and concentrated. The obtained residue was submitted to the next step without further purification (85% yield). ^1H NMR (300 MHz, CDCl_3) δ 7.53 (dd, 1H, $J_1 = 1.8$ Hz, $J_2 = 8.1$ Hz), 7.41 (s, 1H), 6.83 (d, 2H, $J = 8.4$ Hz), 6.02 (s, 1H), 2.52 (s, 3H); ESI-MS m/z 165.0 $[\text{M}+\text{H}]^+$.

4.1.40 Methyl 2-(benzo[*d*][1,3]dioxol-5-yl)-2-hydroxyacetate (10f). 2-(Benzo[*d*][1,3]dioxol-5-yl)-2-hydroxyacetic acid. To a suspension of compound **41** (2800 mg, 16.96 mmol) in a 3:1 mixture of 1,4-dioxane and water (24 mL), Amberlyst A-26 (1696 mg, 16.96 mmol) and SeO_2 (3763 mg, 33.92 mmol) were added at 25 °C. The reaction was heated to 90 °C and stirred for 24 h. After cooling to room temperature, the mixture was filtered and the filtrate was further filtered over a celite pad to remove residual SeO_2 . The reaction mixture was treated with 1 N NaOH (20 mL) and extracted with DCM (3 x 20 mL). The aqueous layer was then acidified to pH = 1 with 6 N HCl and extracted with EtOAc (3 x 25 mL). The combined organic layers were dried over anhydrous sodium sulfate, filtered and concentrated. The obtained yellow solid residue was submitted to the next step without further purification (84% yield). ^1H NMR (300 MHz, $(\text{CD}_3)_2\text{CO}$) δ 6.97 (m, 2H), 6.81 (d, 1H, $J = 8.4$ Hz), 5.98 (s, 2H), 5.10 (s, 1H); ESI-MS m/z

194.9 [M-H]⁻. To a solution of the crude 2-(benzo[d][1,3]dioxol-5-yl)-2-hydroxyacetic acid (465 mg, 2.37 mmol) in dry DMF (12 mL), anhydrous K₂CO₃ (818 mg, 5.92 mmol) and methyl iodide (442 μ L, 7.11 mmol) were added at 25 °C. The resulting mixture was stirred at 25 °C for 3 h, and then poured in water (10 mL) and extracted with DCM (3 x 20 mL). The combined organic layers were dried over anhydrous sodium sulfate, filtered and concentrated. The residue was purified by flash chromatography on silica gel (10% EtOAc in petroleum ether) to afford title compound as an amorphous white solid (29% yield). ¹H NMR (300 MHz, CDCl₃) δ 6.94-6.87 (m, 2H), 6.79 (d, 1H, *J* = 8.7 Hz), 5.96 (s, 2H), 5.07 (s, 2H), 3.76 (s, 3H); ESI-MS *m/z* 232.9 [M+Na]⁺.

4.1.41 Ethyl 2-([1,1'-biphenyl]-2-yl)-2-oxoacetate (43). Compound **43** was prepared starting from **42** following the procedure described for the preparation of **34a**. The residue was purified by flash chromatography on silica gel (2% EtOAc in petroleum ether) to afford the title compound as a yellow oil (18%). ¹H NMR (300 MHz, CDCl₃) δ 7.82 (d, *J* = 7.5 Hz, 1H), 7.63 (t, *J* = 7.4 Hz, 1H), 7.52-7.25 (m, 7H), 3.75 (t, *J* = 6.9 Hz, 2H), 1.25 (q, *J* = 7.2 Hz, 3H); ESI-MS *m/z* 276.9 [M+Na]⁺.

4.1.42 Ethyl 2-([1,1'-biphenyl]-2-yl)-2-hydroxyacetate (10g). Compound **10g** was obtained starting from **43** following the procedure described for **10a**. The residue was purified by column chromatography on silica gel (10% EtOAc in petroleum ether) to afford the title compound as a yellow oil (56%). ¹H NMR (300 MHz, CDCl₃) δ 7.55-7.28 (m, 9H), 5.35 (d, *J* = 5.1 Hz, 1H), 4.19-4.02 (m, 2H), 1.12 (t, *J* = 7.2 Hz, 3H); ESI-MS *m/z* 279.9 [M+Na]⁺.

4.1.43 General Procedure A. Alkylation protocol employed for the synthesis of aryl-alkyl ethers 44a-e. To a stirred solution of pyrrolylphenol compounds (**8a** or **8b**, 1.0 mmol) in dry DMF (10 mL/mmol) were added K₂CO₃ (1.5 mmol) and a catalytic amount of 18-crown-6. The

mixture was stirred at 25 °C for 2 h, then the suitable α -bromoderivative (1.2 mmol) dissolved in dry DMF (3 mL/mmol) was added. The reaction mixture was stirred for 12 h at 90 °C. Then DMF was evaporated and the residue was dissolved in EtOAc. The organic layer was washed with water and dried over anhydrous sodium sulfate, filtered and concentrated. The residue was purified by flash chromatography on silica gel.

4.1.44 General Procedure B. Mitsunobu protocol employed for the synthesis of aryl-alkyl ethers 44f-j. The suitable α -hydroxyester derivative (1.0 mmol) was dissolved in dry THF (10 mL/mmol), then triphenylphosphine (1.5 mmol) and DIAD (1.0 mmol) were added at 0 °C. The mixture was stirred at 0 °C for 10 min, then a solution of pyrrolylphenol compounds **8a** or **8b** (1.0 mmol) dissolved in dry THF (8 mL/mmol) was added. The reaction mixture was stirred at 25 °C for 24 h, then THF was evaporated under reduced pressure. The residue was taken up with DCM and washed with water and brine. The organic layer was dried over anhydrous sodium sulfate, filtered and concentrated. The residue was purified by flash chromatography on silica gel.

4.1.45 Methyl 2-[(3-(1H-pyrrol-1-yl)naphthalen-2-yl)oxy]-2-(quinolin-8-yl)acetate (44a). The title compound was prepared following General Procedure A. The residue was purified by flash chromatography on silica gel (30% EtOAc in *n*-hexane) to afford the title compound as a white solid (68% yield). ^1H NMR (CDCl_3 , 300 MHz) δ 9.05 (t, $J = 2.4$ Hz, 1H), 8.20 (dd, $J_1 = 1.5$ Hz, $J_2 = 8.1$ Hz, 1H), 7.94 (d, 1H, $J = 7.5$ Hz), 7.83 (d, 1H, $J = 8.1$ Hz), 7.73 (m, 2H), 7.65 (d, 1H, $J = 8.1$ Hz), 7.60-7.37 (m, 6H), 7.27 (t, 2H, $J = 2.4$ Hz), 6.35 (t, 2H, $J = 1.5$ Hz), 3.70 (s, 3H); ^{13}C NMR (75 MHz, CDCl_3) δ 170.3, 150.1, 149.2, 145.3, 136.4, 133.3, 132.3, 131.5, 128.9, 128.9, 128.5, 128.1, 127.2, 126.6, 126.5, 126.2, 124.8, 123.7, 122.6 (2), 121.4, 109.9, 109.0 (2), 73.3, 52.6. ESI-MS m/z 409 $[\text{M}+\text{H}]^+$.

4.1.46 Methyl 2-[(3-(1*H*-pyrrol-1-yl)naphthalen-2-yl)oxy]-2-(quinolin-5-yl)acetate (44b).

The title compound was prepared following General Procedure A. The residue purified by flash chromatography on silica gel (33% EtOAc in *n*-hexane) to afford the title compound as a yellow solid (49% yield). ¹H NMR (CDCl₃, 300 MHz) δ 8.93 (d, 1H, *J* = 3.9 Hz), 8.62 (d, 1H, *J* = 8.7 Hz), 8.12 (d, 1H, *J* = 8.1 Hz), 7.77-7.66 (m, 5H), 7.48-7.36 (m, 4H), 7.12 (t, 2H, *J* = 2.1 Hz), 6.32 (t, 2H, *J* = 2.1 Hz), 6.27 (s, 1H), 3.67 (s, 3H); ESI-MS *m/z* 409 [M+H]⁺, 431 [M+Na]⁺, 447 [M+K]⁺.

4.1.47 Methyl 2-[(3-(1*H*-pyrrol-1-yl)naphthalen-2-yl)oxy]-2-(quinolin-3-yl)acetate (44c).

The title compound was prepared following General Procedure A. The residue was purified by flash chromatography on silica gel (25% EtOAc in *n*-hexane) to afford the title compound as a yellow solid (39% yield). ¹H NMR (CDCl₃, 300 MHz) δ 9.03 (d, 1H, *J* = 2.4 Hz), 8.27 (d, 1H, *J* = 2.1 Hz), 8.11 (d, 1H, *J* = 8.7 Hz), 7.83-7.72 (m, 5H), 7.58 (t, 1H, *J* = 6.6 Hz), 7.51-7.40 (m, 2H), 7.36 (s, 1H), 7.21 (t, 2H, *J* = 2.1 Hz), 6.42 (t, 2H, *J* = 2.1 Hz), 5.94 (s, 1H), 3.73 (s, 3H); ESI-MS *m/z* 409 [M+H]⁺, 431 [M+Na]⁺, 447 [M+K]⁺.

4.1.48 Methyl 2-[(3-(1*H*-pyrrol-1-yl)naphthalen-2-yl)oxy]-2-(7-chloroquinolin-5-yl)acetate (44d). The title compound was prepared following General Procedure A. The residue was purified by flash chromatography on silica gel (33% EtOAc in petroleum ether) to afford the title compound as a brown oil (44% yield). ¹H NMR (300 MHz, CDCl₃) δ 8.92 (d, 1H, *J* = 2.7 Hz), 8.66 (s, 1H), 8.24 (s, 1H), 7.81 (t, 4H, *J* = 3.0 Hz), 7.52-7.40 (m, 4H), 7.07 (t, 2H, *J* = 1.8 Hz), 6.33 (t, 2H, *J* = 2.1 Hz), 6.16 (s, 1H), 3.68 (s, 3H); ESI-MS *m/z* 443.0 [M+H]⁺, 465.0 [M+Na]⁺, 481.0 [M+K]⁺.

4.1.49 Ethyl 2-[(3-(1*H*-pyrrol-1-yl)naphthalen-2-yl)oxy]-2-(5-methoxynaphthalen-1-yl)acetate (44e). The title compound was prepared following General Procedure A. The residue

was purified by flash chromatography on silica gel (30% EtOAc in petroleum ether) to afford the title compound as an amorphous orange solid (75% yield). ^1H NMR (400 MHz, CDCl_3) δ 8.30 (d, $J = 8.4$ Hz, 1H), 7.86 (d, $J = 8.7$ Hz, 1H), 7.76-7.72 (m, 3H), 7.65 (d, $J = 7.6$ Hz, 1H), 7.51-7.33 (m, 4H), 7.30 (s, 1H), 7.21 (s, 2H), 6.84 (d, $J = 7.6$ Hz, 1H), 6.40 (s, 1H), 6.33 (s, 2H), 4.12 (q, $J = 3.6$ Hz, 2H), 3.99 (s, 3H), 1.11 (t, $J = 6.8$ Hz, 3H); ^{13}C NMR (75 MHz, CDCl_3) δ 169.3, 155.8, 149.1, 134.3, 132.2, 131.6, 131.6, 130.1, 129.0, 127.3, 127.2, 126.8, 126.6, 126.3, 125.3, 125.0, 124.8, 124.7, 124.1, 123.5, 122.5, 115.8, 110.2, 109.1, 108.9, 103.9, 61.7, 55.5, 13.9. ESI-MS m/z 452.2 $[\text{M}+\text{H}]^+$.

4.1.50 Ethyl 2-((3-(1H-pyrrol-1-yl)naphthalen-2-yl)oxy)-2-(2-methylquinolin-8-yl)acetate (44f). The title compound was prepared following General Procedure B. The residue was purified by flash chromatography on silica gel (10% EtOAc in *n*-hexane) to afford the title compound as a white amorphous solid (66% yield). ^1H NMR (300 MHz, CDCl_3) δ 8.04 (d, $J = 8.4$ Hz, 1H), 7.86 (d, $J = 7.3$ Hz, 1H), 7.81-7.64 (m, 3H), 7.64 (d, $J = 7.6$ Hz, 1H), 7.59 (s, 1H), 7.51-7.22 (m, 6H), 6.33 (t, $J = 2.2$ Hz, 2H), 4.25-4.07 (m, 3H), 2.81 (s, 3H), 1.18 (t, $J = 7.1$ Hz, 3H); ESI-MS m/z 437.0 $[\text{M}+\text{H}]^+$, 458.9 $[\text{M}+\text{Na}]^+$, 474.9 $[\text{M}+\text{K}]^+$.

4.1.51 Ethyl 2-((3-(1H-pyrrol-1-yl)naphthalen-2-yl)oxy)-2-(2-ethylquinolin-8-yl)acetate (44g). The title compound was prepared following General Procedure B. The residue was purified by flash chromatography on silica gel (5% EtOAc in petroleum ether) to afford the title compound as an amorphous light pink solid (55% yield). ^1H NMR (300 MHz, CDCl_3) δ 8.06 (d, $J = 8.4$ Hz, 1H), 7.87 (d, $J = 7.2$ Hz, 1H), 7.78-7.72 (m, 3H), 7.63 (d, $J = 8.1$ Hz, 1H), 7.56 (s, 1H), 7.48 (s, 1H), 7.45 (s, 1H), 7.43-7.32 (m, 3H), 7.29 (t, $J = 3.0$ Hz, 2H), 6.35 (t, $J = 2.1$, 2H), 4.26-4.12 (m, 2H), 3.09 (q, $J = 7.5$, 2H), 1.48 (t, $J = 7.2$, 3H), 1.19 (t, $J = 7.5$); ESI-MS m/z 450.9 $[\text{M}+\text{H}]^+$, 473.0 $[\text{M}+\text{Na}]^+$.

4.1.52 Ethyl 2-((3-(1*H*-pyrrol-1-yl)naphthalen-2-yl)oxy)-2-(isoquinolin-5-yl)acetate (44h).

The title compound was prepared following General Procedure B. The residue was purified by flash chromatography on silica gel (1% MeOH in DCM) to afford the title compound as colorless oil (35% yield). ¹H NMR (400 MHz, CDCl₃) δ 9.25 (s, 1H), 8.56 (d, *J* = 6.0 Hz, 1H), 8.06 (d, *J* = 6.0 Hz, 1H), 7.94 (dd, *J*₁ = 11.2, *J*₂ = 7.8 Hz, 2H), 7.77 (s, 1H), 7.74 (s, 1H), 7.70 (d, *J* = 8.0 Hz, 1H), 7.58 (t, *J* = 8 Hz, 1H), 7.46-7.36 (m, 2H), 7.34 (s, 1H), 7.16 (s, 2H), 6.34 (s, 2H), 6.30 (s, 1H), 4.21-4.05 (m, 2H), 1.11 (t, *J* = 7.1 Hz, 3H); ESI-MS *m/z* 423.0 [M+H]⁺, 445.0 [M+Na]⁺.

4.1.53 Methyl 2-((3-(1*H*-pyrrol-1-yl)naphthalen-2-yl)oxy)-2-(benzo[*d*][1,3]dioxol-5-yl)acetate (44i). The title compound was prepared following General Procedure B. The residue was purified by flash chromatography on silica gel (7% Et₂O in petroleum ether) to afford the title compound as a white amorphous solid (18% yield). ¹H NMR (300 MHz, CDCl₃) δ 7.78-7.72 (m, 3H), 7.48-7.38 (m, 3H), 7.22-7.20 (m, 2H), 7.01-6.96 (m, 2H), 6.78 (d, 2H, *J* = 8.1 Hz), 6.39-6.37 (m, 2H), 5.96 (s, 2H), 3.71 (s, 3H); ESI-MS *m/z* 402.0 [M+H]⁺, 404.0 [M+Na]⁺, 440.0 [M+K]⁺.

4.1.54 Ethyl 2-(2-(1*H*-pyrrol-1-yl)phenoxy)-2-([1,1'-biphenyl]-2-yl)acetate (44j). The title compound was prepared following General Procedure B. The residue was purified by column chromatography on alumina (4% EtOAc in petroleum ether) to provide the title compound as a colorless oil (56%). ¹H NMR (300 MHz, CDCl₃) δ 7.81-7.76 (m, 1H), 7.47-7.30 (m, 8H), 7.19-7.01 (m, 4H), 6.72 (t, *J* = 7.8 Hz, 1H), 6.39 (dd, *J*₁ = 1.8 Hz, *J*₂ = 2.7 Hz, 2H), 5.81 (d, *J* = 11.4 Hz, 1H), 4.31-4.16 (m, 2H), 1.31-1.21 (m, 3H); ESI-MS *m/z* 398.0 [M+H]⁺, 420.9 [M+Na]⁺.

4.1.55 2-[(3-(1*H*-Pyrrol-1-yl)naphthalen-2-yl)oxy]-2-(quinolin-8-yl)acetic acid (45a). To a stirred solution of compound **44a** (100 mg, 0.24 mmol) in a THF/MeOH mixture (3.5 mL/4.0

mL), 5% aqueous NaOH (1.7 mL) was added dropwise and the mixture was stirred at 25 °C for 2 h. The organic solvents were evaporated and the aqueous layer acidified to pH = 2 with a 1 N solution of HCl and extracted twice with DCM. The organic layer was dried over anhydrous sodium sulfate, filtered and concentrated. The title compound was obtained as a yellow amorphous solid and was submitted to the next step without further purification. (85% yield). ¹H NMR (CDCl₃, 300 MHz) δ 8.93 (d, 1H, *J* = 4.5 Hz), 8.35 (d, 1H, *J* = 8.4 Hz), 8.00 (d, 1H, *J* = 7.2 Hz), 7.86 (d, 1H, *J* = 8.4 Hz), 7.78-7.74 (m, 3H), 7.62-7.56 (m, 2H), 7.45-7.39 (m, 3H), 7.26-7.23 (m, 2H), 6.72 (s, 1H), 6.36 (s, 2H); ESI-MS *m/z* 395 [M+H]⁺, 417 [M+Na]⁺.

4.1.56 2-[(3-(1*H*-Pyrrol-1-yl)naphthalen-2-yl)oxy]-2-(quinolin-5-yl)acetic acid (45b).

Compound **45b** was obtained following the procedure described for **45a**. The title compound was obtained as a yellow amorphous solid and submitted to the next step without further purification (88% yield). ¹H NMR (300 MHz, CD₃OD) δ 8.88 (dd, *J*₁ = 11.5 Hz, *J*₂ = 6.5 Hz, 1H), 8.04 (d, *J* = 8.5 Hz, 1H), 7.90 (d, *J* = 6.6 Hz, 1H), 7.84-7.74 (m, 4H), 7.65 (s, 1H), 7.55-7.35 (m, 4H), 7.14-7.09 (m, 2H), 6.61 (s, 1H), 6.25-6.21 (m, 2H); ¹³C NMR (75 MHz, DMSO) δ 171.1, 150.5, 149.7, 148.3, 135.1, 134.4, 132.5, 131.2, 129.7, 129.1, 128.6, 127.7, 127.1, 126.7 (2C), 126.5, 124.8, 123.4, 122.7 (2C), 121.4, 109.8, 109.1 (2C), 78.2. ESI-MS *m/z* 395 [M+H]⁺, 417 [M+Na]⁺.

4.1.57 2-[(3-(1*H*-Pyrrol-1-yl)naphthalen-2-yl)oxy]-2-(quinolin-3-yl)acetic acid (45c).

Compound **45c** was obtained following the procedure described for **45a**. The title compound was obtained as an orange amorphous solid and submitted to the next step without further purification (83% yield). ¹H NMR (CDCl₃, 300 MHz) δ 10.66 (br s, 1H), 9.27 (s, 1H), 8.42 (s, 1H), 8.01 (d, 1H, *J* = 8.1 Hz), 7.65-7.57 (m, 4H), 7.51-7.38 (m, 3H), 7.29-7.19 (m, 4H), 6.31 (d, 2H, *J* = 1.5 Hz), 5.98 (s, 1H); ESI-MS *m/z* 395 [M+H]⁺.

4.1.58 2-((3-(1*H*-Pyrrol-1-yl)naphthalen-2-yl)oxy)-2-(7-chloroquinolin-5-yl)acetic acid (45d). To a solution of compound **44d** (80 mg, 0.189 mmol) in acetonitrile (2.5 mL), a 0.25 N solution of LiOH (1 mL) was added dropwise. The reaction was stirred at 25 °C for 30 min, then acetonitrile was evaporated under reduced pressure and the residue partitioned between EtOAc and water. The aqueous layer was acidified to pH = 1 with 2 N HCl and extracted with EtOAc. The organic layer was dried over anhydrous sodium sulfate, filtered and concentrated. The title compound was obtained as a brown oil and was submitted to the next step without further purification (78% yield). ¹H NMR (300 MHz, CD₃OD), δ 8.86 (s, 1H), 8.01 (d, 1H, *J* = 1.5 Hz), 7.88 (d, 1H, *J* = 1.8 Hz), 7.82-7.79 (m, 3H), 7.67 (s, 1H), 7.52-7.39 (m, 4H), 7.11 (t, 2H, *J* = 1.8 Hz), 6.63 (s, 1H), 6.26 (t, 2H, *J* = 2.10 Hz); ESI-MS *m/z* 429.0 [M+H]⁺.

4.1.59 2-((3-(1*H*-Pyrrol-1-yl)naphthalen-2-yl)oxy)-2-(5-methoxynaphthalen-1-yl)acetic acid (45e). Compound **45e** was obtained following the procedure described for **45a**. The title compound was obtained as an orange amorphous solid and submitted to the next step without further purification (99% yield). ¹H NMR (300 MHz, CDCl₃) δ 8.32 (d, *J* = 8.1 Hz, 1H), 7.82-7.68 (m, 4H), 7.59 (d, *J* = 7.6 Hz, 1H), 7.52-7.34 (m, 5H), 7.25 (s, 2H), 7.15 (s, 1H), 6.86 (d, *J* = 8.2 Hz, 1H), 6.37 (s, 2H), 3.99 (s, 3H); ESI-MS *m/z* 424.0 [M+H]⁺, 446.0 [M+Na]⁺.

4.1.60 2-((3-(1*H*-Pyrrol-1-yl)naphthalen-2-yl)oxy)-2-(2-methylquinolin-8-yl)acetic acid (45f). Compound **45f** was obtained following the procedure described for **45a**. The title compound was obtained as a dark yellow oil and submitted to the next step without further purification (98% yield). ¹H NMR (300 MHz, CD₃OD) δ 8.42 (d, *J* = 8.9 Hz, 2H), 7.96 (t, *J* = 8.6 Hz, 2H), 7.76 (t, *J* = 8.6 Hz, 2H), 7.72-7.40 (m, 4H), 7.40-7.33 (m, 1H), 7.16-7.02 (m, 2H), 6.94 (s, 1H), 6.29-6.10 (m, 2H), 2.76 (s, 3H); ESI-MS *m/z* 409.0 [M+H]⁺, 431.0 [M+Na]⁺.

4.1.61 2-((3-(1*H*-Pyrrol-1-yl)naphthalen-2-yl)oxy)-2-(2-ethylquinolin-8-yl)acetic acid (45g). Compound **45g** was obtained following the procedure described for **45a**. The title compound was obtained as an orange solid and submitted to the next step without further purification (99% yield). ¹H NMR (300 MHz, CDCl₃) δ 8.26 (d, *J* = 8.5 Hz, 1H), 7.97 (d, *J* = 7.3 Hz, 1H), 7.85-7.73 (m, 4H), 7.54 (t, *J* = 7.4 Hz, 1H), 7.50-7.35 (m, 4H), 7.23-7.20 (m, 2H), 6.59 (s, 1H), 6.37-6.31 (m, 2H), 3.14 (q, *J* = 7.8 Hz, 2H), 1.48 (t, *J* = 7.1 Hz, 3H); ESI-MS *m/z* 422.0 [M+H]⁺, 445.0 [M+Na]⁺.

4.1.62 2-((3-(1*H*-Pyrrol-1-yl)naphthalen-2-yl)oxy)-2-(isoquinolin-5-yl)acetic acid (45h). Compound **45h** was obtained following the procedure described for **45a**. The title compound was obtained as an orange amorphous solid and submitted to the next step without further purification (98% yield). ¹H NMR (400 MHz, CD₃OD) δ 9.24 (s, 1H), 8.36 (d, *J* = 6.4 Hz, 1H), 8.28 (d, *J* = 6.4 Hz, 1H), 8.10 (d, *J* = 8.4 Hz, 1H), 8.04 (d, *J* = 7.2 Hz, 1H), 7.80-7.74 (m, 3H), 7.66 (t, *J* = 7.6 Hz, 1H), 7.62 (s, 1H), 7.40 (dt, *J*₁ = 15.2 Hz, *J*₂ = 7.2 Hz, 2H), 7.12 (s, 2H), 6.50 (s, 1H), 6.20 (s, 2H); ¹³C NMR (75 MHz, CD₃OD) δ 175.6, 148.7, 136.3, 136.1, 135.9, 132.6, 131.6, 131.0, 130.9, 130.1, 129.4, 129.3, 127.0 (2), 126.5, 126.3, 124.9, 124.3, 122.4 (2), 122.0, 110.6, 108.6 (2), 77.1. ESI-MS *m/z* 395.0 [M+H]⁺.

4.1.63 2-((3-(1*H*-Pyrrol-1-yl)naphthalen-2-yl)oxy)-2-(benzo[*d*][1,3]dioxol-5-yl)acetic acid (45i). Compound **45i** was obtained following the procedure described for **45d**. The title compound was obtained as an orange amorphous solid and submitted to the next step without further purification (98% yield). ¹H NMR (300 MHz, CDCl₃) δ 7.90-7.82 (m, 3H), 7.58 (s, 1H), 7.54-7.40 (m, 2H), 7.33 (s, 2H), 7.18-7.10 (m, 2H), 6.86 (d, 1H, *J* = 6.00 Hz), 6.29 (s, 2H), 6.06 (s, 1H), 6.01 (s, 2H); ESI-MS *m/z* 386.0 [M-H]⁻, 773.0 [2M-H]⁻.

4.1.64 2-(2-(1*H*-Pyrrol-1-yl)phenoxy)-2-([1,1'-biphenyl]-2-yl)acetic acid (45j). Compound **45j** was obtained following the procedure described for **45a**. The title compound was obtained as a brown amorphous solid and submitted to the next step without further purification (quantitative yield). ¹H NMR (300 MHz, CDCl₃) δ 9.83 (s, 1H), 7.70-7.67 (m, 9H), 7.45-7.27 (m, 9H), 7.11-7.02 (m, 4H), 6.63 (d, 1H, *J* = 7.5 Hz), 6.35-6.33 (m, 2H), 5.74 (s, 1H); ¹³C NMR (75 MHz, CDCl₃) δ 174.7, 149.3, 142.6, 139.6, 132.2, 131.6, 130.2, 129.6 (2), 129.1, 128.3 (2), 128.2, 127.7, 127.6, 127.0, 125.8, 122.9, 121.9 (2), 116.2, 109.1 (2), 75.2. ESI-MS *m/z* 369.9 [M+H]⁺.

4.1.65 5-(Quinolin-8-yl)naphtho[2,3-*b*]pyrrolo[1,2-*d*][1,4]oxazepin-4(5*H*)-one (7a). To a stirred solution of acid **45a** (80 mg, 0.20 mmol) in dry DCM (50.0 mL) phosphorus pentachloride (46 mg, 0.22 mmol) was added in 5 small portions. The reaction was refluxed for 12 h. Then saturated aqueous NaHCO₃ was added dropwise and the aqueous layer was extracted with DCM (3 x 20 mL). The combined organic layers were dried over anhydrous sodium sulfate, filtered and concentrated. The residue was purified by flash chromatography on silica gel (25% EtOAc in *n*-hexane) to afford the title compound as a yellow amorphous solid (52% yield). ¹H NMR (CDCl₃, 300 MHz) δ 8.81(s, 1H), 8.14 (dd, 1H, *J*₁ = 1.2 Hz, *J*₂ = 8.1 Hz), 7.87-7.78 (m, 4H), 7.62-7.26 (m, 8H), 6.86 (br s, 1H), 6.58 (q, 1H, *J*₁ = 2.4 Hz, *J*₂ = 4.2 Hz); ESI-MS *m/z* 377 [M+H]⁺, 399 [M+Na]⁺.

4.1.66 5-(Quinolin-5-yl)naphtho[2,3-*b*]pyrrolo[1,2-*d*][1,4]oxazepin-4(5*H*)-one (7b). Compound **7b** was obtained following the procedure described for **7a**. The residue was purified by chromatography on Al₂O₃ (10% EtOAc in *n*-hexane) to afford the title compound as a white amorphous solid (42% yield). ¹H NMR (CDCl₃, 300 MHz) δ 8.97 (d, 1H, *J* = 3.9 Hz), 8.53 (d, 1H, *J* = 8.1 Hz), 8.09 (d, 1H, *J* = 8.7 Hz), 7.88-7.82 (m, 2H), 7.60-7.36 (m, 9H), 6.64-6.61 (m, 1H), 6.13 (s, 1H); ¹³C NMR (75 MHz, CDCl₃) δ 189.2, 150.4, 148.6, 147.3, 133.2, 132.9, 132.8,

132.1, 131.2, 131.1, 131.0, 128.5, 127.9, 127.4 (2C), 127.1, 126.7, 126.5, 121.6, 121.4, 120.6, 120.4, 112.5, 89.0. ESI-MS m/z 377 $[M+H]^+$.

4.1.67 5-(Quinolin-3-yl)naphtho[2,3-*b*]pyrrolo[1,2-*d*][1,4]oxazepin-4(5*H*)-one (7c).

Compound **7c** was obtained following the procedure described for **7a**. The residue was purified by flash chromatography on silica gel (25% EtOAc in petroleum ether) to afford the title compound as a brown solid (53% yield). ^1H NMR (CDCl_3 , 300 MHz) δ 9.02 (d, 1H, $J = 2.1$ Hz), 8.19 (d, 1H, $J = 0.9$ Hz), 8.12 (d, 1H, $J = 8.7$ Hz), 7.85-7.69 (m, 5H), 7.65 (s, 1H), 7.56-7.46 (m, 4H), 7.39 (d, 1H, $J = 3.3$ Hz), 6.58 (t, 1H, $J = 3.9$ Hz), 5.73 (s, 1H); ESI-MS m/z 377 $[M+H]^+$, 399 $[M+Na]^+$, 775 $[2M+Na]^+$.

4.1.68 5-(7-Chloroquinolin-5-yl)naphtho[2,3-*b*]pyrrolo[1,2-*d*][1,4]oxazepin-4(5*H*)-one (7d).

Compound **7d** was obtained following the procedure described for **7a**. The residue was purified by flash chromatography on silica gel (20% EtOAc in *n*-hexane) to afford the title compound as a white amorphous solid (19% yield). ^1H NMR (300 MHz, CDCl_3), δ 8.95 (dd, 1H, $J_1 = 1.50$ Hz, $J_2 = 4.20$ Hz), 8.43 (d, 1H, $J = 8.70$ Hz), 8.15 (s, 1H), 7.91-7.86 (m, 2H), 7.69 (d, 1H, $J = 7.50$ Hz), 7.55-7.43 (m, 7H), 6.64-6.62 (m, 1H), 5.98 (s, 1H); ESI-MS m/z 411.0 $[M+H]^+$.

4.1.69 5-(5-Methoxynaphthalen-1-yl)naphtho[2,3-*b*]pyrrolo[1,2-*d*][1,4]oxazepin-4(5*H*)-one (7e).

Compound **7e** was obtained following the procedure described for **7a**. The residue was purified by flash chromatography on silica gel (10% Et_2O in petroleum ether) to afford the title compound as a pale yellow amorphous solid (40% yield). ^1H NMR (400 MHz, CDCl_3) δ 8.22 (d, 1H, $J = 8.0$ Hz), 7.82 (s, 2H), 7.79 (d, 1H, $J = 8.7$ Hz), 7.54-7.45 (m, 5H), 7.33-7.44 (m, 4H), 6.87 (d, 1H, $J = 8.0$ Hz), 6.59 (t, 1H, $J = 3.2$ Hz), 6.24 (s, 1H), 3.99 (s, 3H); ESI-MS m/z 406.2 $[M+H]^+$, 427.9 $[M+Na]^+$, 443.1 $[M+K]^+$.

4.1.70 5-(2-Methylquinolin-8-yl)naphtho[2,3-*b*]pyrrolo[1,2-*d*][1,4]oxazepin-4(5*H*)-one (7f). Compound **7f** was obtained following the procedure described for **7a**. The residue was purified by flash chromatography on silica gel (20% EtOAc in *n*-hexane) to afford the title compound as a yellow amorphous solid (62% yield). ¹H NMR (300 MHz, CDCl₃) δ 8.00-7.66 (m, 5H), 7.58-7.29 (m, 6H), 7.25 (s, 2H), 7.09 (s, 1H), 6.62-6.54 (m, 1H), 2.36 (s, 3H); ESI-MS *m/z* 391.0 [M+H]⁺, 412.9 [M+Na]⁺.

4.1.71 5-(2-Ethylquinolin-8-yl)naphtho[2,3-*b*]pyrrolo[1,2-*d*][1,4]oxazepin-4(5*H*)-one (7g). Compound **7g** was obtained following the procedure described for **7a**. The residue was purified by flash chromatography on Al₂O₃ (5% EtOAc in petroleum ether) to afford the title compound as an orange amorphous solid (56% yield). ¹H NMR (300 MHz, CDCl₃) δ 7.95 (d, *J* = 8.4 Hz, 1H), 7.86-7.72 (m, 4H), 7.56 (d, *J* = 7.5 Hz, 1H), 7.52 (s, 1H), 7.50-7.46 (m, 2H), 7.46-7.28 (m, 4H), 7.15 (d, *J* = 8.3 Hz, 1H), 6.62-6.56 (m, 1H), 2.79-2.59 (m, 2H), 1.15 (t, *J* = 7.4 Hz, 3H); ¹³C NMR (75 MHz, CDCl₃) δ 190.8, 162.8, 148.0, 145.0, 136.0, 134.8, 134.5, 134.3, 131.9, 130.9, 130.8, 128.9, 127.3, 127.0, 126.5, 126.1, 125.9, 125.9, 125.7, 125.2, 121.0, 120.6, 119.9, 119.8, 111.6, 31.5, 12.7.

4.1.72 5-(Isoquinolin-5-yl)naphtho[2,3-*b*]pyrrolo[1,2-*d*][1,4]oxazepin-4(5*H*)-one (7h). Compound **7h** was obtained following the procedure described for **7a**. The residue was purified by flash chromatography on silica gel (10% EtOAc in *n*-hexane) to afford the title compound as a white amorphous solid (60% yield). ¹H NMR (400 MHz, CDCl₃) δ 9.26 (s, 1H), 8.60 (d, *J* = 5.6 Hz, 1H), 7.96-7.91 (m, 2H), 7.85-7.80 (m, 3H), 7.59-7.35 (m, 7H), 6.61 (dd, *J*₁ = 4 Hz, *J*₂ = 2.8 Hz, 1H), 6.13 (s, 1H); ESI-MS *m/z* 377.0 [M+H]⁺.

4.1.73 5-(Benzo[*d*][1,3]dioxol-5-yl)naphtho[2,3-*b*]pyrrolo[1,2-*d*][1,4]oxazepin-4(5*H*)-one (7i). Compound **7i** was obtained following the procedure described for **7a**. The residue was

purified by flash chromatography on silica gel (10% EtOAc in *n*-hexane) to afford the title compound as a white amorphous solid (13% yield). ¹H NMR (300 MHz, CDCl₃) δ 7.86-7.83 (m, 2H), 7.76-7.73 (m, 1H), 7.58 (s, 1H), 7.52-7.44 (m, 3H), 7.37-7.35 (m, 1H), 6.86-6.74 (m, 2H), 6.57-6.55 (m, 1H), 5.94 (s, 1H), 5.49 (s, 1H); ESI-MS *m/z* 370.0 [M+H]⁺, 392.0 [M+Na]⁺, 408.0 [M+K]⁺.

4.1.74 6-([1,1'-Biphenyl]-2-yl)benzo[*b*]pyrrolo[1,2-*d*][1,4]oxazepin-7(6*H*)-one (7j).

Compound **7j** was obtained following the procedure described for **7a**. The residue was purified by column chromatography on alumina (5% EtOAc in petroleum ether) to afford the title compound as a yellow oil (37%). ¹H NMR (300 MHz, CDCl₃) δ 7.59-7.52 (m, 2H), 7.45-7.27 (m, 12H), 7.08-7.02 (m, 1H), 6.49 (dd, *J*₁ = 3.0 Hz, *J*₂ = 0.9 Hz, 1H), 5.61 (s, 1H); ¹³C NMR (75 MHz, CDCl₃) δ 190.8, 149.0, 142.7, 140.4, 139.8, 135.0, 133.6, 130.1, 129.5 (2), 128.6, 128.4, 128.2 (2), 127.7, 127.6, 127.4, 126.1, 125.8, 123.6, 122.2, 120.5, 111.8, 88.0. ESI-MS *m/z* 352.0 [M+H]⁺, 374.9 [M+Na]⁺.

4.1.75 5-(Quinolin-8-yl)naphtho[2,3-*b*]pyrrolo[1,2-*d*][1,4]oxazepin-4-yl acetate (6a). To a suspension of potassium *tert*-butoxide (30 mg, 0.26 mmol) in dry THF (1.0 mL) a solution of compound **7a** (40 mg, 0.11 mmol) in dry THF (1.0 mL) was added, and the solution immediately turned orange. After 1 h acetyl chloride (15 μL, 0.21 mmol) was added dropwise. The mixture was stirred at 25 °C for 8 h, then saturated aqueous NH₄Cl was added dropwise and the resulting mixture was extracted with EtOAc (3 x 15 mL). The combined organic layers were dried over anhydrous sodium sulfate, filtered and concentrated. The residue was purified by flash chromatography on silica gel (16% EtOAc in *n*-hexane) to afford the title compound as a pale yellow solid (18% yield). ¹H NMR (CDCl₃, 300 MHz) δ 9.02-9.04 (m, 1H), 8.22 (dd, 1H, *J*₁ = 1.5 Hz, *J*₂ = 8.4 Hz), 7.90-7.83 (m, 4H), 7.69 (dt, 1H, *J*₁ = 1.5 Hz, *J*₂ = 7.2 Hz), 7.62 (d, 1H, 7.8

Hz), 7.54-7.38(m, 7H), 6.50-6.43 (m, 2H), 1.92 (s, 3H); ^{13}C NMR (CDCl_3 , 75 MHz) δ 169.3, 151.3, 151.0, 146.7, 145.4, 136.5, 134.6, 133.2, 132.6, 132.4, 131.5, 130.5, 130.4, 129.8, 128.9, 127.8, 127.7, 127.3, 126.3, 126.2, 122.3, 121.7, 120.9, 119.6, 111.2, 110.7, 20.9; FT-IR (neat) ν_{max} = 1751 cm^{-1} . ESI-MS m/z 419 $[\text{M}+\text{H}]^+$, 441 $[\text{M}+\text{Na}]^+$, 457 $[\text{M}+\text{K}]^+$. Anal. ($\text{C}_{27}\text{H}_{18}\text{N}_2\text{O}_3$) C, H, N.

4.1.76 5-(Quinolin-8-yl)naphtho[2,3-*b*]pyrrolo[1,2-*d*][1,4]oxazepin-4-yl dimethylcarbamate (6b). To a suspension of potassium *tert*-butoxide (23 mg, 0.20 mmol) in dry THF (2.0 mL), a solution of compound **7a** (30 mg, 0.08 mmol) in dry THF (2.0 mL) was added. After 1 h dimethylcarbamoyl chloride (15 μL , 0.16 mmol) was added dropwise. The mixture was stirred at 25 $^\circ\text{C}$ for 8 h, then saturated aqueous NH_4Cl was added dropwise and the resulting mixture was extracted EtOAc (3 x 10 mL). The combined organic layers were dried over anhydrous sodium sulfate, filtered and concentrated. The residue was purified by chromatography on Al_2O_3 (50% DCM in petroleum ether) to afford the title compound as a pale yellow solid (8% yield). ^1H NMR (CDCl_3 , 300 MHz) δ 9.07 (d, 1H, J = 3.6 Hz), 8.24 (d, 1H, J = 7.8 Hz), 7.91-7.81 (m, 3H), 7.61-7.31 (m, 8H), 6.45 (dd, 2H, J_1 = 5.1 Hz, J_2 = 8.1 Hz), 2.75 (d, 6H, J = 26.7 Hz); ^{13}C NMR (CDCl_3 , 75 MHz) δ 154.7, 151.5, 150.7, 137.5, 133.3, 132.4, 131.5, 131.2, 131.1, 130.0, 129.9, 129.5, 128.8, 127.7, 127.3, 126.4, 126.2, 126.1, 124.3, 122.1, 121.6, 120.9, 119.5 (2), 111.1, 110.5, 36.5, 29.9; ESI-MS m/z 448 $[\text{M}+\text{H}]^+$. Anal. ($\text{C}_{28}\text{H}_{21}\text{N}_3\text{O}_3$) C, H, N.

4.1.77 5-(Quinolin-8-yl)naphtho[2,3-*b*]pyrrolo[1,2-*d*][1,4]oxazepin-4-yl ethylcarbamate (6c). To a suspension of potassium *tert*-butoxide (23 mg, 0.20 mmol) in dry THF (2.0 mL) was added a solution of compound **7a** (30 mg, 0.08 mmol) in dry THF (2.0 mL). After 1 h diethylcarbamoyl chloride (22 μL , 0.16 mmol) was added dropwise. The mixture was stirred at

25 °C for 8 h, then saturated aqueous NH_4Cl was added dropwise and the resulting mixture was extracted with EtOAc (3 x 10 mL). The combined organic layers were dried over anhydrous sodium sulfate, filtered and concentrated. The residue was purified by chromatography on silica gel (17% EtOAc in *n*-hexane) to afford the title compound as a pale yellow solid (16 % yield). ^1H NMR (CDCl_3 , 300 MHz) δ 9.05 (d, 1H, J = 2.4 Hz), 8.21 (d, 1H J = 8.4 Hz), 7.89-7.78 (m, 4H), 7.60 (d, 1H, J = 8.1 Hz), 7.51-7.32 (m, 6H), 6.45 (d, 2H, J = 5.7 Hz), 3.09 (dd, 4H J_1 = 6.6 Hz, J_2 = 40.8 Hz), 0.98 (t, 3H, J = 6.6 Hz), 0.68 (t, 3H, J = 6.6 Hz); ^{13}C NMR (CDCl_3 , 75 MHz) δ 154.0, 151.6, 150.9, 146.9, 145.4, 136.4, 135.1, 133.3, 132.9, 132.4, 131.5, 130.8, 129.4, 128.8, 128.6, 127.6, 127.3, 126.2, 126.1, 122.1, 122.0, 121.6, 120.9, 119.5, 111.1, 110.43, 42.3, 41.7, 13.9, 13.5; ESI-MS m/z 477 $[\text{M}+\text{H}]^+$, 498 $[\text{M}+\text{Na}]^+$, 514 $[\text{M}+\text{K}]^+$. Anal. ($\text{C}_{30}\text{H}_{25}\text{N}_3\text{O}_3$) C, H, N.

4.1.78 5-(Quinolin-8-yl)naphtho[2,3-*b*]pyrrolo[1,2-*d*][1,4]oxazepin-4-yl (5-(diethylamino)pentan-2-yl)carbamate (6d). A solution of compound **7a** (50 mg, 0.13 mmol) in dry THF (2 mL) was added to a two-necked round bottom flask containing KO^tBu in 2 mL of dry THF. The resulting suspension immediately turned dark orange. The reaction mixture was stirred for 30 min at 25 °C, and then added *via* cannula to a solution containing triphosgene (39 mg, 0.13 mmol) in dry THF (1 mL). After 5 min stirring, *N*,*N*-diethylbutan-1,3-diamine (52 μL , 0.27 mmol) and *N,N*-DIPEA (91 μL , 0.52 mmol) were sequentially added. The reaction mixture was stirred for 14 h at 25 °C, and then neutralized with saturated aqueous NaHCO_3 . THF was evaporated under reduced pressure and the residue was extracted with EtOAc (2 x 10 mL). The combined organic layers were dried over anhydrous sodium sulfate, filtered and concentrated. The residue was purified by chromatography on silica gel (10% EtOAc in *n*-hexane) to afford title compound as an amorphous white solid (15% yield). ^1H NMR (300 MHz, CDCl_3) δ 9.03 (s, 1H), 8.24 (m, 1H), 8.16 (m, 1H), 7.91-7.75 (m, 5H), 7.62-7.27 (m, 5H), 6.47

(d, 2H, $J = 13.1$ Hz), 5.59 (br, 1H), 3.53 (m, 1H), 2.66-2.17 (m, 4H), 1.69-1.58 (m, 2H), 1.43-1.11 (m, 6H), 0.86 (m, 6H); ESI-MS m/z 560.8 $[M+H]^+$. Anal. ($C_{35}H_{36}N_4O_3$) C, H, N.

4.1.79 5-(2-Methylquinolin-8-yl)naphtho[2,3-*b*]pyrrolo[1,2-*d*][1,4]oxazepin-4-yl acetate (6e). Compound **6e** was obtained following the procedure described for **6a**. The residue was purified by flash chromatography on silica gel (20% EtOAc in *n*-hexane) to afford the title compound as a pale yellow amorphous solid (77% yield). 1H NMR (300 MHz, $CDCl_3$) δ 8.05 (d, $J = 8.2$ Hz, 1H), 7.97-7.71 (m, 4H), 7.64 (d, $J = 7.1$ Hz, 1H), 7.57-7.14 (m, 6H), 6.47 (s, 2H), 2.54 (s, 3H), 1.93 (s, 3H); ^{13}C NMR (75 MHz, $CDCl_3$) δ 169.3, 159.6, 151.7, 146.4, 146.0, 136.1, 134.0, 133.2, 132.4, 131.4, 130.8, 129.5, 128.0, 127.7, 127.3, 127.0, 126.2, 126.1, 125.56, 125.1, 122.6, 122.2, 120.6, 120.4, 111.2, 110.6, 25.7, 21.0; FT-IR (neat) $\nu_{max} = 1751$ cm^{-1} . ESI-MS m/z 433.9 $[M+H]^+$. Anal. ($C_{28}H_{20}N_2O_3$) C, H, N.

4.1.80 5-(2-Methylquinolin-8-yl)naphtho[2,3-*b*]pyrrolo[1,2-*d*][1,4]oxazepin-4-yl diethylcarbamate (6f). Compound **6f** was obtained following the procedure described for **6c**. The residue was purified by flash chromatography on silica gel (10% EtOAc in *n*-hexane) to afford the title compound as a pale yellow amorphous solid (46% yield). 1H NMR (300 MHz, $CDCl_3$) δ 8.04 (d, $J = 8.3$ Hz, 1H), 7.87-7.74 (m, 4H), 7.65 (d, $J = 7.7$ Hz, 1H), 7.48-7.36 (m, 4H), 7.34-7.20 (m, 2H), 6.46 (d, $J = 1.8$ Hz, 2H), 3.21-2.92 (m, 4H), 2.56 (s, 3H), 0.99 (t, $J = 6.5$ Hz, 3H), 0.66 (t, $J = 6.5$ Hz, 3H); ^{13}C NMR (75 MHz, $CDCl_3$) δ 159.4, 154.0, 151.9, 146.7, 146.2, 136.0, 134.4, 133.4, 132.6, 132.3, 131.4, 131.3, 129.2, 128.9, 127.6, 127.3, 126.9, 126.1, 126.0, 125.1, 122.4, 121.8, 120.6, 120.3, 111.2, 110.4, 42.3, 41.7, 25.9, 13.9, 13.5; FT-IR (neat) $\nu_{max} = 2923, 1711$ cm^{-1} . ESI-MS m/z 490.0 $[M+H]^+$, 527.9 $[M+K]^+$. Anal. ($C_{31}H_{27}N_3O_3$) C, H, N.

4.1.81 5-(2-Ethylquinolin-8-yl)naphtho[2,3-*b*]pyrrolo[1,2-*d*][1,4]oxazepin-4-yl acetate (6g). Compound **6g** was obtained following the procedure described for **6a**. The residue was purified by flash chromatography on silica gel (20% EtOAc in *n*-hexane) to afford the title compound as a colorless oil (77% yield). ¹H NMR (300 MHz, CDCl₃) δ 8.08 (d, *J* = 8.4 Hz, 1H), 7.86-7.82 (m, 3H), 7.77 (d, *J* = 7.2 Hz, 1H), 7.65 (d, *J* = 7.7 Hz, 1H), 7.51-7.38 (m, 5H), 7.37-7.23 (m, 2H), 6.48 (d, *J* = 2.2 Hz, 2H), 2.79 (q, *J* = 7.6 Hz, 2H), 1.88 (s, 3H), 1.11 (t, *J* = 8.1 Hz, 3H); ¹³C NMR (75 MHz, CDCl₃) δ 169.3, 164.3, 151.8, 146.4, 146.1, 136.2, 133.9, 133.2, 132.5, 132.4, 131.4, 131.2, 130.8, 129.5, 129.2, 128.0, 127.7, 127.6, 126.4, 125.2, 122.2, 121.4, 120.6, 120.3, 111.2, 110.5, 32.2, 20.9, 13.5; ESI-MS *m/z* 447.8 [M+H]⁺. Anal. (C₂₉H₂₂N₂O₃) C, H, N.

4.1.82 5-(2-Ethylquinolin-8-yl)naphtho[2,3-*b*]pyrrolo[1,2-*d*][1,4]oxazepin-4-yl dimethylcarbamate (6h). Compound **6h** was obtained following the procedure described for **6b**. The residue was purified by flash chromatography on silica gel (10% EtOAc in *n*-hexane) to afford the title compound as a pale yellow amorphous solid (50% yield). ¹H NMR (300 MHz, CDCl₃) δ 8.07 (d, *J* = 8.5 Hz, 1H), 7.89-7.79 (m, 4H), 7.64 (m, 1H), 7.50-7.36 (m, 4H), 7.34-7.30 (m, 2H), 6.51-6.44 (m, 2H), 2.89-2.76 (m, 5H), 2.63 (s, 3H), 1.19 (t, *J* = 7.6 Hz, 3H); ¹³C NMR (75 MHz, CDCl₃) δ 164.1, 154.7, 152.0, 146.6, 146.0, 136.2, 134.5, 133.3, 132.7, 132.4, 131.4, 131.2, 129.2, 128.8, 127.6, 127.3, 127.1, 126.1, 126.0, 125.1, 121.9, 121.2, 120.6, 120.1, 111.2, 110.3, 36.8, 36.3, 32.3, 13.7; FT-IR (neat) ν_{\max} = 1718 cm⁻¹. ESI-MS *m/z* 475.8 [M+H]⁺, 513.7 [M+K]⁺. Anal. (C₃₀H₂₅N₃O₃) C, H, N.

4.1.83 5-(2-Ethylquinolin-8-yl)naphtho[2,3-*b*]pyrrolo[1,2-*d*][1,4]oxazepin-4-yl diethylcarbamate (6i). Compound **6i** was obtained following the procedure described for **6c**. The residue was purified by flash chromatography on silica gel (10% EtOAc in *n*-hexane) to afford the title compound as a yellow amorphous solid (33% yield). ¹H NMR (300 MHz, CDCl₃)

δ 8.07 (d, J = 8.5 Hz, 1H), 7.89-7.77 (m, 4H), 7.65 (d, J = 7.4 Hz, 1H), 7.48-7.37 (m, 4H), 7.37-7.28 (m, 2H), 7.26 (s, 1H), 6.53-6.43 (m, 2H), 3.21-2.91 (m, 4H), 2.82 (q, J = 7.6 Hz, 2H), 1.18 (t, J = 7.6 Hz, 3H), 1.03-0.84 (m, 3H), 0.69-0.53 (m, 3H); ^{13}C NMR (75 MHz, CDCl_3) δ 164.1, 154.0, 152.1, 146.6, 146.0, 136.1, 134.4, 133.4, 132.8, 132.4, 131.4, 131.2, 130.0, 129.1, 128.9, 127.6, 127.3, 127.1, 126.0, 126.0, 125.1, 121.8, 121.2, 120.6, 120.0, 111.2, 110.4, 42.2, 41.7, 32.3, 29.9, 13.8, 13.6, 13.5; ESI-MS m/z 503.9 $[\text{M}+\text{H}]^+$. Anal. ($\text{C}_{32}\text{H}_{29}\text{N}_3\text{O}_3$) C, H, N.

4.1.84 5-(Quinolin-5-yl)naphtho[2,3-*b*]pyrrolo[1,2-*d*][1,4]oxazepin-4-yl acetate (6j). To a solution of **46b** (20 mg, 0.053 mmol) in dry THF (1.0 mL) sodium *bis*(trimethylsilyl)amide (1 M solution in THF, 133 μL , 0.13 mmol) was added dropwise at -78°C . After 45 min at -78°C acetyl chloride (8 μL , 0.11 mmol) was added. The mixture was stirred for 4 h at -78°C . Subsequently 1 mL of aqueous saturated NH_4Cl was added. The aqueous phase was extracted with EtOAc. The organic layer was dried over anhydrous sodium sulfate, filtered and concentrated. The residue was purified by chromatography on Al_2O_3 (30% petroleum ether in DCM) to afford the title compound as a white solid (17 % yield). ^1H NMR (CDCl_3 , 300 MHz) δ 8.97 (dd, 1H, J_1 = 1.5 Hz, J_2 = 3.9 Hz), 8.52 (d, 1H, J = 8.4 Hz), 8.21 (d, 1H, J = 8.4 Hz), 7.85-7.87 (m, 2H), 7.38-7.72 (m, 7H), 7.31 (s, 1H), 6.50 (t, 2H, J = 1.2 Hz), 1.88 (s, 3H); ^{13}C NMR (CDCl_3 , 75 MHz) δ 168.8, 150.9, 150.2, 135.0, 132.7, 132.4, 131.6, 131.3, 130.8, 129.3, 128.0, 127.7 (2), 127.4, 127.3, 126.9, 126.6 (2), 122.8, 121.6, 121.7, 121.1, 119.3, 111.5, 111.1, 104.4, 20.7; FT-IR (neat) ν_{max} = 1756 cm^{-1} . ESI-MS m/z 419 $[\text{M}+\text{H}]^+$, 441 $[\text{M}+\text{Na}]^+$, 457 $[\text{M}+\text{K}]^+$. HRMS-ESI (m/z): $[\text{M}+\text{H}]^+$ calcd for $\text{C}_{27}\text{H}_{19}\text{N}_2\text{O}_3$ 419,13957; found 419,13815. Anal. ($\text{C}_{27}\text{H}_{18}\text{N}_2\text{O}_3$) C, H, N.

4.1.85 5-(7-Chloroquinolin-5-yl)naphtho[2,3-*b*]pyrrolo[1,2-*d*][1,4]oxazepin-4-yl acetate (6k). Compound **6k** was obtained following the procedure described for **6j**. The residue was

purified by flash chromatography on silica gel (4% acetone in DCM) to afford the title compound as an amorphous white solid (27% yield). ^1H NMR (300 MHz, CDCl_3) δ 8.97 (dd, 1H, $J_1 = 1.8$ Hz, $J_2 = 4.5$ Hz), 8.53 (d, 1H, $J = 8.4$ Hz), 8.24 (s, 1H), 7.86-7.88 (m, 2H), 7.66 (d, 1H, $J = 7.8$ Hz), 7.40-7.55 (m, 5H), 7.32 (s, 1H), 6.51 (d, 2H, $J = 2.40$ Hz), 1.94 (s, 1H); ^{13}C NMR (75 MHz, CDCl_3) δ 168.7, 150.7, 132.5, 132.4 (2), 131.6 (2), 128.9, 127.7 (2), 127.5 (2), 126.8 (2), 125.5, 123.3, 121.7 (2), 121.3 (2), 119.3 (2), 111.6, 29.9, 20.7; ESI-MS m/z 452.9 $[\text{M}+\text{H}]^+$, 475.0 $[\text{M}+\text{Na}]^+$, 491.0 $[\text{M}+\text{K}]^+$. Anal. ($\text{C}_{27}\text{H}_{17}\text{ClN}_2\text{O}_3$) C, H, N.

4.1.86 5-(Quinolin-3-yl)naphtho[2,3-*b*]pyrrolo[1,2-*d*][1,4]oxazepin-4-yl acetate (6l).

Compound **6l** was obtained following the procedure described for **6j**. The residue was purified by flash chromatography on silica gel (0.5% methanol in DCM) to afford the title compound as a yellow oil (28% yield). ^1H NMR (CDCl_3 , 300 MHz) δ 9.32 (s, 1H), 8.62 (s, 1H), 8.13 (d, 1H, $J = 8.7$ Hz), 7.92 (d, 1H, $J = 7.8$ Hz), 7.72-7.85 (m, 4H), 7.68 (s, 1H), 7.61 (t, 1H, $J = 7.5$ Hz), 7.42-7.50 (m, 2H), 7.37 (s, 1H), 6.49-6.53 (m, 2H), 2.26 (s, 3H); ^{13}C NMR (CDCl_3 , 75 MHz) δ 168.8, 150.8, 148.2, 142.1, 135.0, 134.6, 132.6, 132.4, 131.6, 130.9, 128.7, 128.6, 127.9 (2), 127.7, 127.6, 127.5, 127.4, 127.1, 126.8, 126.7, 123.1, 121.1, 119.0, 111.8, 111.7, 21.3; ESI-MS m/z 419 $[\text{M}+\text{H}]^+$, 441 $[\text{M}+\text{Na}]^+$. Anal. ($\text{C}_{27}\text{H}_{18}\text{N}_2\text{O}_3$) C, H, N.

4.1.87 5-(Isoquinolin-5-yl)naphtho[2,3-*b*]pyrrolo[1,2-*d*][1,4]oxazepin-4-yl acetate (6m).

Compound **6m** was obtained following the procedure described for **6j**. The residue was purified by flash chromatography on silica gel (1% acetone in DCM) to afford the title compound as a colorless oil (30% yield). ^1H NMR (300 MHz, CDCl_3) δ 9.34 (s, 1H), 8.54 (d, $J = 6.4$ Hz, 1H), 8.06 (d, $J = 8.2$ Hz, 1H), 7.98 (d, $J = 6.4$ Hz, 1H), 7.87-7.85 (m, 2H), 7.74 (d, $J = 6.7$ Hz, 1H), 7.65-7.61 (m, 3H), 7.49-7.35 (m, 4H), 7.31 (s, 1H), 6.50 (d, $J = 3.2$ Hz, 2H), 1.87 (s, 3H); ^{13}C NMR (CDCl_3 , 75 MHz) δ 168.6, 152.4, 150.7, 143.7, 142.9, 134.7, 134.2, 132.5, 132.1, 131.5,

131.3, 130.0, 129.3, 128.87, 127.4, 127.1, 127.0, 126.8, 126.4 (2), 122.6, 120.9, 119.4, 119.0, 111.2, 110.9, 20.5; ESI-MS m/z 419.1 $[M+H]^+$. Anal. ($C_{27}H_{18}N_2O_3$) C, H, N.

4.1.88 5-(Benzo[*d*][1,3]dioxol-5-yl)naphtho[2,3-*b*]pyrrolo[1,2-*d*][1,4]oxazepin-4-yl acetate (6n). Compound **6n** was obtained following the procedure described for **6j**. The residue was purified by flash chromatography on silica gel (10% EtOAc in *n*-hexane) to afford the title compound as a white amorphous solid (37% yield). 1H NMR (300 MHz, $CDCl_3$) δ 7.84-7.73 (m, 3H), 7.63 (s, 1H), 7.46-7.43 (m, 2H), 7.36-7.26 (m, 3H), 6.87 (d, 1H, $J = 8.4$ Hz), 6.45-6.42 (m, 2H), 6.02 (s, 2H), 2.22 (s, 3H); ^{13}C NMR (75 MHz, $CDCl_3$) δ 169.0, 151.0, 148.2, 145.0, 144.6, 132.9, 132.5, 132.4, 131.5, 128.2, 127.7, 127.4, 127.2, 126.6 (2), 122.2, 121.7, 120.7, 118.9, 111.3, 110.7, 108.5, 107.6, 101.6, 21.3; ESI-MS m/z 411.9 $[M+H]^+$, 433.8 $[M+Na]^+$, 449.9 $[M+K]^+$. Anal. ($C_{25}H_{17}NO_5$) C, H, N.

4.1.89 5-(5-Methoxynaphthalen-1-yl)naphtho[2,3-*b*]pyrrolo[1,2-*d*][1,4]oxazepin-4-yl acetate (6o). Compound **6o** was obtained following the procedure described for **6j**. The residue was purified by flash chromatography on silica gel (5% EtOAc in *n*-hexane) to afford the title compound as a colorless oil (65% yield). 1H NMR (400 MHz, $CDCl_3$) δ 8.35 (d, $J = 8.0$ Hz, 1H), 7.84 (d, $J = 7.7$ Hz, 1H), 7.69 (d, $J = 8.5$ Hz, 1H), 7.61 (d, $J = 8.0$ Hz, 1H), 7.47-7.34 (m, 6H), 7.31 (s, 2H), 6.86 (d, $J = 7.6$ Hz, 1H), 6.47 (s, 2H), 4.02 (s, 3H), 1.84 (s, 3H); ^{13}C NMR ($CDCl_3$, 75 MHz) δ 168.8, 155.5, 150.9, 145.9, 134.1, 132.7, 132.4, 132.2, 131.3, 130.2, 127.8, 127.5, 127.4, 127.2, 126.5, 126.2, 126.1, 126.0, 124.4, 123.7, 122.2, 120.7, 119.3, 118.7, 111.1, 110.4, 104.1, 55.6, 20.8; ESI-MS m/z 448.3 $[M+H]^+$, 470.2 $[M+Na]^+$. Anal. ($C_{29}H_{21}NO_4$) C, H, N.

4.1.90 6-([1,1'-Biphenyl]-2-yl)benzo[*b*]pyrrolo[1,2-*d*][1,4]oxazepin-7-yl acetate (6p). Compound **6p** was obtained following the procedure described for **6j**. The residue was purified by flash chromatography on silica gel (5% EtOAc in petroleum ether) to afford the title

compound as a yellow oil (84%). ^1H NMR (300 MHz, CDCl_3) δ 7.49-7.41 (m, 5H), 7.37-7.30 (m, 1H), 7.28-7.18 (m, 4H), 7.12-7.05 (m, 2H), 6.95 (td, $J_1 = 6.6$ Hz, $J_2 = 1.2$ Hz, 1H), 6.58 (d, $J = 7.2$ Hz, 1H), 6.33 (m, 1H), 6.26 (dd, $J_1 = 1.5$ Hz, $J_2 = 2.1$ Hz, 1H), 1.99 (s, 3H); ^{13}C NMR (300 MHz, CDCl_3) δ 168.6, 152.1, 146.4, 141.7, 141.2, 132.8, 132.5, 131.6, 130.6, 130.4, 129.4, 128.6, 128.2, 127.2, 127.1, 126.8, 126.7, 125.2, 122.3, 122.2, 121.3, 110.6, 109.9, 20.6; ESI-MS m/z 416.1 $[\text{M}+\text{Na}]^+$. Anal. ($\text{C}_{26}\text{H}_{19}\text{NO}_3$) C, H, N.

4.1.91 5-(Naphthalen-1-yl)naphtho[2,3-*b*]pyrrolo[1,2-*d*][1,4]oxazepin-4(5*H*)-one oxime (47). To a solution of compound **46** (50 mg, 0.13 mmol) in dry MeOH (1 mL) hydroxylamine hydrochloride (185 mg, 2.66 mmol) and pyridine (1.06 mL, 2.66 mmol) were sequentially added. The reaction mixture was stirred at reflux for 12 h, then methanol was evaporated under reduced pressure. The residue was partitioned between water and EtOAc. The organic layer was dried over anhydrous sodium sulfate, filtered and concentrated. The residue was purified by chromatography on silica gel (1% acetone in DCM) to afford the title compound as a yellow amorphous solid (60% yield). ^1H NMR (300 MHz, CDCl_3) δ 8.51 (d, 1H, $J = 8.4$ Hz), 8.40 (s, 1H), 7.91 (d, 1H, $J = 8.1$ Hz), 7.78-7.72 (m, 3H), 7.74-7.55 (m, 4H), 7.50-7.40 (m, 4H), 7.13 (s, 1H), 6.81 (m, 1H), 6.45 (t, 1H, $J = 3.0$ Hz); ESI-MS m/z 390.9 $[\text{M}+\text{H}]^+$, 413.9 $[\text{M}+\text{Na}]^+$.

4.1.92 *N*-(5-(Naphthalen-1-yl)naphtho[2,3-*b*]pyrrolo[1,2-*d*][1,4]oxazepin-4-yl)acetamide (6q). To a solution of **47** (70 mg, 0.18 mmol) in 1,2-dichloroethane (4 mL), acetic anhydride (42 μL , 0.45 mmol), sodium bisulfite (56 mg, 0.54 mmol) and copper(I) iodide (10 mol%) were added in sequence at 25 °C. The reaction mixture was heated to reflux and stirred for 12 h. The mixture was then cooled to room temperature and extracted with EtOAc (3 x 10 mL). The combined organic layers were dried over anhydrous sodium sulfate, filtered and concentrated. The residue was purified by chromatography on silica gel (36% EtOAc in *n*-hexane) to afford the

title compound as a yellow amorphous solid (22% yield). ^1H NMR (300 MHz, CDCl_3) δ 8.11-8.04 (m, 1H), 7.84 (m, 4H), 7.62-7.29 (m, 9H), 6.60-6.37 (m, 3H), 1.79 (s, 3H); ^{13}C NMR (75 MHz, CDCl_3) δ 134.0, 133.2, 132.4, 132.0, 131.5 (2), 131.2, 129.8, 129.0, 128.6, 127.7 (2), 127.4, 126.9, 126.6, 126.4, 126.3, 125.5 (2), 123.3, 122.6, 121.0, 119.2, 111.3, 111.2, 23.5; FT-IR (neat) ν_{max} = 1733 cm^{-1} . ESI-MS m/z 417.0 $[\text{M}+\text{H}]^+$, 439.0 $[\text{M}+\text{Na}]^+$, 455.0 $[\text{M}+\text{K}]^+$. Anal. ($\text{C}_{28}\text{H}_{20}\text{N}_2\text{O}_2$) C, H, N.

4.1.93 5-(Naphthalen-1-yl)naphtho[2,3-*b*]pyrrolo[1,2-*d*][1,4]oxazepin-4-yl (5-(diethylamino)pentan-2-yl)carbamate (6r). A solution of compound **46** (100 mg, 0.26 mmol) in dry THF (3 mL) was added to a two-necked round bottom flask containing potassium hydride (30% suspension in mineral oil, 40 mg, 0.26 mmol). The resulting suspension immediately turned dark orange. The reaction mixture was stirred for 1 h at 25 °C, and then added via cannula to a solution containing triphosgene (78 mg, 0.26 mmol) in dry THF (1 mL). After 5 min stirring, N^1,N^1 -diethylbutan-1,3-diamine (103 μL , 0.53 mmol) and N,N -DIPEA (185 μL , 1.06 mmol) were sequentially added. The reaction mixture was stirred for 14 h at 25 °C, and then neutralized with saturated aqueous NaHCO_3 . THF was evaporated under reduced pressure and the residue was extracted with EtOAc (3 x 8 mL). The combined organic layers were dried over anhydrous sodium sulfate, filtered and concentrated. The residue was purified by chromatography on silica gel (100% EtOAc to 5% MeOH/5% trimethylamine in EtOAc) to afford the title compound as yellow oil (10% yield). ^1H -NMR (300 MHz, CDCl_3) δ 8.09 (d, 1H, J = 8.0 Hz), 8.04 (s, 1H), 7.93 (d, 3H, J = 7.6 Hz), 7.70 (d, 1H, J = 8.0 Hz), 7.27-7.53 (m, 8H), 6.43 (d, 2H, J = 13.2 Hz), 3.38 (s, 1H), 2.40 (q, 2H, J = 7.2 Hz), 2.31 (q, 4H, J = 6.8 Hz), 1.26 (s, 2H), 0.83 (t, 6H, J = 6.8 Hz); ESI-MS m/z 561.0 $[\text{M}+\text{H}]^+$. Anal. ($\text{C}_{36}\text{H}_{37}\text{N}_3\text{O}_3$) C, H, N.

4.2 Crystallization, Data Collection, and Structure Solution

Crystals of T₂R-TTL were grown as previously described [43, 44] and soaked 30 min or 3 h at 20 °C in the reservoir solution (10% PEG 4k, 12.5% glycerol) containing 5 mM of **6j**. Crystals were fished directly from the drop and flash-cooled in a nitrogen stream at the beamline after a transfer into cryo-solution containing 20% glycerol. Standard data collection at beamline x06DA at the Swiss Light Source (Paul Scherrer Institut, Villigen, Switzerland), data processing, and structure solution using the difference Fourier method were performed as described previously [43, 44]. Data collection and refinement statistics are given in the Table S2. Chains in the T₂R-TTL complex were defined as follows: chain A, α -tubulin-1; chain B, β -tubulin-1; chain C, α -tubulin-2; chain D, β -tubulin-2; chain E, RB3; and chain F, TTL. Chains B and D were used throughout for the structural analyses and figure preparation.

4.3 Computational Details

4.3.1 Protein and ligands preparation.

The crystal structure of **6j**-tubulin was prepared by means of Protein Preparation Wizard protocol implemented in Maestro (Maestro, version 10.1, Schrödinger, LLC, New York, NY, 2015) for acquiring an appropriate starting complex for the subsequent computational analyses [16, 50-52]. Regarding the **6j**-tubulin used in MD simulation we maintained the chain C and D of the complex removing the water molecules and the compounds used for the crystallization but maintaining the co-factors such as GDP and GTP. The **6j**-tubulin used in molecular docking studies was prepared in a similar way reported for **6j**-tubulin employed in MD simulation maintaining the structural water molecules obtained by the crystallographic study. The derivatives used in molecular docking calculation were generated by using the building panel in Maestro. Molecules were treated by means of MacroModel (MacroModel, version 10.7,

Schrödinger, LLC, New York, NY, 2015) for retrieving the lower energy conformers [53] to use as input in molecular docking experiments. The calculation was performed using the Optimized Potentials for Liquid Simulations-all atom (OPLS-AA) force field 2005 [54, 55] and the Generalized-Born/Surface-Area (GB/SA) model to simulate the solvent effects [56]. No cutoff for non-bonded interactions was used. Polak-Ribiere conjugate gradient (PRCG) method was employed with 2500 maximum iterations and 0.001 gradient convergence threshold for performing the molecular energy minimizations. MCMM (Monte Carlo Multiple Minimum) was employed as torsional sampling method for the conformational searches, performing automatic setup with 21 kJ/mol (5.02 kcal/mol) in the energy window for saving structure and 0.5 Å was used as cutoff distance for redundant conformers. The lower conformers were treated by LigPrep application (LigPrep, version 3.3, Schrödinger, LLC, New York, NY, 2015), generating the most plausible ionization state at cellular pH value (7.4 ± 0.2) [57].

All the compounds presented in this study were evaluated for their potential capability to behave as Pan Assay Interference Compounds (PAINS) by FAF-Drugs4 web server. The compounds filtered for PAINS indicated that none of them contain sub-structural features that would label them as “frequent hitters” in high throughput screens (<http://fafdrugs4.mti.univ-paris-diderot.fr/>).

4.3.2 Molecular Dynamics simulation.

MD simulations studies were performed by means of Desmond 4.8 academic version, providing by D. E. Shaw Research ("DESRES"), using Maestro as graphical interface (Desmond Molecular Dynamics System, version 4.8, D. E. Shaw Research, New York, NY, 2016. Maestro-Desmond Interoperability Tools, version 4.8, Schrödinger, New York, NY, 2016). The calculation was performed using the Compute Unified Device Architecture (CUDA) API [58]

employing two NVIDIA GPU. The calculation was performed on a system comprising 72 Intel Xeon E5-2695 v4@2.10 GHz processors and two NVIDIA GeForce 1070 GTX GPU. The complex **6j**-tubulin was prepared as above reported. The complex was positioned into an orthorhombic box filled with water (TIP3P model). OPLS_2005 force field was used in MD calculation. The physiological concentration of monovalent ions (0.15 M) was simulated by adding Na⁺ and Cl⁻ ions. Constant temperature (300 K) and pressure (1.01325 bar) were employed with NPT (constant number of particles, pressure, and temperature) as ensemble class. RESPA integrator [59] was used in order to integrate the equations of motion, with an inner time step of 2.0 fs for bonded interactions and nonbonded interactions within the short-range cutoff. Nose-Hoover thermostats [60] were used to maintain the constant simulation temperature, and the Martyna-Tobias-Klein method [61] was used to control the pressure. Long-range electrostatic interactions were evaluated adopting particle-mesh Ewald method (PME). The cut-off for van der Waals and short-range electrostatic interactions was set at 9.0 Å. The equilibration of the system was performed with the default protocol provided in Desmond, which consists of a series of restrained minimizations and MD simulations used to slowly relax the system. By following this protocol, a single trajectory of 100 ns was obtained. We performed five independent MD runs for the mentioned complex with an aggregate simulation time of 0.5 μs to provide a more reliable result. The trajectory files were investigated by simulation interaction diagram tools, simulation quality analysis and simulation event. The described applications were used to generate all plots regarding MD simulations analysis included in the manuscript (Figure 10).

4.3.3. Molecular Docking.

Genetic Optimization for Ligand Docking (GOLD, version 5.2, Cambridge Crystallographic Data Center, UK) software was employed in molecular docking studies using the Genetic

algorithm (GA) [62, 63]. This technique allows a partial flexibility of protein and full flexibility of ligand. For each of the 100 independent GA runs, a maximum number of 125,000 GA operations were performed. The default search efficiency value was employed. The active site radius of 4 Å was chosen from the ligand (**6j**) of the crystal structure of **6j**-tubulin. Default cutoff values of 2.5 Å (dH-X) for hydrogen bonds and 4.0 Å for van der Waals distance were used. When the top three solutions attained RMSD values within 1.5 Å, GA docking was terminated. The fitness function GoldScore was evaluated. The main contacts of ligands with tubulin were calculated employing ligand-interaction diagram and a script for displaying hydrophobic interactions (*display_hydrophobic_interactions.py*) downloaded from Schrödinger website and implemented in Maestro. The RMSD between the docked pose and the crystal structure of compound **6j** was calculated by using the script *rmsd.py* available in Maestro.

4.3.4. Pictures preparation.

Figures 8,9 and 11 were prepared by means of PyMOL (The PyMOL Molecular Graphics System, v1.8.4.0, Schrödinger LLC, New York, 2015).

4.4 Biological evaluation

4.4.1 Cell lines.

Human ovarian carcinomas A2780, A2780AD (MDR overexpressing P-glycoprotein) and Human promyelocytic leukemia cells HL-60 were cultured in RPMI1640 medium supplemented with 10% fetal calf serum (FCS), glutamine (2 mM), gentamycin (40 µg/mL) penicillin (100 IU/mL), streptomycin (100 µg/mL) and 0.25 units/mL of bovine insulin. NIH3T3 Mouse fibroblasts and NIH-MDR-G185 3T3 cells (colchicine resistant fibroblasts) were maintained in Dulbecco's modified Eagle's medium (DMEM) supplemented with 10% FCS, glutamine (2

mM), penicillin (100 IU/mL), streptomycin (100 µg/mL) and **4** (60 ng/mL) and were a generous gift of Carol O. Cardarelli and Michael. M. Gottesman [64].

The human lung carcinoma A549 cells were obtained from European Collection of Cell Cultures (Salisbury, UK). The mouse melanoma cells B16F1 and B16F10 (metastatic), the non-small cell lung carcinoma cells PC9, and the NSC lung adenocarcinoma with EGFR mutation HCC827, were obtained from the American Type Culture Collection. Cells were maintained in DMEM (Sigma-Aldrich) supplemented with 10% fetal bovine serum (FBS) (Hyclone, Celbio, Milan, Italy) and 2 mM glutamine, 100 units penicillin and 0.1 mg/l streptomycin (Sigma Aldrich, St. Louis, MO, USA).

NB4 is a cell line derived from human acute promyelocytic leukemia and has been obtained from ATCC. The cells were grown at 37 °C in a humidified atmosphere containing 5% CO₂ in RPMI-1640 medium (SIGMA) supplemented with 10% heat-inactivated fetal bovine serum (HYCLONE), penicillin G (100 units/mL), streptomycin (100 µg/mL), L-glutamine (2 mM), amphotericin B (250 mg/mL).

Human multiple myeloma cell line NCI-H929 was obtained from the DSMZ cell bank (Braunschweig, Germany) and were cultured in RPMI-1640 GlutaMAXTM. The SCC4 cell line was cultured in DMEM GlutaMAXTM from Gibco (Grand Island, NY, USA). All media was supplemented with 10% (v/v) foetal bovine serum (FBS) (Gibco) and 100 U/mL penicillin and cells were incubated at 37 °C containing 5% CO₂.

4.4.2 Flow cytometry analysis

Differentiation: the cells were resuspended in 10 µL of conjugate phycoerythrine CD11c (CD11c-PE, PharMingen). Control samples were incubated 10 µL of mouse IgG1 PE conjugated; after incubation for 1 h at 4 °C in the dark, the cells were washed in PBS and re-

suspended in 500 μ L PBS containing propidium iodide (0.25 μ g/mL). The samples were then analyzed according to standard flow cytometry (FACSCalibur, BD). In particular, it has been applied statistics, Kolmogorov-Smirnov (KS) for data validation. Histograms obtained represent the distribution of real data obtained from the cells.

4.4.3. Cell cycle analysis and apoptosis

Cells were plated (2×10^5 cells/mL) and collected after treatment with title compounds. Then they were centrifuged and suspended in a solution containing 1X PBS, sodium citrate 0.1%, NP40 0.1% and propidium iodide 50 mg/mL. After 30 min of incubation at room temperature in the dark, cell cycle was evaluated by flow cytometry (FACSCalibur, Becton Dickinson Inc.) and analyzed with the program Mod Fit V3 (Verity). Apoptosis was quantified by propidium iodide staining and evaluated by flow cytometry. Alternatively, cell cycle distribution was quantified by flow cytometric analysis of propidium iodide (PI Invitrogen UK) stained cells. Briefly, cells treated with 10 μ M **6a-r** for 24 h or DMSO were fixed and permeabilized with 70% ethanol o.n. at 4 °C and incubated with 100 μ g RNAsi and 20 μ g/ml PI (Sigma) for 30 min. Samples were acquired in a GUAVA flow cytometer (Merck) and analyzed with the FlowJo software. Doublets were excluded and 20,000 events were acquired for each sample.

4.4.4 Short term cytotoxicity assays.

B16F1, B16F10, A549, PC9 and HCC827 were seeded at the density of 2,500 cells/well in 96 multiwell plates in medium with 10% serum. After adhesion, cells were treated with **PNOX** and **6a,j,l** (0.1, 1 and 10 μ M) in presence of 5% serum. After 18 h, medium was removed and cells were incubated for 4 h with fresh medium in the presence of 1.2 mM MTT (3-(4,5-dimethylthiazol-2-yl)-2,5-diphenyltetrazolium bromide) (Sigma, Milan, Italy). Alive cells reduce MTT to a strongly pigmented formazan product. After solubilization in DMSO, absorbance of

the formazan was measured with a microplate reader at 540 nm. Data are expressed as % of basal response.

4.4.5 Long term cytotoxicity assays.

Cells were seeded in 96-well plates at a density of 12,000 to 17,000 cells in 0.08 mL per well depending on the cell line and incubated overnight. Next day cells were exposed to serial dilutions of ligands for 48 h and then MTT at 2.5 mg/mL was added to each well. MTT was incubated for 4 h at 37 °C and then treated with an MTT solubilizer (10% SDS, 45% dimethylformamide, pH 5.5). Plates were incubated overnight at 37 °C in order to solubilize the formazan precipitate and the next day absorbance were measured at 595/690 nm in an automated Appliskan microplate reader (Thermo Scientific). Control Wells containing medium were used as blanks. The IC₅₀ was calculated from the log-dose response curves.

4.4.6 Tubulin polymerization assay.

Polymerization of tubulin in the presence of the different compounds was monitored by absorbance at 355 nm (Filter A00019x) in 96 well plates (Falcon, transparent, flat bottom) with an Appliskan (Thermo Scientific). 25 µM of Tubulin in GAB buffer (10 mM Sodium Phosphate, 30% Glycerol, 1 mM EGTA, 6 mM MgCl₂ and 1 mM GTP, pH 6.7) was supplemented with 27.5 µM of the compounds or DMSO as vehicle control. The turbidity was measured for 70 min at 37 °C. Data was exported using Thermo Scientific SKanIt Software for Appliskan (version 2.3) and SigmaPlot 13.0 was used to plot the charts. In order to correct the absorbance of the compounds at 350 nm data were normalized to absorbance value of the initial stable plateau.

4.4.7 Binding constant determination.

In order to determine the binding constant, we first attempted a fluorometric assay. Firstly, the spectroscopy properties of each compound were determined. Their ultraviolet-visible absorbance spectrum was determined in 10 mM NaPi 1% SDS it show a maximal absorbance of 320 nm. Absorbance was measured in a double haz Evolution 201 (Thermo Scientific) in 1 cm path length quartz cuvettes at 25 °C. Fluorescence was measured in a Horiba Jovin Yvon Fluoromax-2 at 25 °C. The fluorescence spectra with 10 μ M of each compound exciting at 320 nm (10 mM NaPi and 0.1 mM GTP) showed a maximum emission around 450 nm. When incubated with an excess of tubulin, the compounds an increment of the fluorescence intensity was observed. However, when a displacement assay using podophyllotoxin was attempted, turbidity due to precipitation was observed, which we attributed to the insolubility of the compounds. To determine the solubility of each compound in 10 mM NaPi, different concentrations (5, 10, 25, 50 and 100 μ M) were centrifugated for 20 min at 50 krpm (110.00 g) in a Beckman Optima TLX in 1mL polycarbonate tubes. Concentration of compound was determined spectrophotometrically before and after centrifugation. None of the compound were soluble at the lower concentration assayed, so we had to design an experiment in which the displaced insoluble compound does not interfere with the measurement. We decided to determine the binding constants using analytical ultracentrifugation. In this experiment the compound bound to tubulin is soluble and the non-bound compound will precipitate allowing determining the bound concentration without the interference of the free compound. Samples of 10 μ M GTP-tubulin equilibrated in 10 mM Sodium Phosphate and 1 mM GTP were incubated with 15 μ M of the different derivatives (**PNOX**, **6a-h**, **6j**, **6m**, **6n**) compounds and growing amounts of podophyllotoxin (5, 10, 25, 50 and 100 μ M). Displacement of the compound by podophyllotoxin was measured by using analytical ultracentrifugation. Analysis were performed in a Beckman

Optima XL-I ultracentrifuge equipped with dual detection system, one of UV-visible absorbance and another by Rayleigh interference [65]. An angular speed of 45 krpm (163.300 g) and a An50Ti rotor equipped with a 1.2 cm optical pathway double sector cells with quartz windows. The sedimentation profiles were analyzed as described [66, 67] and the average sedimentation coefficient $c(s)$ was calculated using *Sedfit* [68]. The data obtained were corrected by the density and viscosity of the media using *Sednterp* [69]. The concentration of the compound-tubulin complex was measured by the absorbance at 320 nm of the peak which contains the protein (this at 6S). Given the concentrations of ligand and tubulin, and the outcome of preliminary experiments that indicate that the binding is saturated at these concentrations, the absorbance of the peak in the absence of podophyllotoxin can be considered the absorbance of 10 μ M ligand-tubulin complex. Then, since the concentrations of tubulin and podophyllotoxin are far over the dissociation constant of podophyllotoxin (54 nM [70]) it could be also considered that all the sites not bound to the compound are bound to podophyllotoxin allowing determining the concentration of the podophyllotoxin-tubulin complex. The free concentration of podophyllotoxin (soluble at the conditions of the assay) can be determined from the difference between the total podophyllotoxin added and the bound podophyllotoxin. In this way we just need the free concentration of the ligands. To measure it the samples with 15 μ M of each compound in 10 mM NaPi buffer were centrifuged for 20 min at 70 krpm (163.300 g) in a Beckman Optima TLX in 1 mL polycarbonate tubes. We prepared duplicated samples without centrifugation. Supernatants were collected and 10 μ M docetaxel was added as internal standard to the supernatant and the samples which were not centrifuged. The compounds were extracted with three volumes of DCM. The extracts were dried and solved in the mobile phase to analyze with an Agilent 1100 chromatograph connected to a reverse phase column Zorbax

Eclipse XDB-C18 (mobile phase gradient 50 to 100% acetonitrile) with detection at 220, 2890 and 320 nm. In the assay conditions, the concentration remaining in the supernatant was considered the maximal free concentration of the ligand in solution, and the apparent solubility of it (**PNOX** 0.62 μM , **6a** 0.36 μM , **6d** 2.89 μM , **6e** 0.34 μM , **6f** 0.39 μM , **6g** 0.064 μM , **6h** 0.27 μM , **6j** 0.17 μM , **6m** 0.22 μM , **6n** 0.14 μM). K_b of each compound can be calculated using the next equation:

$$\frac{K_c}{K_p} = \frac{\frac{[C]b}{[T]f \cdot [C]f}}{\frac{[P]b}{[T]f \cdot [P]f}}$$

$$K_c = \frac{[C]b \cdot [P]f}{[P]b \cdot [C]f} \cdot K_p$$

K_c is the binding constant of the compound, K_p the binding constant of podophyllotoxin, $[C]b$ the concentration of bound compound, $[C]f$ the concentration of free compound, $[P]b$ the concentration of bound podophyllotoxin and $[P]f$ the free concentration of podophyllotoxin. The previous described experimental procedure result in the values of all the data requested considering K_b of podophyllotoxin ($185 \pm 7 \times 10^5 \text{ M}^{-1}$) [70].

4.4.8 Alamar blue viability assay.

NCI-H929 cells were seeded at 5×10^4 cells/well in 96 well plates while SCC4 cells were seeded at 5×10^3 cells/well in 96 well plates. Cells were treated in triplicate with either vehicle (1% (v/v) ethanol) or a range of concentrations (6-5,000 nM) of the indicated compound. After 48 h, 10% alamar blue (v/v) was added to each well. Plates were incubated in the dark for up to 5 h until a color change was observed in the vehicle. Fluorescence was measured using a SpectraMax Gemini plate reader at excitation wavelength 544 nm and emission wavelength 590 nm.

4.4.9 Flow cytometric analysis of Annexin V/PI stained cells.

The Annexin V/Propidium iodide (PI) double stain assay was employed to detect both early and late stage apoptosis using flow cytometry. Early stage apoptosis is detected by the presence of phosphatidyl serine (PS) on the outer surface of the cell membrane which is bound by the phospholipid binding protein Annexin V. Early stage apoptotic cells have an intact cell membrane and therefore stain Annexin V⁺/PI⁻. Late stage apoptosis is characterized by the ability of PI to permeate the cell membrane therefore these cells stain Annexin V⁺/PI⁺. For this apoptosis assay, SCC4 cells were seeded at a density of 15×10^4 cells/mL while NCI-H929 cells were seeded at a density of 30×10^4 cells/mL. Cells were treated with either vehicle control (1% EtOH (v/v)) or 500 nM of **PNOX** or **6j** for 48 h. After incubation, cells were harvested and stained with Annexin V/Propidium Iodide (PI) and were analyzed by flow cytometry using BD FACs Accuri software. 10,000 cells were gated on vehicle treated cells.

4.4.10 Autophagy.

HL-60 cells (1×10^6 cells/sample) were resuspended in RPMI1640 medium supplemented with 10% bovine calf serum (BCS) or in Earle's Balanced Salts (EBS) medium incubated at 37 °C for 15 min and treated with 10 μ M of compounds **PNOX**, **6g**, **6j** or **6n** in presence or absence of 40 μ M chloroquine (CQ) for 1 h 45 min. Alternatively, cells were resuspended in RPMI1640 medium supplemented with 10% BCS and treated as above for 16 h. Cells were harvested and lysed in 1% (v/v) Triton X-100 in 20 mM Tris-HCl (pH 8), 150 mM NaCl (in the presence of 0.2 mg/mL Na orthovanadate; 1 mg/mL pepstatin, leupeptin, and aprotinin; 10 mM phenyl methyl sulfonyl fluoride; and 50 mM NaF), resolved by SDS-PAGE, and transferred to nitrocellulose. Immunoblot analysis was carried out by chemiluminescence (SuperSignal West Pico Chemiluminescent Substrate kit from Pierce) using anti-LC3B (D11) XP (Cell Signaling

Technology), as well as control anti-actin mAb (catalogue MAB1501; Millipore) and secondary peroxidase-labeled Abs (Amersham Pharmacia Biotech). Immunoblots were scanned and quantitated using ImageJ software.

4.4.11 Western blot for cell cycle and apoptosis proteins.

PC9 and HCC827 were seeded at the density of 300,000 cells/well in 6 multiwell plates in medium with 10% serum. After adhesion, cells were treated with **PNOX** and **6j** (10 μ M) in presence of 5% serum. After 18 h of incubation, cells were lysed as described [71]. Cell lysates were centrifuged at 15,000 x g for 20 min at 4 °C. Following gel electrophoresis, proteins were blotted onto activated nitrocellulose membranes. Non-specific protein-binding sites were blocked by incubation with 5% milk 0.5% Tween-20 in PBS for 1 h at room temperature and membranes were then incubated overnight at 4 °C with appropriate dilutions of specific primary antibodies: anti p21 (1:1000, Cell Signaling, Celbio, Milan, Italy), anti-cyclin D1 (1:1000, Cell Signaling), anti-cleaved-caspase-3 (1:1000, Cell Signaling), anti-caspase-3 (1:1000, Cell Signaling) monoclonal antibodies. Membranes were then washed with PBS/0.1% Tween-20 and incubated for 1 h at room temperature with horseradish peroxidase- conjugated anti-mouse (1:2500, Promega, Madison, USA) or anti-rabbit (1:10,000, Merck Millipore) secondary antibody, followed by enhanced chemiluminescence detection system (Bio-Rad, Hercules, USA). As an internal control for protein loading, membranes were reprobed with antibodies for the house-keeping protein β -actin (mouse anti β -actin Ab 1:1000, Sigma). Images were digitalized with Image Quant LAS4000.

Acknowledgements

This work was supported in part by a grant from the Swiss National Science Foundation (31003A_166608; to M.O.S), grant BFU2016-75319-R (AEI/FEDER, UE) from Ministerio de

Economia y Competitividad, Blueprint 282510, AIRC-17217. The authors acknowledge networking contribution by the COST Action CM1407 “Challenging organic syntheses inspired by nature - from natural products chemistry to drug discovery” (to M.O.S. and J.F.D.) and the COST Action EPICHEMBIO CM-1406 (to L.A. and G.C.). This work has also received partial funding from the European Union’s Horizon 2020 research and innovation programme under the Marie Skłodowska-Curie grant agreement No 721906. Finally, this work was partially funded by MIUR-PRIN project n. 2015Y3C5KP (to L.M.).

The Authors thank V. Olieric and M. Wang for excellent technical assistance with the collection of X-ray data at beamlines X06DA of the Swiss Light Source (Paul Scherrer Institut, Villigen, Switzerland). We also thank Dr. Federica Finetti for technical assistance on cell biology studies and Dr. Nicola Gaggelli for technical support during IR experiments.

Additional Information

The atomic coordinates and structure factors of the T₂R-TTL-**6j** complex have been deposited to the RCSB PDB (www.rcsb.org) with the PDB ID 6GJ4. Authors will release the atomic coordinates and the experimental data upon article publication.

Supplementary data

Supplementary data associated to this article can be found at....

REFERENCES

- [1] E. Mukhtar, V.M. Adhami, H. Mukhtar, Targeting microtubules by natural agents for cancer therapy, *Mol Cancer Ther*, 13 (2014) 275-284.
- [2] C. Dumontet, M.A. Jordan, Microtubule-binding agents: a dynamic field of cancer therapeutics, *Nat Rev Drug Discov*, 9 (2010) 790-803.
- [3] R. Mackeh, D. Perdiz, S. Lorin, P. Codogno, C. Pous, Autophagy and microtubules - new story, old players, *J Cell Sci*, 126 (2013) 1071-1080.
- [4] T. Mitchison, M. Kirschner, Dynamic instability of microtubule growth, *Nature*, 312 (1984) 237-242.

- [5] E. Pasquier, M. Kavallaris, Microtubules: a dynamic target in cancer therapy, *IUBMB Life*, 60 (2008) 165-170.
- [6] J. Yang, Y. Wang, T. Wang, J. Jiang, C.H. Botting, H. Liu, Q. Chen, J.H. Naismith, X. Zhu, L. Chen, Pironetin reacts covalently with cysteine-316 of alpha-tubulin to destabilize microtubule, *Nat Commun*, 7 (2016) 12103.
- [7] P.G. Morris, M.N. Fornier, Microtubule active agents: beyond the taxane frontier, *Clin Cancer Res*, 14 (2008) 7167-7172.
- [8] Y. Lu, J. Chen, M. Xiao, W. Li, D.D. Miller, An overview of tubulin inhibitors that interact with the colchicine binding site, *Pharm Res*, 29 (2012) 2943-2971.
- [9] A.E. Prota, K. Bargsten, J.F. Diaz, M. Marsh, C. Cuevas, M. Liniger, C. Neuhaus, J.M. Andreu, K.H. Altmann, M.O. Steinmetz, A new tubulin-binding site and pharmacophore for microtubule-destabilizing anticancer drugs, *Proc Natl Acad Sci U S A*, 111 (2014) 13817-13821.
- [10] A.E. Prota, J. Setter, A.B. Waight, K. Bargsten, J. Murga, J.F. Diaz, M.O. Steinmetz, Pironetin Binds Covalently to alphaCys316 and Perturbs a Major Loop and Helix of alpha-Tubulin to Inhibit Microtubule Formation, *J Mol Biol*, 428 (2016) 2981-2988.
- [11] R.A. Veldhoen, S.L. Banman, D.R. Hemmerling, R. Odsen, T. Simmen, A.J. Simmonds, D.A. Underhill, I.S. Goping, The chemotherapeutic agent paclitaxel inhibits autophagy through two distinct mechanisms that regulate apoptosis, *Oncogene*, 32 (2013) 736-746.
- [12] B.R. Acharya, S. Bhattacharyya, D. Choudhury, G. Chakrabarti, The microtubule depolymerizing agent naphthazarin induces both apoptosis and autophagy in A549 lung cancer cells, *Apoptosis*, 16 (2011) 924-939.
- [13] R. Kochl, X.W. Hu, E.Y. Chan, S.A. Tooze, Microtubules facilitate autophagosome formation and fusion of autophagosomes with endosomes, *Traffic*, 7 (2006) 129-145.
- [14] S. Bhattacharya, A. Das, S. Datta, A. Ganguli, G. Chakrabarti, Colchicine induces autophagy and senescence in lung cancer cells at clinically admissible concentration: potential use of colchicine in combination with autophagy inhibitor in cancer therapy, *Tumour Biol*, 37 (2016) 10653-10664.
- [15] S. He, Q. Li, X. Jiang, X. Lu, F. Feng, W. Qu, Y. Chen, H. Sun, Design of Small Molecule Autophagy Modulators: A Promising Druggable Strategy, *J Med Chem*, (2017) 10.1021/acs.jmedchem.1027b01019.
- [16] M. Brindisi, S. Maramai, S. Brogi, E. Fanigliulo, S. Butini, E. Guarino, A. Casagni, S. Lamponi, C. Bonechi, S.M. Nathwani, F. Finetti, F. Ragonese, P. Arcidiacono, P. Campiglia, S. Valenti, E. Novellino, R. Spaccapelo, L. Morbidelli, D.M. Zisterer, C.D. Williams, A. Donati, C. Baldari, G. Campiani, C. Ulivieri, S. Gemma, Development of novel cyclic peptides as pro-apoptotic agents, *Eur J Med Chem*, 117 (2016) 301-320.
- [17] M.M. Mc Gee, S. Gemma, S. Butini, A. Ramunno, D.M. Zisterer, C. Fattorusso, B. Catalanotti, G. Kukreja, I. Fiorini, C. Pisano, C. Cucco, E. Novellino, V. Nacci, D.C. Williams, G. Campiani, Pyrrolo[1,5]benzoxa(thia)zepines as a new class of potent apoptotic agents. Biological studies and identification of an intracellular location of their drug target, *J Med Chem*, 48 (2005) 4367-4377.
- [18] M. Brindisi, S. Maramai, A. Grillo, S. Brogi, S. Butini, E. Novellino, G. Campiani, S. Gemma, Development of a practical and scalable route for the preparation of the deacetyltubovaline (dTuv) fragment of pretubulysin and analogs, *Tetrahedron Lett*, 57 (2016) 920-923.
- [19] S.M. Nathwani, L.M. Greene, S. Butini, G. Campiani, D.C. Williams, A. Samali, E. Szegezdi, D.M. Zisterer, The pyrrolo-1,5-benzoxazepine, PBOX-15, enhances TRAIL-induced

apoptosis by upregulation of DR5 and downregulation of core cell survival proteins in acute lymphoblastic leukaemia cells, *Int J Oncol*, 49 (2016) 74-88.

[20] S.M. Nathwani, S. Butler, D. Fayne, N.N. McGovern, B. Sarkadi, M.J. Meegan, D.G. Lloyd, G. Campiani, M. Lawler, D.C. Williams, D.M. Zisterer, Novel microtubule-targeting agents, pyrrolo-1,5-benzoxazepines, induce apoptosis in multi-drug-resistant cancer cells, *Cancer Chemother Pharmacol*, 66 (2010) 585-596.

[21] K. O'Callaghan, E. Palagano, S. Butini, G. Campiani, D.C. Williams, D.M. Zisterer, J. O'Sullivan, Induction of apoptosis in oral squamous carcinoma cells by pyrrolo-1,5-benzoxazepines, *Mol Med Rep*, 12 (2015) 3748-3754.

[22] J.C. Lennon, S. Butini, G. Campiani, A. O'Meara, D.C. Williams, D.M. Zisterer, Involvement of AMP-activated protein kinase in mediating pyrrolo-1,5-benzoxazepine-induced apoptosis in neuroblastoma cells, *Invest New Drugs*, 34 (2016) 663-676.

[23] L.M. Greene, D.P. Nolan, D. Regan-Komito, G. Campiani, D.C. Williams, D.M. Zisterer, Inhibition of late-stage autophagy synergistically enhances pyrrolo-1,5-benzoxazepine-6-induced apoptotic cell death in human colon cancer cells, *Int J Oncol*, 43 (2013) 927-935.

[24] F.T. Bane, J.H. Bannon, S.R. Pennington, G. Campiani, D.C. Williams, D.M. Zisterer, M.M. Mc Gee, The microtubule-targeting agents, PBOX-6 [pyrrolobenzoxazepine 7-[(dimethylcarbamoyl)oxy]-6-(2-naphthyl)pyrrolo-[2,1-d] (1,5)-benzoxazepine] and paclitaxel, induce nucleocytoplasmic redistribution of the peptidyl-prolyl isomerases, cyclophilin A and pin1, in malignant hematopoietic cells, *J Pharmacol Exp Ther*, 329 (2009) 38-47.

[25] L.M. Greene, M. Fleeton, J. Mulligan, C. Gowda, B.J. Sheahan, G.J. Atkins, G. Campiani, V. Nacci, M. Lawler, D.C. Williams, D.M. Zisterer, The pyrrolo-1,5-benzoxazepine, PBOX-6, inhibits the growth of breast cancer cells in vitro independent of estrogen receptor status and inhibits breast tumour growth in vivo, *Oncol Rep*, 14 (2005) 1357-1363.

[26] L.M. Greene, S. Butini, G. Campiani, D.C. Williams, D.M. Zisterer, Pre-clinical evaluation of a novel class of anti-cancer agents, the Pyrrolo-1, 5-benzoxazepines, *J Cancer*, 7 (2016) 2367-2377.

[27] M. Brindisi, S. Gemma, G. Alfano, G. Kshirsagar, E. Novellino, G. Campiani, S. Butini, A stereoselective route to 6-substituted pyrrolo-1,5-benzoxazepinones and their analogues, *Tetrahedron Lett*, 54 (2013) 5387-5390.

[28] K. Wada, T. Mizutani, S. Kitagawa, Synthesis of functionalized porphyrins as oxygen ligand receptors, *J Org Chem*, 68 (2003) 5123-5131.

[29] S. Gemma, S. Brogi, P.R. Patil, S. Giovani, S. Lamponi, A. Cappelli, E. Novellino, A. Brown, M.K. Higgins, K. Mustafa, T. Szeszak, A.G. Craig, G. Campiani, S. Butini, M. Brindisi, From (+)-epigallocatechin gallate to a simplified synthetic analogue as a cytoadherence inhibitor for *P. falciparum*, *RSC Adv*, 4 (2014) 4769-4781.

[30] C. McDonald, H. Holcomb, K. Kennedy, E. Kirkpatrick, T. Leathers, P. Vanemon, N-Iodosuccinimide-Mediated Conversion of Aldehydes to Methyl-Esters, *J Org Chem*, 54 (1989) 1213-1215.

[31] S. Lin, C.P. Stevenson, E.R. Parmee, L. Xu, X. Liao, E. Metzger, R. Liang, F. Zhang, J.E. Stelmach, Glucagon receptor antagonist compounds, compositions containing such compounds and methods of use, in, *PCT Int. Appl.*, 2010030722, 2010 March 18

[32] W.B. Choi, D.S. Menaldino, D.I. Kim, M. Bouygues, M.W. Hager, Gram-positive carbapenem antibacterials and processes for their preparation, in, *WO 2005123069*, 2005 December 29.

- [33] A. Crespo-Pena, D. Monge, E. Martin-Zamora, E. Alvarez, R. Fernandez, J.M. Lassaletta, Asymmetric formal carbonyl-ene reactions of formaldehyde tert-butyl hydrazone with alpha-keto esters: dual activation by bis-urea catalysts, *J Am Chem Soc*, 134 (2012) 12912-12915.
- [34] A.M. Lord, M.F. Mahon, M.D. Lloyd, M.D. Threadgill, Design, synthesis, and evaluation in vitro of quinoline-8-carboxamides, a new class of poly(adenosine-diphosphate-ribose)polymerase-1 (PARP-1) inhibitor, *J Med Chem*, 52 (2009) 868-877.
- [35] W.D. Brown, A.H. Gouliaev, Bromination of isoquinoline, quinoline, quinazoline and quinoxaline in strong acid, *Synthesis-Stuttgart*, (2002) 83-86.
- [36] M.G. Shen, S.B. Shang, Z.Q. Song, D. Wang, X.P. Rao, H. Gao, H. Liu, Amberlyst A-26: an efficient and reusable heterogeneous catalyst for a one-pot oxidation-Cannizzaro reaction, *J Chem Res*, (2013) 51-52.
- [37] D.C. Williams, D.M. Zisterer, V. Nacci, G. Campiani, Apoptosis-inducing compounds, in, WO 2001058904 A1, 2001 August 16.
- [38] Z.H. Guan, Z.Y. Zhang, Z.H. Ren, Y.Y. Wang, X. Zhang, Synthesis of enamides via CuI-catalyzed reductive acylation of ketoximes with NaHSO₃, *J Org Chem*, 76 (2011) 339-341.
- [39] S. Gemma, C. Camodeca, M. Brindisi, S. Brogi, G. Kukreja, S. Kunjir, E. Gabellieri, L. Lucantoni, A. Habluetzel, D. Taramelli, N. Basilico, R. Gualdani, F. Tadini-Buoninsegni, G. Bartolommei, M.R. Moncelli, R.E. Martin, R.L. Summers, S. Lamponi, L. Savini, I. Fiorini, M. Valoti, E. Novellino, G. Campiani, S. Butini, Mimicking the intramolecular hydrogen bond: synthesis, biological evaluation, and molecular modeling of benzoxazines and quinazolines as potential antimalarial agents, *J Med Chem*, 55 (2012) 10387-10404.
- [40] C.M. Henry, E. Hollville, S.J. Martin, Measuring apoptosis by microscopy and flow cytometry, *Methods*, 61 (2013) 90-97.
- [41] M. Mirigian, K. Mukherjee, S.L. Bane, D.L. Sackett, Measurement of in vitro microtubule polymerization by turbidity and fluorescence, *Methods Cell Biol*, 115 (2013) 215-229.
- [42] J.F. Diaz, R.M. Buey, Characterizing ligand-microtubule binding by competition methods, *Methods Mol Med*, 137 (2007) 245-260.
- [43] A.E. Prota, K. Bargsten, D. Zurwerra, J.J. Field, J.F. Diaz, K.H. Altmann, M.O. Steinmetz, Molecular mechanism of action of microtubule-stabilizing anticancer agents, *Science*, 339 (2013) 587-590.
- [44] A.E. Prota, M.M. Magiera, M. Kuijpers, K. Bargsten, D. Frey, M. Wieser, R. Jaussi, C.C. Hoogenraad, R.A. Kammerer, C. Janke, M.O. Steinmetz, Structural basis of tubulin tyrosination by tubulin tyrosine ligase, *J Cell Biol*, 200 (2013) 259-270.
- [45] A.E. Prota, F. Danel, F. Bachmann, K. Bargsten, R.M. Buey, J. Pohlmann, S. Reinelt, H. Lane, M.O. Steinmetz, The novel microtubule-destabilizing drug BAL27862 binds to the colchicine site of tubulin with distinct effects on microtubule organization, *J Mol Biol*, 426 (2014) 1848-1860.
- [46] R.B. Ravelli, B. Gigant, P.A. Curmi, I. Jourdain, S. Lachkar, A. Sobel, M. Knossow, Insight into tubulin regulation from a complex with colchicine and a stathmin-like domain, *Nature*, 428 (2004) 198-202.
- [47] J.A. Shabbits, R. Krishna, L.D. Mayer, Molecular and pharmacological strategies to overcome multidrug resistance, *Expert Rev Anticancer Ther*, 1 (2001) 585-594.
- [48] R. Matesanz, I. Barasoain, C.G. Yang, L. Wang, X. Li, C. de Ines, C. Coderch, F. Gago, J.J. Barbero, J.M. Andreu, W.S. Fang, J.F. Diaz, Optimization of taxane binding to microtubules: binding affinity dissection and incremental construction of a high-affinity analog of paclitaxel, *Chem Biol*, 15 (2008) 573-585.

- [49] E. White, The role for autophagy in cancer, *J Clin Invest*, 125 (2015) 42-46.
- [50] S. Brogi, S. Butini, S. Maramai, R. Colombo, L. Verga, C. Lanni, E. De Lorenzi, S. Lamponi, M. Andreassi, M. Bartolini, V. Andrisano, E. Novellino, G. Campiani, M. Brindisi, S. Gemma, Disease-Modifying Anti-Alzheimer's Drugs: Inhibitors of Human Cholinesterases Interfering with beta-Amyloid Aggregation, *CNS Neurosci Ther*, 20 (2014) 624-632.
- [51] S. Butini, M. Brindisi, S. Brogi, S. Maramai, E. Guarino, A. Panico, A. Saxena, V. Chauhan, R. Colombo, L. Verga, E. De Lorenzi, M. Bartolini, V. Andrisano, E. Novellino, G. Campiani, S. Gemma, Multifunctional cholinesterase and amyloid Beta fibrillization modulators. Synthesis and biological investigation, *ACS Med Chem Lett*, 4 (2013) 1178-1182.
- [52] L. Zaccagnini, S. Brogi, M. Brindisi, S. Gemma, G. Chemi, G. Legname, G. Campiani, S. Butini, Identification of novel fluorescent probes preventing PrP(Sc) replication in prion diseases, *Eur J Med Chem*, 127 (2017) 859-873.
- [53] S. Gemma, S. Kunjir, S.S. Coccone, M. Brindisi, V. Moretti, S. Brogi, E. Novellino, N. Basilico, S. Parapini, D. Taramelli, G. Campiani, S. Butini, Synthesis and antiparasitic activity of bicyclic dioxanes as simplified dihydroplakortin analogues, *J Med Chem*, 54 (2011) 5949-5953.
- [54] W.L. Jorgensen, D.S. Maxwell, J. TiradoRives, Development and testing of the OPLS all-atom force field on conformational energetics and properties of organic liquids, *J Am Chem Soc*, 118 (1996) 11225-11236.
- [55] G.A. Kaminski, R.A. Friesner, J. Tirado-Rives, W.L. Jorgensen, Evaluation and reparametrization of the OPLS-AA force field for proteins via comparison with accurate quantum chemical calculations on peptides, *J Phys Chem B*, 105 (2001) 6474-6487.
- [56] W.C. Still, A. Tempczyk, R.C. Hawley, T. Hendrickson, Semianalytical Treatment of Solvation for Molecular Mechanics and Dynamics, *J Am Chem Soc*, 112 (1990) 6127-6129.
- [57] M. Brindisi, S. Gemma, S. Kunjir, L. Di Cerbo, S. Brogi, S. Parapini, S. D'Alessandro, D. Taramelli, A. Habluetzel, S. Tapanelli, S. Lamponi, E. Novellino, G. Campiani, S. Butini, Synthetic spirocyclic endoperoxides: new antimalarial scaffolds, *Medchemcomm*, 6 (2015) 357-362.
- [58] J. Nickolls, I. Buck, M. Garland, K. Skadron, Scalable Parallel Programming with CUDA, *Queue*, 6 (2008) 40-53.
- [59] D.D. Humphreys, R.A. Friesner, B.J. Berne, A Multiple-Time-Step Molecular-Dynamics Algorithm for Macromolecules, *J Phys Chem*, 98 (1994) 6885-6892.
- [60] W.G. Hoover, Canonical Dynamics - Equilibrium Phase-Space Distributions, *Phys Rev A*, 31 (1985) 1695-1697.
- [61] G.J. Martyna, D.J. Tobias, M.L. Klein, Constant-Pressure Molecular-Dynamics Algorithms, *J Chem Phys*, 101 (1994) 4177-4189.
- [62] G. Jones, P. Willett, Docking small-molecule ligands into active sites, *Curr Opin Biotechnol*, 6 (1995) 652-656.
- [63] A. Gasser, S. Brogi, K. Urayama, T. Nishi, H. Kurose, A. Tafi, N. Ribeiro, L. Desaubry, C.G. Nebigil, Discovery and cardioprotective effects of the first non-Peptide agonists of the G protein-coupled prokineticin receptor-1, *Plos One*, 10 (2015) e0121027.
- [64] C.O. Cardarelli, I. Aksentijevich, I. Pastan, M.M. Gottesman, Differential effects of P-glycoprotein inhibitors on NIH3T3 cells transfected with wild-type (G185) or mutant (V185) multidrug transporters, *Cancer Res*, 55 (1995) 1086-1091.
- [65] J.S. Philo, A critical review of methods for size characterization of non-particulate protein aggregates, *Curr Pharm Biotechnol*, 10 (2009) 359-372.

- [66] P. Schuck, Size-distribution analysis of macromolecules by sedimentation velocity ultracentrifugation and lamm equation modeling, *Biophys J*, 78 (2000) 1606-1619.
- [67] P.H. Brown, P. Schuck, A new adaptive grid-size algorithm for the simulation of sedimentation velocity profiles in analytical ultracentrifugation, *Comput Phys Commun*, 178 (2008) 105-120.
- [68] P. Schuck, B. Demeler, Direct sedimentation analysis of interference optical data in analytical ultracentrifugation, *Biophys J*, 76 (1999) 2288-2296.
- [69] T.M. Laue, B.D. Shah, T.M. Ridgeway, S.L. Pelletier, Computer-Aided Interpretation of Analytical Sedimentation Data For Proteins, in: S.E. Harding, A.J. Rowe, J.C. Horton (Eds.) *Analytical ultracentrifugation in biochemistry and polymer science*, Royal Society of Chemistry, Cambridge [England] 1992, pp. 90-125.
- [70] M. Antunez-Mojica, J. Rodriguez-Salarichs, M. Redondo-Horcajo, A. Leon, I. Barasoain, A. Canales, F.J. Canada, J. Jimenez-Barbero, L. Alvarez, J.F. Diaz, Structural and Biochemical Characterization of the Interaction of Tubulin with Potent Natural Analogues of Podophyllotoxin, *J Nat Prod*, 79 (2016) 2113-2121.
- [71] F. Finetti, E. Terzuoli, S. Donnini, M. Uva, M. Ziche, L. Morbidelli, Monitoring Endothelial and Tissue Responses to Cobalt Ferrite Nanoparticles and Hybrid Hydrogels, *Plos One*, 11 (2016) e0168727.

Highlights

- We explored structure-activity relationships for a novel series of MDAs
- The crystal structure of compound **6j** in complex with tubulin was solved
- Binding to isolated tubulin was evaluated for the most promising derivatives
- Compound **6j** showed potent proapoptotic activity on a variety of cancer cell lines
- The best performing compounds were assessed on cell differentiation and autophagy